

2023

## Development of a pseudotype-based neutralization test for SARS-COV-2 antibody measurement

Kunlanan Charsangbong  
*Graduate School*

Follow this and additional works at: <https://digital.car.chula.ac.th/chulaetd>



Part of the [Medical Sciences Commons](#)

---

### Recommended Citation

Charsangbong, Kunlanan, "Development of a pseudotype-based neutralization test for SARS-COV-2 antibody measurement" (2023). *Chulalongkorn University Theses and Dissertations (Chula ETD)*. 9960. <https://digital.car.chula.ac.th/chulaetd/9960>

This Thesis is brought to you for free and open access by Chula Digital Collections. It has been accepted for inclusion in Chulalongkorn University Theses and Dissertations (Chula ETD) by an authorized administrator of Chula Digital Collections. For more information, please contact [ChulaDC@car.chula.ac.th](mailto:ChulaDC@car.chula.ac.th).

DEVELOPMENT OF A PSEUDOTYPE-BASED NEUTRALIZATION TEST FOR SARS-CoV-2  
ANTIBODY MEASUREMENT



A Thesis Submitted in Partial Fulfillment of the Requirements  
for the Degree of Master of Science in Medical Microbiology  
Medical Microbiology, Interdisciplinary Program  
Graduate School  
Chulalongkorn University  
Academic Year 2023

การพัฒนาการวัดระดับแอนติบอดีต่อไวรัสซาร์สโควิทูโดยการทดสอบนิวทรัลไลเซชันด้วยชุดโตะ



วิทยานิพนธ์นี้เป็นส่วนหนึ่งของการศึกษาตามหลักสูตรปริญญาวิทยาศาสตรมหาบัณฑิต  
สาขาวิชาจุลชีววิทยาทางการแพทย์ (สหสาขาวิชา) สหสาขาวิชาจุลชีววิทยาทางการแพทย์  
บัณฑิตวิทยาลัย จุฬาลงกรณ์มหาวิทยาลัย  
ปีการศึกษา 2566

Thesis Title	DEVELOPMENT OF A PSEUDOTYPE-BASED NEUTRALIZATION TEST FOR SARS-CoV-2 ANTIBODY MEASUREMENT
By	Miss Kunlanan Charsangbong
Field of Study	Medical Microbiology
Thesis Advisor	Associate Professor EAKACHAI PROMPETCHARA, Ph.D.
Thesis Co Advisor	NAVAPON TECHAKRIENGKRAI, D.V.M., M.Sc., Ph.D.

---

Accepted by the GRADUATE SCHOOL, Chulalongkorn University in Partial  
Fulfillment of the Requirement for the Master of Science

----- Dean of the GRADUATE SCHOOL  
(Assistant Professor YOOTTHANA CHUPPUNNARAT, Ph.D.)

THESIS COMMITTEE

----- Chairman  
(Associate Professor SIWAPORN BOONYASUPPAYAKORN,  
Ph.D.)

----- Thesis Advisor  
(Associate Professor EAKACHAI PROMPETCHARA, Ph.D.)

----- Thesis Co-Advisor  
(NAVAPON TECHAKRIENGKRAI, D.V.M., M.Sc., Ph.D.)

----- External Examiner  
(Assistant Professor ROJJANAPORN PULMANAUSAHAKUL,  
Ph.D.)

กุลนันท์ ขาแสงบง : การพัฒนาการวัดระดับแอนติบอดีต่อไวรัสซาร์สโควิทูโดยการทดสอบ  
 นิวทรัลไลเซชันด้วยซูโดไทป์. ( DEVELOPMENT OF A PSEUDOTYPE-BASED NEUTRALIZATION  
 TEST FOR SARS-CoV-2 ANTIBODY MEASUREMENT) อ.ที่ปรึกษาหลัก : รศ. ดร.เอกชัย พรหม  
 เพชร, อ.ที่ปรึกษาร่วม : อ.น.สพ. ดร.นवल เตชะเกรียงไกร

วิธีมาตรฐานของการตรวจวัดระดับนิวทรัลไลเซชันแอนติบอดีต่อไวรัสซาร์สโควิทูคือ live-virus neutralization test (VNT) ที่มีกระบวนการที่ซับซ้อนและต้องปฏิบัติงานในห้องชีวนิรภัยระดับ 3 การศึกษานี้จึงได้พัฒนาไวรัสซาร์สโควิทูซูโดไทป์บนพื้นฐานของเลนติไวรัสโดยออกแบบยีนที่ถอดรหัสเป็นโปรตีนหนามของไวรัสสายพันธุ์ดั้งเดิมเพื่อใช้แทนไวรัสที่มีชีวิตซึ่งทำให้สามารถปฏิบัติงานในห้องชีวนิรภัยระดับ 2 ได้ ผลการทดลองพบว่าเลนติไวรัสซูโดไทป์รุ่นที่ 2 ที่ใช้ green fluorescent protein (GFP) และเลนติไวรัสซูโดไทป์รุ่นที่ 3 ที่ใช้เอนไซม์ luciferase เป็นตัวแสดงผลตามลำดับ ให้ปริมาณไวรัส (TCID<sub>50</sub>/mL) สูงเพียงพอที่จะทำการทดสอบนิวทรัลไลเซชัน อย่างไรก็ตามระบบติดตามด้วยเอนไซม์ luciferase มีความแปรปรวนค่อนข้างสูง ผู้วิจัยจึงเลือกใช้เลนติไวรัสซูโดไทป์รุ่นที่ 2 ที่ติดตามด้วย GFP ในการทดสอบนิวทรัลไลเซชัน (Pseudotype neutralization test, PVNT) ผลการตรวจวัดระดับนิวทรัลไลเซชันด้วยซูโดไทป์ซาร์สโควิทูในตัวอย่างซีรัมอาสาสมัครโครงการ ChulaCoV-19 จำนวน 128 ตัวอย่าง พบว่า มีความไว (sensitivity) และความจำเพาะ (specificity) ร้อยละ 98.91 และ 100 ตามลำดับเมื่อเปรียบเทียบกับวิธี VNT และเพื่อให้การรายงานผลมีมาตรฐาน ผู้วิจัยได้ทำการทดสอบโดยใช้ตัวอย่างมาตรฐานที่ทราบระดับนิวทรัลไลเซชันและแปลงค่า PVNT<sub>50</sub> ไตเตอร์เป็นหน่วยสากล (international unit, IU/mL) พบว่าค่าไตเตอร์ที่อ่านได้จาก PVNT เปรียบเทียบกับวิธีมาตรฐาน VNT มีความสอดคล้องกันระดับปานกลาง โดยมีค่าสัมประสิทธิ์สหสัมพันธ์เท่ากับ 0.740 ( $p$ -value <0.0001) นอกจากนี้เมื่อทำการเปรียบเทียบผล PVNT กับห้องปฏิบัติการคู่เทียบ พบว่ามีความสอดคล้องกันระดับปานกลาง โดยมีค่าสัมประสิทธิ์สหสัมพันธ์เท่ากับ 0.738 ( $p$ -value <0.0001) และพบว่ามีความสอดคล้องกันต่ำลงเมื่อเปรียบเทียบกับค่า anti-SARS-CoV-2 IgG ที่วัดด้วยวิธี ELISA โดยมีค่าสัมประสิทธิ์สหสัมพันธ์เท่ากับ 0.610 ( $p$ -value <0.0001) จึงกล่าวได้ว่าการตรวจวัดระดับนิวทรัลไลเซชันแอนติบอดีด้วยซูโดไทป์ซาร์สโควิทูที่พัฒนาขึ้นสามารถตรวจวัดระดับแอนติบอดีต่อไวรัสซาร์สโควิทูได้อย่างถูกต้องและแม่นยำ โดยมีค่าสัมประสิทธิ์สหสัมพันธ์ในระดับปานกลางกับค่าที่วิเคราะห์ได้จากวิธีอื่นๆ ความแตกต่างของค่าที่วัดได้อาจเกิดจากขั้นตอนวิธีการทดสอบที่แตกต่างกัน การตรวจวัดระดับนิวทรัลไลเซชันแอนติบอดีด้วยซูโดไทป์ซูโดไทป์ที่พัฒนาขึ้นเป็นอีกทางเลือกสำหรับการตรวจวินิจฉัยทางซีรัมวิทยาสำหรับผู้ที่เคยติดเชื้อซาร์สโควิทูหรือผู้ที่ได้รับวัคซีนได้

สาขาวิชา	จุลชีววิทยาทางการแพทย์ (สหสาขาวิชา)	ลายมือชื่อนิสิต .....
ปีการศึกษา	2566	ลายมือชื่อ อ.ที่ปรึกษาหลัก .....
		ลายมือชื่อ อ.ที่ปรึกษาร่วม .....

# # 6380112020 : MAJOR MEDICAL MICROBIOLOGY

KEYWORD: SARS-CoV-2, COVID-19, Pseudotype, Serum neutralization assay

Kunlanan Charsangbong : DEVELOPMENT OF A PSEUDOTYPE-BASED NEUTRALIZATION TEST FOR SARS-CoV-2 ANTIBODY MEASUREMENT. Advisor: Assoc. Prof. EAKACHAI PROMPETCHARA, Ph.D. Co-advisor: NAVAPON TECHAKRIENGKRAI, D.V.M., M.Sc., Ph.D.

The gold standard for measuring anti-SARS-CoV-2 neutralizing antibody is a live-virus neutralization test (VNT). However, VNT is rather complex and must be performed in a biosafety level 3 facility. Therefore, a gene-encoding spike protein of the original SARS-CoV-2 variant was designed to develop a lentivirus-based SARS-CoV-2 pseudotype in this study to replace the live virus, which can be conducted in a biosafety level 2 facility. The 2<sup>nd</sup> generation lentiviral pseudotype with green fluorescent protein (GFP) and the 3<sup>rd</sup> generation lentiviral pseudotype with luciferase as a reporter system, respectively, provided a sufficient titer (TCID<sub>50</sub>/mL) for a neutralization test. However, the 3<sup>rd</sup> generation lentivirus with luciferase reporter system was inconsistent, with high variability. Therefore, the 2<sup>nd</sup> generation lentiviral pseudotype with GFP was selected and developed further into a pseudotype neutralization test (PVNT). When tested against 128 serum samples from the ChulaCoV-19 trial, the diagnostic sensitivity and specificity of this test were 98.91% and 100%, respectively, in comparison with the VNT. Standard serum samples with known titers were tested to convert the PVNT<sub>50</sub> titer into international units (IU/mL) and compared with the standard VNT method. A moderate level of agreement was observed between the 2 tests, with a correlation coefficient of 0.740 ( $p$ -value <0.0001). The PVNT titer was further compared with the titer obtained from another laboratory, which also gave a moderate level of agreement with a correlation coefficient of 0.738 ( $p$ -value <0.0001). However, a lower correlation coefficient of 0.610 ( $p$ -value <0.0001) was observed when compared with anti-SARS-CoV-2 IgG levels analyzed by ELISA. It is apparent that the developed SARS-CoV-2 pseudotype-based neutralization test can be used for anti-SARS-CoV-2 neutralizing antibody measurement with high sensitivity and specificity, with a moderate correlation with other methods. The differences in the titer may be due to the different testing protocols. Altogether, the developed test is an alternative SARS-CoV-2 serological test for individuals who have been previously infected or vaccinated.

Field of Study: Medical Microbiology

Student's Signature .....

Academic Year: 2023

Advisor's Signature .....

Co-advisor's Signature .....

## ACKNOWLEDGEMENTS

I would like to express my deepest gratitude to my advisor, Associate Professor Eakachai Prompetchara, Ph.D., for his invaluable patience, guidance, assistance, and support. His help allowed me to complete my research and write my thesis successfully.

I extend my gratitude to my co-advisor, Dr. Navapon Techakriengkrai, DVM, MSc, Ph.D., for his guidance, assistance, and instruction in completing this study.

I am also thankful to Associate Professor Chutitorn Ketloy, Ph.D., for her guidance, assistance, support, and suggestion.

I want to express my thanks to all the members of the ChulaVRC laboratory, including Dr. Sunee Sirivichayakul, Ms. Pattarawadee Pitakpolrak, Ms. Suwanna Mekprasan, Dr. Supichcha Saithong, Mr. Kittiphan Tarakhet, Ms. Prapatsara Kaewpang, Ms. Nongnapat Yostrirat, and Mr. Pachara Wangsoontorn. I also appreciate the members of the Virology Unit, Faculty of Veterinary Science, Chulalongkorn University for their instructions and assistances.

I am also thankful to Associate Professor Dr. Arunee Thitithanyanont from the Faculty of Sciences at Mahidol University and Dr. Anan Jongkaewwattana from the National Science and Technology Development Agency for providing the live-virus neutralization and pseudotype neutralization test results, respectively. Additionally, I am very appreciate Dr.Sasiwimol Ubolyam (HIV-NAT) for the ELISA (Abbott SARS-CoV-2 IgG II Quant assay) results.

I am thankful to the committee members, Associate Professor Siwaporn Boonyasuppayakorn, M.D., Ph.D., and Assistant Professor Rojjanaporn Pulmanausahakul, Ph.D. for their excellent suggestions on the thesis proposal and for ensuring the completeness of the thesis.

Kunlanan Charsangbong

## TABLE OF CONTENTS

	Page
ABSTRACT (THAI) .....	iii
ABSTRACT (ENGLISH) .....	iv
ACKNOWLEDGEMENTS .....	v
TABLE OF CONTENTS .....	vi
LIST OF TABLES.....	viii
LIST OF FIGURES.....	ix
LIST OF ABBREVIATIONS.....	1
CHAPTER I INTRODUCTION .....	4
CHAPTER II HYPOTHESIS AND OBJECTIVE.....	9
CHAPTER III LITERATURE REVIEW.....	11
CHAPTER IV MATERIALS AND METHODS .....	27
CHAPTER V RESULTS .....	39
CHAPTER VI DISCUSSION AND CONCLUSION.....	66
APPENDIX A REAGENTS.....	70
APPENDIX B INSTRUMENTS AND MATERIALS.....	71
APPENDIX C ENZYMES .....	73
APPENDIX D ANTIBODY.....	74
APPENDIX E REAGENTS PREPARATION.....	75
APPENDIX F AMINO ACID SEQUENCE.....	76
APPENDIX G PLASMID MAP .....	79
APPENDIX H SUMMARY NEUTRALIZING DATA.....	83

REFERENCES.....89

VITA.....98



จุฬาลงกรณ์มหาวิทยาลัย  
**CHULALONGKORN UNIVERSITY**

## LIST OF TABLES

	Page
<i>Table 1: Characteristic comparison of three generations of pseudotype.....</i>	21
<i>Table 2: Characteristic comparison of reporter systems. ....</i>	25
<i>Table 3: Comparison of the SARS-CoV-2 antibody testing platform. ....</i>	26
<i>Table 4: Detail of the plasmids used in the study.....</i>	28
<i>Table 5: Plasmids concentration for 1<sup>st</sup> generation SARS-CoV-2-pseudotype production.....</i>	31
<i>Table 6: Plasmids concentration for 2<sup>nd</sup> generation SARS-CoV-2-pseudotype production.....</i>	32
<i>Table 7: Plasmids concentration for 3<sup>rd</sup> generation SARS-CoV-2-pseudotype production.....</i>	32
<i>Table 8: Summary of cell or antigen target and signal detection of the different testing platforms. ....</i>	37
<i>Table 9: The titer of SARS-CoV-2 pseudotype produced at different collection time. ....</i>	41
<i>Table 10: Titer comparison between different pseudotype generations and reporter systems.....</i>	49
<i>Table 11: Sensitivity and specificity results of PVNT.....</i>	51
<i>Table 12: Validation of PVNT<sub>50</sub> titers using standard sera. ....</i>	53
<i>Table 13: Summary of results comparison between PVNT and other techniques. ...</i>	60
<i>Table 14: Titer summary of SARS-CoV-2-S-Delta (B.1.617.2) and Omicron BA.4/5.....</i>	65

## LIST OF FIGURES

	Page
<i>Figure 1: The details of SARS-CoV-2 Spike Glycoprotein.</i> .....	11
<i>Figure 2: SARS-CoV-2 viral entry and replication cycle.</i> .....	13
<i>Figure 3: Schematic representation of HIV and HIV lentiviral system.</i> .....	23
<i>Figure 4: Plate design for pseudotype viral titration.</i> .....	33
<i>Figure 5: Plate design for pseudotype neutralization assay.</i> .....	38
<i>Figure 6: Restriction digestion products in 1% agarose gel electrophoresis</i> .....	39
<i>Figure 7: Immunofluorescence staining of SARS-CoV-2-S protein expression in HEK293T cells.</i> .....	40
<i>Figure 8: Relationship between RLU on X-axis and dilution on Y-axis at 60-hr post-titration of 1<sup>st</sup> generation of pseudotype SARS-CoV-2-WT, VSVG and bald controls.</i> .42	
<i>Figure 9: Relationship between RLU on X-axis and dilution on Y-axis at 60-hr post-titration of 2<sup>nd</sup> generation of pseudotype SARS-CoV-2-WT, VSVG and bald controls.</i> 43	
<i>Figure 10: Relationship between RLU on X-axis and dilution on Y-axis at 60-hr post-titration of 3<sup>rd</sup> generation of pseudotype SARS-CoV-2-WT, VSVG and bald controls.</i> .44	
<i>Figure 11: HEK293T cell 24-hr post transfection with 2<sup>nd</sup> generation (left) and 3<sup>rd</sup> generation (right) plasmids.</i> .....	47
<i>Figure 12: HEK-Blue™ hACE2 cell 60-hr post titration using 2<sup>nd</sup> generation of SARS-CoV-2 detected GFP signal (green) and counted by CTL-Immunospot® S6 Ultimate.</i> .....	47
<i>Figure 13: HEK-Blue™ hACE2 cell 60-hr post titration using 3<sup>rd</sup> generation of SARS-CoV-2 detected GFP signal (green) and counted by CTL-Immunospot® S6 Ultimate.</i> .....	48

Figure 14: The 96-well plate configuration of SARS-CoV-2 WT 2 <sup>nd</sup> generation neutralization test. GFP signal (green) in HEK-Blue™ hACE2 was detected and counted by CTL-Immunospot® S6 Ultimate.....	50
Figure 15: Demonstrates the comparison of results between Accuset™ Seracare panel for CMIA (Abbott ARCHITECT SARS-CoV-2 IgG) (A) and PVNT <sub>50</sub> (B). .....	52
Figure 16: Correlation of PVNT <sub>50</sub> and neutralizing antibody concentration after validated against the standardized serum panel. ....	54
Figure 17: Passing-bablok regression analysis of log VNT and log PVNT (A), Bland-Altman analysis for mean difference of log VNT and log PVNT (B). .....	55
Figure 18: Passing-bablok regression of log PVNT and log PVNT-NSTDA (IU/mL) (A) and Bland-Altman analysis of log PVNT and log PVNT-NSTDA (IU/mL) (B). .....	57
Figure 19: Passing-bablok regression analysis of log PVNT (IU/mL) and log ELISA (BAU/mL) (A) and, Bland-Altman analysis for mean difference of log PVNT (IU/mL) and log ELISA (BAU/mL) (B). .....	58
Figure 20: Passing-bablok regression analysis of log PVNT (IU/mL) and sVNT.....	59
Figure 21: Restriction digestion products in 1% agarose gel electrophoresis .....	61
Figure 22: Immunofluorescence staining SARS-CoV-2 S protein expression in HEK293T cells. ....	62
Figure 23: HEK293T cell 24-hr post transfection with 2 <sup>nd</sup> generation plasmids.....	64

## LIST OF ABBREVIATIONS

µg	=	microgram
µL	=	microliter
ACE2	=	angiotensin converting enzyme 2
bp	=	base pair
BSL	=	biosafety level
CC	=	cell control
CMIA	=	chemiluminescent microparticle immunoassay
DNA	=	deoxyribonucleotide
E	=	envelope
EC	=	extrafollicular
ELISA	=	enzyme-linked immunosorbent assay
FBS	=	fetal bovine serum
FCS	=	furin cleavage site
FITC	=	fluorescein isothiocyanate
G	=	glycoprotein
GC	=	germinal center
GFP	=	green fluorescent protein
gRNA	=	genomic ribonucleic acid
hr	=	hour
HRP	=	horseradish peroxidase
IgA	=	immunoglobulin A
IgG	=	immunoglobulin G
IgM	=	immunoglobulin M
IL	=	interleukin
IU	=	international unit
K	=	Kilo
Kb	=	Kilo base
M	=	membrane

mAb	=	monoclonal antibody
MERS-CoV	=	Middle East respiratory syndrome coronavirus
mg	=	milligram
MHC	=	major histocompatibility complex
mL	=	milliliter
MN	=	microneutralization
N	=	nucleocapsid
NAb	=	neutralizing antibody
NK	=	natural killer
NLRs	=	nucleotide-binding oligomerization domain like receptors
Nsp	=	non structural protein
°C	=	degree celcius
PAb	=	polyclonal antibody
PAMPs	=	pathogen-associated molecular patterns
PBS	=	phosphate buffer saline
PEI	=	polyethyleneimine
PRRs	=	pattern recognition receptors
PVNT	=	pseudotype neutralization test
RBD	=	receptor binding domain
RdRp	=	RNA-dependent RNA polymerase
RDT	=	rapid diagnostic test
RLU	=	relative light unit
RNA	=	ribonucleic acid
rpm	=	Round per minute
S	=	Spike
SARS-CoV	=	Severe acute respiratory syndrome coronavirus
TLRs	=	Toll-like receptors
VC	=	Virus control

VNT	=	Virus neutralization test
VSV	=	Vesicular stomatitis virus
WHO	=	World health organization
WT	=	Wild type



## CHAPTER I

### INTRODUCTION

In late December 2019, several health organizations in Wuhan, Hubei Province, China, reported clusters of patients with pneumonia of uncertain cause. The symptoms ranged from fever, cough, chest pain to dyspnea and bilateral lung infiltration in severe cases. The sign of viral pneumonia was similar to the previous reports in individual with Severe acute respiratory syndrome coronavirus (SARS-CoV) and Middle East respiratory syndrome coronavirus (MERS-CoV) infections [1-3]. Independent teams of Chinese scientists attempted to identify the causative agent of this emerging illness using metagenomic RNA sequencing and virus isolation from bronchoalveolar lavage samples collected from patients with severe pneumonia. The results revealed a novel virus was belong to the *Betacoronavirus* genus of the *Coronaviridae* family [1, 3]. The disease continued to spread throughout China and worldwide. In February 2020, this novel virus was named “Severe Acute Respiratory Syndrome Coronavirus 2 or SARS-CoV-2” by the International Committee on Virus Taxonomy (ICTV) , and the illness caused by this virus was called “Coronavirus disease 2019 (COVID-19)” by the World Health Organization[4].

The cumulative number of confirmed cases has exhibited a consistent upward trend since its initial detection in December 2019, owing to the ongoing mutation of viruses. Up until the present month of September 2023, the number of confirmed infections has exceeded 770 million, with a confirmed mortality of over 6 million. The first notable mutation was identified among the SARS-CoV-2 virus in the early of April 2020. This mutation, known as D614G, is a non-synonymous mutation that leads to the substitution of aspartic acid with glycine at position 614 of the virus's spike protein [5, 6]. Over the course of time, this substitution greatly enhances SARS-CoV-2 transmissibility and fitness [5-7]. Following the advent of D614G substitution, multiple distinct lineages with unique mutations occurred continuously, the emergence of the Alpha (B.1.1.7), characterized by an extensive number of

genetic alterations, took place in the United Kingdom (UK) in December, 2020. Simultaneously, two more variants, namely Beta (B.1.351) and Gamma (P.1), arose autonomously and resulted in a significant increase in the number of new cases in South Africa and Brazil, respectively. In January 2021, the city of Manaus in Brazil had a reemergence of the COVID-19 virus, primarily attributable to the appearance of the Gamma variant. This resurgence occurred despite the region's already high seroprevalence resulting from the initial wave of the epidemic. In April 2021, India saw its fourth wave of the SARS-CoV-2 pandemic, characterized by the Delta (B.1.617.2) variant. This wave emerged even after three previous waves and coincided with a seroprevalence of approximately 50%. The Delta variant subsequently disseminated worldwide, replacing other variants in other countries. In early November 2021, another variant known as Omicron (B.1.1.529) had emerged in Botswana, South Africa. Subsequently, South Africa noticed a notable escalation in the number of cases, with a daily increase from 280 to 800 cases. This surge has been characterized by fast transmission and the displacement of the Delta variant. Consequently, the Omicron variant has emerged as the dominant strain both in South Africa and worldwide. The World Health Organization (WHO) gave a definition for the variants of concern (VOCs) as a variant with transmission benefits when compared to its predecessors. Each VOC showed transmission advantages over preceding variants and became dominant, either regionally in the cases of Alpha, Beta, Gamma, Delta and the many Omicron sublineages (B.1.1.529/BA sublineages, such as BA.1, BA.2 and BA.5) [8, 9].

After infection, the host immune system instantly detects the presence of the whole virus or its surface epitopes, thereby triggering either the innate or adaptive immune response. The humoral immune response against SARS-CoV-2 has been observed to have similarities to the response against previous illnesses caused by coronaviruses. This response is characterized by the synthesis of immunoglobulins G (IgG) and M (IgM). During the initial stages of SARS-CoV infection, B cells initiate an early immune response targeting the N protein. Antibodies specific to the S protein,

on the other hand, become detectable approximately 4-8 days after the start of clinical symptoms. SARS-CoV-specific immunoglobulin A (IgA), IgG, and IgM antibodies were observed to be present in infected patients at various time intervals following the manifestation of symptoms. A prolonged presence of IgG was seen over an extended duration, while IgM levels exhibited a drop after a three-month period [10, 11]. Specific antibody tests can be used as a helpful tool for diagnosis for those who have not been able to detect the presence of the SARS-CoV-2 virus by molecular or antigen-based assays. This includes individuals experiencing persistent symptoms of acute infection beyond the third week or those exhibiting post-acute sequelae of COVID-19. Nevertheless, as the duration of infection increases, the probability of antibody tests detecting an immunological response to the infection also increases. These tests have shown satisfactory performance in identifying past infections for the purpose of sero-epidemiological studies.

There are three major important aspects of serological testing of SARS-CoV-2. Firstly, it is crucial for evaluating the response potential vaccinations and the development of more universally efficacious ones. Quantifying neutralizing antibody titers can serve as an indicator of protection against the original SARS-CoV-2 virus and its variants. Additionally, examining the specific epitopes of neutralizing antibodies can be valuable in identifying crucial antigenic regions of the SARS-CoV-2 virus, which can aid in the development of effective vaccines [12, 13]. Secondly, understanding the humoral response in various patient populations is essential for effective disease screening and provide insights into disease severity [14-16]. Last but not least, the application and utilization of convalescent plasma therapy and particular neutralizing monoclonal antibodies (mAbs), whether they are synthetic or produced from patient B cell clones, has shown promise as a viable therapeutic treatments for patients suffering from severe disease [17].

Recently, several platforms for antibody measurement have been developed such as RBD or S1-specific total IgG [18, 19]. A surrogate viral neutralization assay (sVNT), employing competitive ELISA assay to facilitate the ease of antibody measurement, was also developed [20-22]. Neutralizing antibody (Nab) measurement using live-virus neutralization (VNT) assay is accepted as the gold standard in

depicting the functional antibody level after natural infection and vaccination[22-24]. Although the VNT using live virus could provide an important information about the neutralizing capacity of the induced antibody *in vitro*, the test procedure required a high level of containment and well-trained personnel. As SARS-CoV-2 is a highly contagious virus and could induce a significant pathogenesis especially in individuals who haven't been vaccinated or have some underlying health conditions, VNT was limited to perform in biosafety level (BSL)-3 facility. This limitation could lead to the difficulties in the measurement of NAb levels. An alternative method to overcome the limitation of VNT was then required in order to reduce the risk of SARS CoV-2 exposure and also to maximize the test throughput.

In this study, we aim to develop a SARS-CoV-2 pseudotype virus using lentiviral vector system to express SARS-CoV-2 spike protein and use it as a target virus in a neutralization assay. The major advantage of using SARS-CoV-2 pseudotype is the lower safety concern as it is replicative incompetent and undergoes as a single round of infection after entering the target cells. Thus, the test procedure can be performed in BSL-2 facility. Genetic stability concern of live virus uses in VNT, especially for a high passage cultured virus, are also minimized when using pseudotype neutralization test (PVNT) platform. Moreover, by employing molecular genetics approaches, new viral variants can be rapidly constructed in response to the emergence of viral mutations [11].

Hence, in this study, we developed a SARS-CoV-2 pseudotype expressing spike protein and use as a target virus in a neutralization assay. The test procedures were developed and optimized using two reporter assays, green fluorescent protein (GFP) and luciferase. The assay was evaluated for its sensitivity, specificity and correlation with VNT using both SARS-CoV-2 infected human sera and ChulaCoV-19 immunized samples. Additionally, the results were also compared with those obtained from different methods, including enzyme-linked immunosorbent assay (ELISA), sVNT and PVNT (performed by different laboratory). The developed PVNT

procedures will be further used as a tool for assessing SARS-CoV-2 neutralizing antibody level in both SARS-CoV-2 infection and vaccination individuals.



## CHAPTER II

### HYPOTHESIS AND OBJECTIVE

#### Research question

1. Does the in-house SARS-CoV-2 pseudotype-based neutralization test correlate with live SARS-CoV-2 viral neutralization test?

#### Hypothesis

1. The SARS-CoV-2 pseudotype-based neutralization test correlates well with live SARS-CoV-2 viral neutralization test.

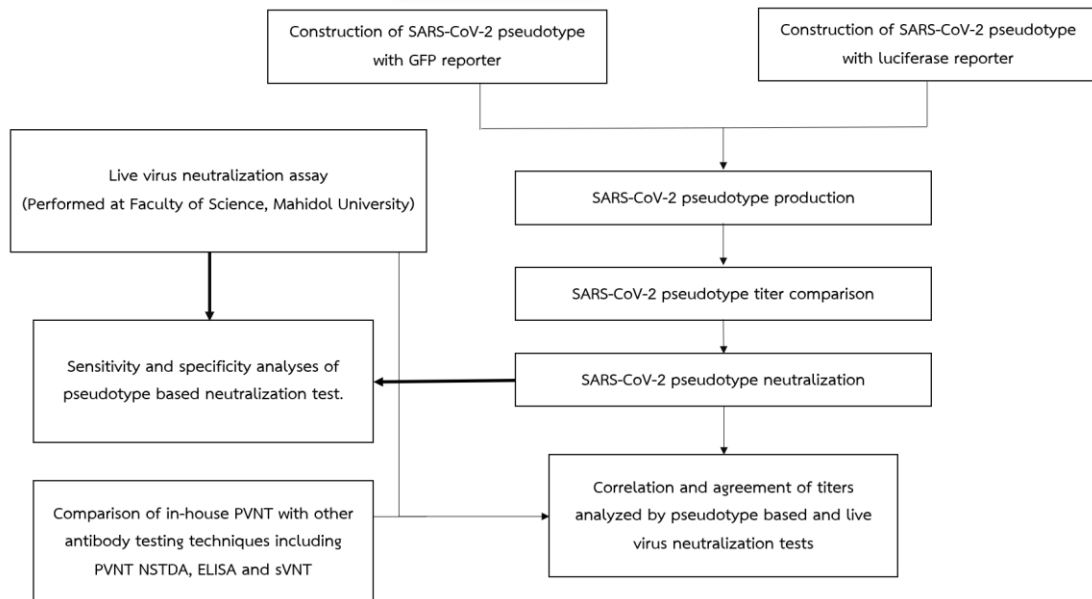
#### Objective

1. To produce and optimize the in-house SARS-CoV-2 pseudotype using lentiviral vector harboring either GFP or luciferase reporter.
2. To determine the analytical sensitivity, specificity and correlation of the in-house SARS-CoV-2 pseudotype-based neutralization test and live SARS-CoV-2 neutralization test (VNT).

#### Expected outcomes

1. Pseudotype SARS-CoV-2 serum neutralization assay has high sensitivity and specificity.
2. Pseudotype SARS-CoV-2 serum neutralization assay shows strong correlation, agreement and low bias when compare with SARS-CoV-2 live viral neutralization assay (VNT).

## Conceptual frameworks



## CHAPTER III

### LITERATURE REVIEW

#### SARS-CoV-2 virology

SARS-CoV-2 is an enveloped spherical virus containing positive single strand RNA belongs to *Coronaviridae* family, *Betacoronavirus* genus. SARS-CoV-2 genome encodes 4 structural proteins including spike (S) that binds to the host cell ACE2 receptor and mediates fusion and entry. Membrane (M) protein is essential for the incorporation of viral components during assembly while envelope (E) forms an ion channel and participates in viral assembly. Nucleocapsid (N) is associated with viral genome and downregulates host immune response. Sixteen nonstructural proteins (NSPs) 1-16 that are the enzymes that essential for viral replication, maturation, and evasion of the host immune responses.

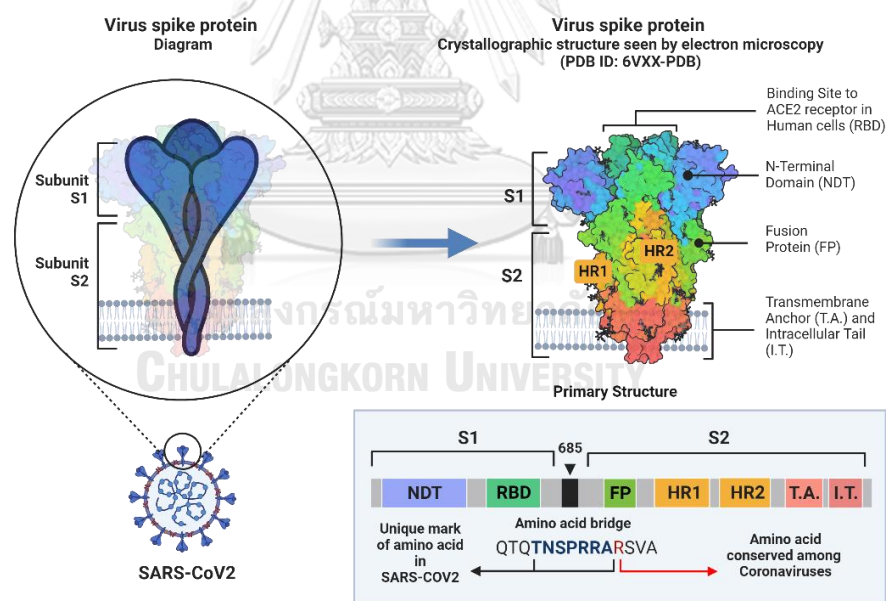


Figure 1: The details of SARS-CoV-2 Spike Glycoprotein. (Reprinted from “An In-depth Look into the Structure of the SARS-CoV-2 Spike Glycoprotein”, by BioRender.com, accessed on 20 October 2023).

In particular, the receptor angiotensin converting enzyme 2 (ACE2), to which the SARS-CoV-2 spike (S) glycoprotein binds, is essential for SARS-CoV-2 entry into the cell (**figure 1**). The two components of the fusogenic spike protein, S1 and S2, mediate the cell membrane fusion and attachment, respectively. To prime its membrane fusion activity, the spike protein must be cleaved by cellular protease like transmembrane serine protease. To get entry into a host cell, the spike protein of the virus interacts with the ACE2, a cellular surface protein. Additionally, the spike protein undergoes cleavage by cellular proteases, including transmembrane serine protease 2 (TMPRSS2), which activates its ability to fuse with the host cell's membrane [25].

The genomic RNA (gRNA) is modified with a 5' cap and a 3' polyadenylation (polyA) tail. Upon release from the viral particle, the gRNA recruits ribosomes from the host cell and undergoes translation to produce two replicase polyproteins, pp1a and pp1ab. The NSP3 and NSP5 have protease activity that are responsible for cleaving pp1a and pp1ab into 16 non-structural proteins. These proteins then come together to form replication-transcription complexes (RTCs). The process of viral RNA synthesis takes place within double-membrane vesicles, which are virus-induced membranous replication organelles. The RTCs generate novel gRNAs and a collection of subgenomic mRNAs (sg-mRNAs) that encompass open reading frames (ORFs) 2-9b. These ORFs are responsible for encoding various proteins such as the structural S, M, E, and N proteins, as well as several auxiliary proteins. The recently generated gRNAs have the potential to undergo translation, resulting in the production of supplementary non-structural proteins. They can also function as a template for subsequent RNA synthesis or be encapsidated within newly formed virions. The process of SARS-CoV-2 assembly initiates by the encapsidation of genomic RNAs (gRNAs) with N proteins, resulting in the formation of N structures. These structures then bud into the endoplasmic reticulum-Golgi intermediate compartment (ERGIC),

where they acquire a lipid bilayer that incorporates the viral S, M, and E proteins as shown in **figure 2** [26, 27].

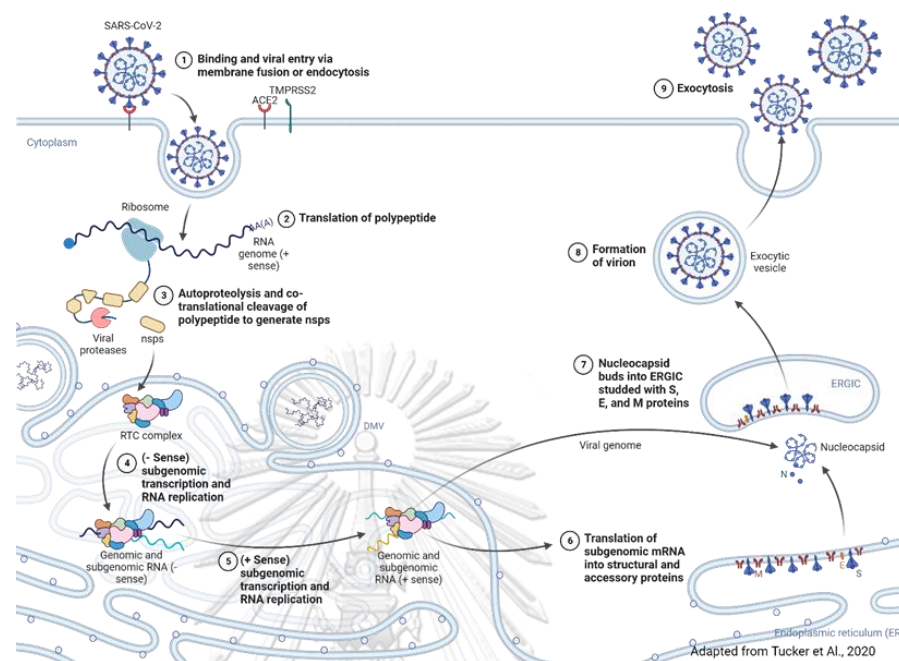


Figure 2: SARS-CoV-2 viral entry and replication cycle. (Adapted from Tucker et Al., 2020, by BioRender.com, accessed on 20 October 2023).

## Immune responses against SARS-CoV-2.

### Innate immunity

The infection caused by SARS-CoV-2 and subsequent damage to lung cells elicits a localized immune responses. The innate immune system such as macrophages, monocytes, dendritic cells, neutrophils, and innate lymphoid cells (ILCs) like natural killer (NK) cells, possess a repertoire of pattern recognition receptors (PRRs). These receptors enable the recognition of pathogen-associated molecular patterns (PAMPs) or damage-associated molecular patterns (DAMPs), thereby initiating inflammatory signaling pathways and immune responses [25, 26]. Multiple pattern recognition receptors (PRRs), specifically Toll-like receptors (TLRs), retinoic acid-inducible gene I-like receptors (RLRs), nucleotide-binding oligomerization domain-like receptors (NLRs), and inflammasomes, have demonstrated the ability to initiate their respective signaling cascades upon encountering SARS-CoV-2. The TLR1,

TLR2, TLR4, and TLR6 can initiate signaling via MyD88, resulting in the activation of NF- $\kappa$ B and MAPK signaling pathways [27, 28]. This activation subsequently leads to the transcription of genes that encode pro-inflammatory cytokines and other sensors. The TLR3 and TLR4 can initiate signaling via the Toll/interleukin-1 receptor (TIR) domain-containing adaptor inducing interferon- $\beta$  (TRIF) pathway [27, 28]. Signaling through RIG-I, MDA5 and STING also activates IRF3 and type I and type III IFN production [29], cytokines (Interleukin (IL)-1, IL-18, and IL-6), and chemokines (CCL-2 and CCL-7). Then, adaptive immune responses are triggered [25, 30, 31].

## Adaptive immunity

### T cell response

Following infection with SARS-CoV-2, T cells exhibit recognition of viral proteins in conjunction with Major Histocompatibility Complex (MHC) classes I and II molecules that are presented on the cellular surface. As a result, CD8+ cytotoxic T lymphocytes, which recognize MHC-class I molecules bound to viral peptides, selectively target cells undergoing viral replication [31]. Activated CD4+ T cells undergo a significant amount of cell division and differentiation, resulting in the emergence of diverse subsets of effector T cells [32]. The most extensively studied subsets among them are T helper 1 ( $T_H1$ ) and  $T_H2$  cells, distinguished by their secretion of interferon- $\gamma$  (IFN- $\gamma$ ) and IL-4 respectively. Follicular helper T ( $T_{FH}$ ) cells, a type of specialized B cell helpers, as well as the pro-inflammatory  $T_H17$  cell subset, are generated alongside regulatory T ( $T_{Reg}$ ) cells. The presence of  $T_{Reg}$  cells is crucial in preventing excessive immune responses and the resulting immunopathology [33].

There exists a strong correlation between the size of CD4+ and CD8+ T cell responses and the majority of proteins. The T cell responses specific to Spike protein are mostly dominated by CD4+ T cells and are expected to facilitate the production of antibodies. In particular, the presence of  $T_{FH}$  cells is associated with the development of humoral immunity during the memory phase [34-36]. Evidence now indicates that T cell responses specific to SARS-CoV-2 play a crucial role in eliminating the virus, potentially preventing infection even in the absence of

seroconversion. These T cell responses also contribute to the development of strong immune memory and facilitate the identification of viral components [34].

### **Antibody response**

The generation of antibodies plays a crucial role in the adaptive immune response to viral infection or vaccination. The humoral immune response to viral infection or vaccinations can be broadly categorized into two phases based on the predominant isotypes and profiles of somatic hypermutations observed in the resultant antibodies. During the extrafollicular (EF) phase, B cells undergo activation and promptly differentiate into plasma cells in localized areas outside of the follicle shortly after infection. These plasma cells generate antibodies that exhibit limited somatic hypermutations. Nevertheless, these antibodies can still possess reasonably high affinities and effectively neutralize the virus. The EF plasma cells observed in this study have a predominant expression of the IgM isotype subsequent to protein-antigen immunization. However, it is noteworthy that these cells have the potential to undergo switching to the IgG or IgA isotypes, particularly in the context of viral infections. In both scenarios, it is widely believed that EF plasma cells exhibit a relatively limited lifespan. During the germinal center (GC) phase, which typically spans several days to a week but can persist for months, B cells that are specific to the antigen undergo somatic hypermutation and affinity-based selection. This process leads to the generation of plasma cells that are predominantly isotype-switched and possess high affinity. These plasma cells establish a durable population that is primarily localized in the bone marrow. Both the EF and GC responses generate antigen-specific memory B cells that have the potential to endure for an extended period of time following the resolution of original infection[37].

Serological tests rely on the presence of IgM and IgG antibodies to facilitate the immune response and monitor disease progression. IgG is often the most abundant antibody in the blood and has an important role in the later stages of SARS-CoV-2 infection and in supporting the establishment of long-term immune

memory. Plasma, serum, or whole blood samples are commonly employed in these analyses. Serological analysis holds significant potential in public health practice, as it enables the swift identification of cases and the tracking of sequential events, such as identifying individuals exposed to a virus and determining high-risk groups [38].

In addition, serological assays play a crucial role in assessing the immune response to SARS-CoV-2. The majority of serological kits, including as enzyme-linked immunosorbent assays (ELISA), chemiluminescence immunoassays (CLIA), and rapid diagnostic tests (RDT), are utilized to quantify the interaction between antibodies and the spike protein of SARS-CoV-2 [39-41]. The tests in question can not effectively measure the quantitative neutralizing activity that occurs after an individual has been infected with SARS-CoV-2, as not all antibodies that bind to the spike protein are capable of inhibiting viral infection, often known as neutralization. The viral neutralization assay is widely regarded as the definitive method for quantifying neutralizing antibodies. The following are the methodologies employed for the quantification and evaluation of antibody responses.

#### **ELISA technique**

ELISA is a widely used analytical technique that employs a solid substrate for the detection and quantification of biomolecules, particularly proteins. The antigens or antibodies were immobilized on a plastic plate. Subsequently, the molecules of interest were introduced and caught by the mounted antigens, or antibodies. The trapped molecules were then treated with secondary or tertiary antibodies that were conjugated with an enzyme. Following this, the unbound conjugates were washed away, and a substrate was added to facilitate the detection of the biomolecules [42].

ELISA is extensively employed for the serological diagnosis of COVID-19, making it the predominant method in use [12]. The fundamental idea underlying this method is the application of a coating to viral proteins, specifically the N and S proteins. The S protein subunit (S1) or RBD was immobilized on a solid support, facilitating its interaction with serum antibodies. The detection process involved the introduction of a secondary antibody, known as enzyme-linked antibodies, which

facilitated the occurrence of a chromogenic reaction. The previous study aimed to assess the analytical performance of two ELISA assays in blood samples by examining the presence of antibodies targeting the SARS-CoV-2 S protein or its S1/S2 subunit. The findings of the study indicated that the full-length S protein had the highest reactivity with IgG antibodies, whilst the S1 protein demonstrated the greatest level of specificity [41, 43, 44]. James, J et al. reported that ELISA required shorter time period of testing than virus neutralization test and useful for diagnosis in asymptomatic patients [45]. Nevertheless, the issue of cross-reactivity to comparable antigens is a substantial challenge for serological testing. The antigens present in the ELISA assay may elicit a reaction from antibodies targeting other coronaviruses such as HKU1, 229E, OC43, and NL63 [16, 46]. Despite the persisting hurdles, the utilization of serological testing through ELISA offers notable benefits as a surveillance technique in the management of the current epidemic and the possible resurgence of coronavirus and other emerging viruses [47].

#### **sVNT technique**

The sVNT method is dependent on the presence of serum antibodies that are specific to the RBD of the SARS-CoV-2 virus. These antibodies work by inhibiting the specific interaction between the recombinant RBD of the virus and the recombinant ACE2 protein that is coated on 96-well plates. Moreover, due to the utilization of a singular pre-established dilution, the assay has the potential to yield a substantial increase in sample throughput [23, 48]. Nevertheless, the determination of the positive titer endpoint is not investigated in this particular single dilution format.

Mouna, L. et al. conducted an assessment of the analytical and clinical performances of a sVNT in comparison to conventional neutralization tests VNTs and anti-SeCLIA assays, the findings of our study suggest that sVNTs exhibited a notable level of selectivity and did not demonstrate any instances of cross-reactivity [49].

### Live-virus neutralization (VNT) technique

SARS-CoV-2 VNT is the gold standard for NAb titer assessment [50]. The evaluation of viral infection is frequently conducted by the assessment of virus-induced cytopathic effect (CPE) [51], which is often complemented by a viral neutralization experiment. This assay aims to detect the presence of antibodies that possess the ability to impede viral infection. Due to its limited ability to identify all antigen-antibody interactions. The process involves the identification of antibodies that possess the ability to inhibit viral replication [52].

Live SARS-CoV-2 neutralization assays have the advantage of not requiring adaptation to newly emerging variants, hence minimizing the response time to novel viral strains. Nevertheless, a significant limitation of conventional live SARS-CoV-2 neutralization experiments is to the necessary duration of incubation, which typically spans from 3 to 5 days. Hence, these assays are not conducive to expedited and extensive screening [50]. Experiments with SARS-CoV-2 necessitate adherence to certain safety protocols, rendering them infeasible in the majority of research and clinical institutions. Consequently, the availability of testing in BSL-3 laboratories is limited [53].

### PVNT technique

Pseudotype is a recombinant virus composing core of one low pathogenic or modified virus, the envelope protein genes responsible for infecting host cells are substituted with reporter genes, including as GFP and luciferase genes [54], which enable the detection of viral infection *in vitro* while another highly pathogenic glycoprotein envelope virus [55]. *In vitro*, a pseudotype is formed by assembling the core genome and envelope proteins obtained from two distinct viruses and secrete into the supernatant of a cell culture. To infect the target cells, the supernatant is then collected and used as a target virus in this approach. Pseudotype particles could infect cells that are susceptible to their specific receptor binding properties. However, their replication is limited to a single round within the host cells that have been successfully infected, therefore pseudotypes can be effectively managed within

a BSL-2 laboratory setting and generally exhibit greater experimental manipulability compared to live viruses [56].

During the onset of the SARS-CoV-2 outbreak, it became imperative to conduct research on live viral specimens within BSL-3 facilities. The utilization of the pseudotype system has significantly advanced the pertinent investigation of SARS-CoV-2, thereby assuming a crucial function in elucidating the mechanisms underlying virus binding and recognition with cellular receptors. Additionally, this system has proven instrumental in the identification of specific small-molecular drugs, as well as the assessment of monoclonal antibodies and vaccine titers [57]. Furthermore, the measurement of neutralizing titers of antibodies and sera using pseudotype shown a strong correlation with the measurement obtained using live viruses [58, 59].

### **Pseudotype systems**

#### **Human immune deficiency virus (HIV-1)-based lentiviral packaging system**

HIV-1 belongs to *retroviridae* family and *lentivirinae* subfamily. Its genome consists of two linear single stranded RNA. The HIV proviral DNA genome is generated through reverse transcription of viral RNA (**figure 3A**). It contains LTR sequences, promoter for transcription of *gag*, *pol* and *env*. The genome also codes for regulatory proteins like Tat, Rev, Nef, Vif, Vpr, and Vpu. These proteins play a crucial role in HIV replication, infectivity, cell cycle, and virus particle release, influencing the rate of virus particle production. Gag, Pol, and Env polyproteins are essential for formation of viral particle. Gag protein is associated with the formation of viral particles, packaging of viral genomic RNA. Pol protein is associated with reverse transcription and integration. Env protein responsible for binding and entry into the host cell [60, 61].

The fundamental component of the pseudotype system, which is taken from the HIV core is pNL4-3.Luc.R-E- or 1<sup>st</sup> generation packaging system (**figure 3B**). The life cycle of the vector is similar to HIV-1, allowing for encapsidation into developing pseudotypes and LTR sections containing the U3 promoter. After integration into the

host genome, *tat* facilitates the expression of the viral proteins. The reporter gene transcript—which serves as this system's output measure—and other viral mRNA can be exported nucleus via the *rev* responsive element (RRE). Transduced cells may be able to manufacture luciferase containing cores in addition to its transcribed enzyme because the HIV core genes are integrated into the same integrated construct as the reporter [60]. The packaging plasmids frequently employed in the 1st generation are pSG3 $\Delta$ env and pNL4-3 [62].

An additional approach makes use of the 2<sup>nd</sup> generation pseudotype lentiviral vector is cytomegalovirus (CMV) promoter [63], in place of LTR-based promoter (**figure 3C**). This means that while the proviral and packaging elements (LTRs, RRE) are transferred to a different plasmid containing the reporter gene. Thus, the reporter plasmid will be added to developing virions and integrated into the genome of the transduced cell. A safety component is added to transfer plasmid, the widely used firefly luciferase or GFP by deleting the 3' LTR (U3 promoter region), resulting in what are known as self-inactivating (SIN) vectors [64]. The packaging plasmid and transfer plasmid frequently employed in this system are psPAX2 and pLenti-GFP [68, 69]

By dividing the viral genome into distinct plasmids, 3<sup>rd</sup> generation lentiviral vectors increased safety even further and increased the likelihood of recombinant virus formation. The vector used in the 3<sup>rd</sup> generation system was created from three distinct plasmids that each had the required viral sequences for packaging since the *gag* and *pol* genes were encoded on a different plasmid than the *rev* and *tat* genes (**figure 3D**) [63, 65].

Currently, the internal ribosome entry site (IRES) element serves as a supplementary location for the recruitment of ribosomes, resulting in the concurrent synthesis of two proteins from a single mRNA molecule. This methodology entails employing a solitary promoter to enable the production of two reporter genes that are linked via an IRES sequence. The plasmid is utilized for the purpose of producing lentiviral vectors, which are capable of encoding an IRES element. This IRES element

facilitates the expression of both luciferase and GFP (see Appendix G). Which IRES plasmids system are compatible with 2<sup>nd</sup> and 3<sup>rd</sup> generation lentiviral production.

The HIV genome parts are assembled with interest envelope plasmid into incomplete and secure HIV pseudotype particles through transfection of the coupled plasmids into HEK293T cells, and the viral particles are then released into the extracellular space by exocytosis. The pseudotype particles will take advantage of the chance to incorporate the heterologously produced envelope proteins into the viral membrane, which is derived from cell membrane, during the secretion phase. Characteristic comparison of 3 generations of pseudotype was summarized in **table 1**.

*Table 1: Characteristic comparison of three generations of pseudotype.*

Features	1 <sup>st</sup> generation	2 <sup>nd</sup> generation	3 <sup>rd</sup> generation
Number of plasmids use for pseudotype production	2	3	5
Packaging plasmid(s)	pNL4-3.Luc.R-E-	psPAX2	HDM-Hgpm2, HDM-tat1b, pRC-CMV-Rev1b
Transfer plasmid		pCCGW	pHAGE-CMV-Luc2- IRES-ZsGreen- W
Envelope plasmid (for SARS-CoV-2)	pMD2.G or pHDM SARS-CoV-S	pMD2.G or pHDM SARS-CoV-S	pMD2.G or pHDM SARS-CoV-S
<i>Tat</i> and <i>rev</i> genes	encode in pNL4-3.Luc.R-E-	encode in psPAX2	<i>tat</i> encodes in HDM-tat1b and <i>rev</i> encode in pRC-CMV-Rev1b
<i>Gag</i> and <i>pol</i> genes	encode in pNL4-3.Luc.R-E-	encode in psPAX2	encode in HDM-Hgpm2

Features	1 <sup>st</sup> generation	2 <sup>nd</sup> generation	3 <sup>rd</sup> generation
Regulatory genes ( <i>vif</i> , <i>vpr</i> , <i>vpu</i> , <i>nef</i> )	✓	Only <i>vif</i> present	✗
3' LTR deletion	✗	✓	✓
Reporter system	Luciferase	GFP	GFP and luciferase



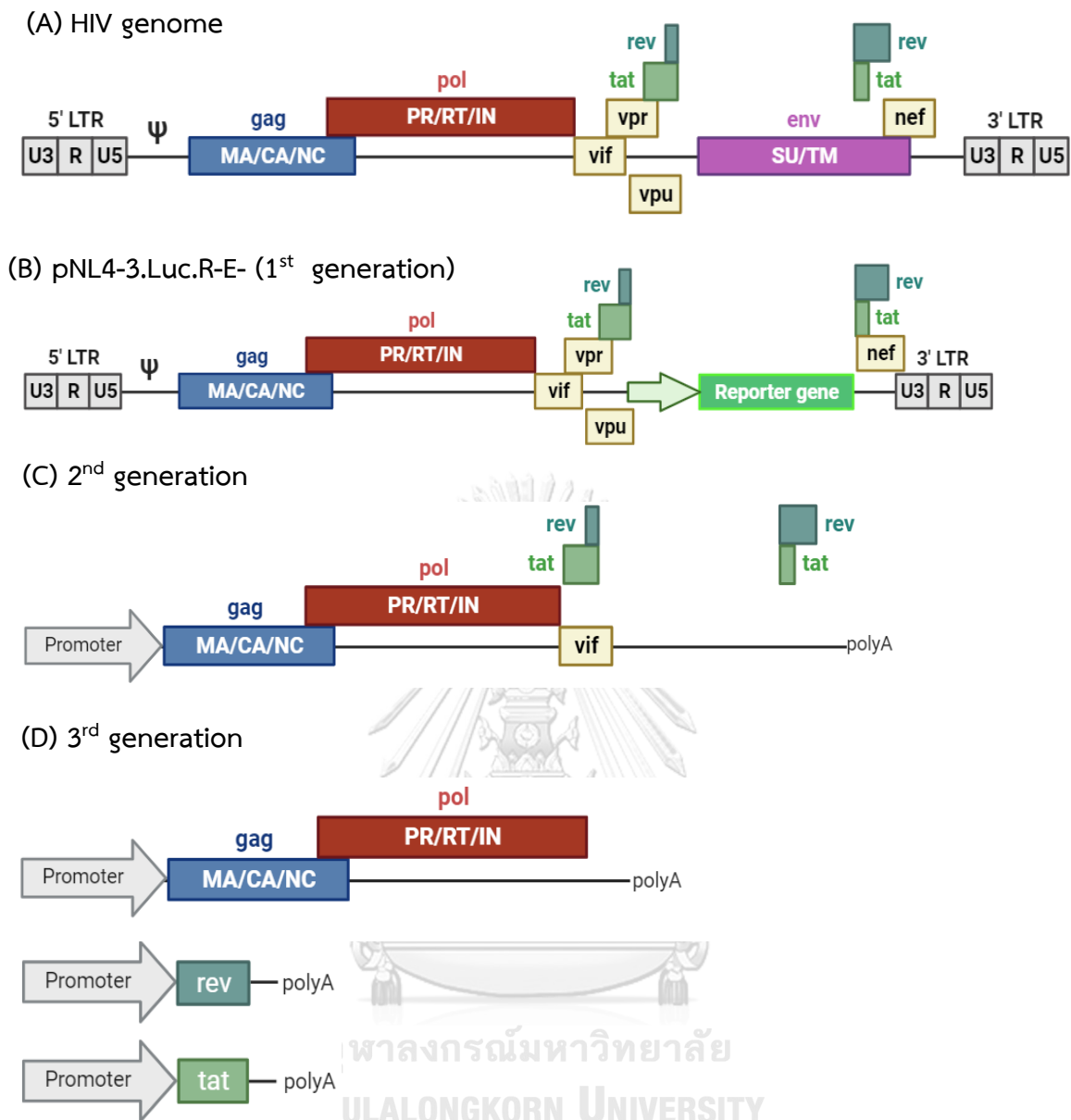


Figure 3: Schematic representation of HIV and HIV lentiviral system. HIV genome (A) pNL4-3.Luc.R-E- (B) (1<sup>st</sup> generation), 2<sup>nd</sup> generation (C) and 3<sup>rd</sup> generation (D), LTR: long terminal repeat, gag; MA: matrix, CA; capsid, NC; nucleocapsid, pol; PR: protease, RT: reverse transcriptase, IN: integrase, vif: viral infectivity factor, vpr; viral protein unique, vpu; viral protein unique, tat: trans activating proteins, rev: regulator of expression of virion proteins, env; envelope glycoproteins, nef; negative regulating factor, SU: surface, TM: transmembrane

Figure 3: (Continued)

(Adapted from Carnell GW et al., 2015 by BioRender.com, accessed on 6 November 2023)

### Vesicular stomatitis virus (VSV) packaging system

VSV is non-segmented, negative stranded RNA, bullet shaped virus belongs to the *Rhabdoviridae* family and *vesiculovirus* genus. VSV composed of five major proteins, glycoprotein (G), Matrix protein (M), nucleoprotein (N), large protein (L), and phosphoprotein (P). Recombinant VSV in which the native envelope G protein is replaced with a reporter gene, such as GFP, luciferase or secreted alkaline phosphatase [54].

In the process of generating recombinant vesicular stomatitis virus (VSV), The recombinant vesicular stomatitis virus (VSV) is engineered by substituting the natural envelope G protein with a reporter gene, such as green fluorescent protein (GFP), luciferase [66]. The first stage involves the construction of a transfer plasmid. This plasmid is designed to facilitate the transcription of the negative strand RNA of the VSV genome. The resulting transcript serves as an RNA template for the RNA-dependent RNA polymerase (RdRp) to synthesis viral RNA. The vector is co-transfected with four auxiliary vectors that express VSV N, P, G, and L proteins, respectively, into packaging cells that express phage T7 RNA polymerase. The T7 RNA polymerase enzyme facilitates the transcription of the negative RNA VSV- $\Delta$ G genome by interacting with the T7 promoter located on the transfer plasmid. The assembly and release of recombinant vesicular stomatitis virus (VSV) occur within packaging cells. The cell supernatant is collected in order to acquire G-deficient VSV virus. Following this, we employ it to re-infect with packaging cells that express G glycoprotein in order to get VSV- $\Delta$ G/G\* stock with a high yield. Additionally, we can utilize VSV- $\Delta$ G virion coated with G protein to infect cells that express different viral glycoproteins, so generating the desired pseudo virus. However, the G protein present in the initial viral particles has the potential to undergo recycling on the newly generated particles, hence potentially leading to a significant increase in background noise levels [55, 67].

Based on the literature, evaluation of two prevalent reporter systems, namely GFP and luciferase, were employed for pseudotype measurement and neutralization. A summary of these systems is included in **table 2** [68-72].

*Table 2: Characteristic comparison of reporter systems.*

Item	GFP reporter system	Luciferase reporter system
Signal detection method	Photoluminescence photon emission-based	Enzymatic chemical reaction
Instrument required	Fluorescence microscopy	Luminometer
Detection acquisition time	Immediately after light exposure	3 minutes of reagent incubation
Throughput	High	High
Cost	70 THB/plate 35 THB/test sample	3,200 THB/plate 1,600 THB/test sample
Substrate/ATPs	Not required	Required
Photostable and thermostable	Higher and repeatable	Lower and non- repeatable
Sensitivity	High	Higher
Readout	GFP Spot count number	Relative light units (RLUs)

Based on 5 SARS-CoV-2 antibody testing methods described above. We summarized all of testing platform in **table 3**.

Table 3: Comparison of the SARS-CoV-2 antibody testing platform.

Testing platform	Advantages	Disadvantages	References
ELISA	<ul style="list-style-type: none"> <li>- Safe</li> <li>- Various platform available</li> <li>- High throughput</li> </ul>	<ul style="list-style-type: none"> <li>- Less correlate with neutralizing antibodies</li> <li>- Cannot provide the neutralizing activity</li> </ul>	[47, 73, 74]
sVNT	<ul style="list-style-type: none"> <li>- Does not require handling of infectious virus</li> <li>- A rapid prescreening of patient serum to identify neutralization activity</li> <li>- High throughput</li> </ul>	<ul style="list-style-type: none"> <li>- Only detect RBD-specific neutralizing antibodies</li> <li>- The samples with low neutralizing activity were underestimated.</li> </ul>	[21, 23, 75]
VNT	<ul style="list-style-type: none"> <li>- Detecting functional antibodies to a specific virus that may suggest protective immunity after vaccination or post-infection</li> </ul>	<ul style="list-style-type: none"> <li>- Need for high level biosafety containment (BSL-3)</li> <li>- Time consuming (require 4 or 5 days)</li> <li>- Labor intensive</li> <li>- Pose a risk of infection</li> <li>- Viral mutation at high passage number</li> </ul>	[55, 74, 76-78]
PVNT	<ul style="list-style-type: none"> <li>- Detecting functional antibodies to a specific virus</li> <li>- Safe, can perform in BSL-2</li> <li>- High throughput</li> </ul>	<ul style="list-style-type: none"> <li>- Time consuming (require 3 days)</li> <li>- Correct conformation structure of surface protein of the target virus is required</li> </ul>	[73-75, 77, 78]

## CHAPTER IV

### MATERIALS AND METHODS

#### Construction of recombinant plasmid expressing SARS-CoV-2 Spike protein

Synthetic gene with humanized codon optimization encoding SARS-CoV-2 spike protein (accession number MN908947.1, available from GenBank database) with 21 amino acid deletion at carboxy-terminal (see Appendix), designated as S wild-type (S-WT) was synthesized by GeneScript (Piscataway, NJ, USA). For subcloning into pHDM expression vector, the gene was flanked with restriction enzymes *EcoRI* (GAATTC) and *SalI* (GTCGAC) at 3' and 5' ends, respectively. pHDM vector contains the cytomegalovirus (CMV) promoter and bovine growth hormone (BGH) polyadenylation signal, and ampicillin resistance gene (see Appendix). The 21 amino acid deletion at carboxy-terminal was designed for eliminate ER retention motif [79].

For SARS-CoV-2 variants including Delta (B.1.617.2) and Omicron BA.4/5, S protein with 21 amino acid deletion, they were also synthesized by GeneScript (Piscataway, NJ, USA) and using the same cloning procedure as S-WT construct.

#### Plasmids

All plasmids enlisted in **table 4** were propagated in *E.coli* DH5-alpha competent cell (Invitrogen™ MAX Efficiency™, Carlsbad, USA) and grown in 50 mL Luria-Bertani (LB) broth with selective antibiotics. The transformed competent cells were incubated at 37 °C with continuously shaking at 200 round per minute (rpm) for 16 hrs. The plasmid DNAs were then harvested and extracted by using MidiPrep® extraction kit (QIAGEN, Hilden, Germany) according to manufacturer procedure. The details and function of plasmids were described in **table 4**.

Table 4: Detail of the plasmids used in the study.

Recombinant agents	Function	Source
psPAX2	Expressing lentiviral structural proteins and essential enzyme	A gift from Didier Trono (Addgene plasmid #12260)
pCCGW	Encoding the green fluorescent protein gene (GFP)	Zhang et al., PLOS Pathogens.7(5): e1002039. Doi10.1371/journal.ppat.1002039
pNL4-3.Luc.R-E-	Encoding lentiviral structural proteins and essential enzyme, encoding Firefly luciferase gene	A gift from Dr. Nathaniel Landau, Aaron Diamond AIDS Research Center, The Rockefeller University.
pHAGE-CMV-Luc2-IRES-ZsGreen-W	Encoding luciferase followed by an IRES and ZsGreen.	Obtained through BEI Resources, NR-52516
HDM-Hgpm2	Encoding HIV Gag-Pol	Obtained through BEI Resources, NR-52517
HDM-tat1b	Encoding HIV Tat	Obtained through BEI Resources, NR-52518
pRC-CMV-Rev1b	Encoding HIV Rev	Obtained through BEI Resources, NR-52519
pMD2.G	Encoding envelope glycoprotein of vesicular stomatitis virus	A gift from Didier Trono (Addgene plasmid #12259)
pUC57-SARS-CoV-2-S-WT	Encoding spike glycoprotein of SARS-CoV-2 WT with deletion the C-terminal 21 amino	Synthesize by Genscript (Genscript, Piscataway, NJ, USA)

Recombinant agents	Function	Source
	acids	
pUC57-SARS-CoV-2-S-Delta (B1.617.2)	Encoding spike glycoprotein of SARS-CoV-2 Delta (B1.617.2)	Synthesize by Genscript (Genscript, Piscataway, NJ, USA)
pUC57-SARS-CoV-2 -S-Omicron BA.4/5	Encoding spike glycoprotein of SARS-CoV-2 Omicron BA.4.5	Synthesize by Genscript (Genscript, Piscataway, NJ, USA)

All pUC57-SAR-CoV-2-S including WT, Delta (B.1.617.2) and Omicron BA.4/5 were grown in LB broth with 100 µg/mL ampicillin for 16 hrs then harvested and extracted using DNA extraction kit, Presto™ Mini plasmid Kit (Geneaid, Taiwan). Restriction endonuclease digestion with *EcoRI* (NEB, England) and *Sall* (NEB, England) was performed for both expression and insert vectors. The restriction products were analyzed on 1% agarose gel in 1X TAE buffer (see appendix). The expected size of S gene at approximately 3.8 kb was excised and purified then ligated into linearized pHDM expression plasmid using U4 DNA ligase (NEB, England). The ligation reactions were transformed into DH5 $\alpha$  competent cells and plated on LB-Ampicillin plate then incubate at 37 °C for 16 hrs. The candidate colonies were grown, harvested and extracted to confirm the recombinant plasmid (pHDM-S-WT) by restrictions endonuclease digestion.

### Cell lines

Human embryonic kidney (HEK) 293T (ATCC CRL-11268) used for viral propagation, were maintained in Dulbecco's modified Eagles's Medium (DMEM) and supplemented with 10% heat-inactivated fetal bovine serum (FBS), 2 mM (100X) L-glutamine and 10,000 units/mL of penicillin, 10,000 µg/mL of streptomycin, and 25 µg/mL of Gibco Amphotericin B (Antibiotic-Antimycotic (100X) (all reagents were from Gibco™, MD, USA).

HEK Blue™ hACE2, procured from (Invivogen, CA, USA) were maintained in DMEM and supplemented with 10% heat-inactivated FBS, 2 mM (100X) L-glutamine

(Gibco™, MD, USA), Normocin™, Zeocin® and Puromycin™ (Invivogen, CA, USA) and used as a target cells for pseudotype titration. All cells were incubated in 37 °C, 5% CO<sub>2</sub> and serially subculture twice a week.

#### **Target protein expression analysis by indirect immunofluorescent assay (IFA)**

One day before transfection HEK 293T cells were seeded into 6-well plate with cover glass at  $6 \times 10^5$  cells/well. On the next day, cells was transfected with 2 ug of pHDM-SARS-CoV-2 expression plasmids of SARS-CoV-2 Spike using PEI 6 ug (DNA:PEI, 1:3). At 24 hr post-transfection, cells were fixed using cold-acetone for 10 minutes, then incubated with primary antibody anti-S1 SARS-CoV-2 (2019-nCoV), Rabbit pAb, Antigen Affinity Purified (Cat no. 40591-T62, Sino Biological, United States) at 4 °C for 16 hrs. Cells were then washed with 1X PBS then incubated with donkey anti-rabbit IgG (Cat no. 406403) tagged with fluorescein isothiocyanate (FITC) (Biolegend, San Diego, CA, USA) and counter stained with 4', 6'-diamidino-2-phenylindole (DAPI). Stained cells were visualized under fluorescence microscope (Nikon T2s, Japan).

#### **Clinical Specimen**

Serum sample (n=128) were retrieved from serum archive of participants previously immunized with ChulaCoV-19 vaccine (NCT04566279) spanning low (20-160), medium (>160-2,560), and high (>2,560) of MN<sub>50</sub> titers analyzed by live virus neutralization [80] with at least 20 samples of each analytical range. Negative control sample were also obtained from serum archive of ChulaCoV-19 project who were screening negative for anti-SARS-CoV-2 before enrolling the trials.

Panel of naturally infected human serum with different SARS-CoV-2 specific antibody titers were procured from SeraCare Life Sciences, US. In detail, the panel composed of 11 samples of undiluted AccuSet™ Seracare SARS-CoV-2 Performance Panel (0820-0410 / Batch #10497051).

For assay standardization, another panel of SARS-CoV-2 infected sera with known international unit (IU) of neutralizing antibody titer, verified by National Institute for Biological Standard and Control (NIBSC, Hertfordshire, UK), NIBSC code 20/268, version 3.0, dated 17/12/2020 were also used.

### SARS-CoV-2-lentiviral pseudotype production

One day before transfection,  $1 \times 10^6$  cells of HEK293T were seeded into 10 mm tissue culture dishes and incubated at 37 °C with 5% CO<sub>2</sub>. After 24 hrs of incubation, the cells were transfected with 12 µg of plasmids using 36 µg of branched 25K Polyethyleneimine (PEI, Merck, Germany) at ratio of 1:3 (DNA:PEI) with each generation (**detailed in table 5-7**) and incubated for 4 hrs at 37 °C, 5% CO<sub>2</sub>. The media was then replaced with 10% DMEM. The supernatant was harvested at 48 hrs and 72 hrs post-transfection and pooled together. To remove cell debris, the supernatant was centrifuged at 2,000 rpm at 4 °C for 5 minutes and filtered through a 0.45 µm PES syringe filter (Corning, USA), aliquoted into 0.5 ml, and stored at -80 °C.

*Table 5: Plasmids concentration for 1<sup>st</sup> generation SARS-CoV-2-pseudotype production.*

Producer cell	Plasmid and component	Plasmid concentration (µg)
HEK 293T	pNL4-3.Luc.R-E-	8
	pHDM-SARS-CoV-2-S-WT	4
	Polyethyleneimine	36

Table 6: Plasmids concentration for 2<sup>nd</sup> generation SARS-CoV-2-pseudotype production.

Producer cell	Plasmid and component	Plasmid concentration (µg)
HEK 293T	pCCGW(GFP)/ pHAGE-CMV-Luc2-IRES- ZsGreen-W(Luciferase)	6
	pSPAX2	4
	pHDM-SARS-CoV-2 spike	2
	Polyethyleneimine	36

Table 7: Plasmids concentration for 3<sup>rd</sup> generation SARS-CoV-2-pseudotype production.

Producer cell	Plasmid and component	Plasmid concentration (µg)
HEK 293T	pHAGE-CMV-Luc2-IRES- ZsGreen-W	6
	pHDM-Hgpm2	1.32
	pHDM-tat1b	1.32
	pRC-CMV-Rev1b	1.32
	pHDM-SARS-CoV-2 spike	2.04
	Polyethyleneimine	36

### Pseudotype collection time optimization

Following the aforementioned procedures, the producer cell was transfected with a total of 12 µg of both 2<sup>nd</sup> and 3<sup>rd</sup> generation plasmids. The supernatant samples were obtained at 48- and 72-hr post-transfection for assessing and comparing the maximum TCID<sub>50</sub> titer in HEK Blue™ hACE2. The Spearman and Karber method was employed to facilitate further neutralization testing [81, 82].

### SARS-CoV-2-lentiviral pseudotype titer determination

The SARS-CoV-2-lentiviral pseudotype was titrated by 3-fold serially dilution on HEK Blue™ hACE2 and quadruplicated for each sample in 96 well plates (**figure 4**). The titers were compared between 2 reporting systems including (1) GFP system, (which analyzed and quantified on CTL-Immunospot® S6 Ultimate (CTL, Cleveland, OH, USA) after 60 hrs of infection or (2) luciferase reporting system which was analyzed by Thermo Scientific Varioskan® Flash (Thermo Scientific, Finland) after adding equal volume of ONE-Glo™ Luciferase substrate (Promega, Madison, USA) to culture medium. The titer was calculated using Spearman and Karber method [81, 82] and reported as TCID<sub>50</sub>. The optimizations of SARS-CoV-2 pseudotype lentiviral production with different generations were explored. The procedure that yielded the highest titer was chosen for PVNT.

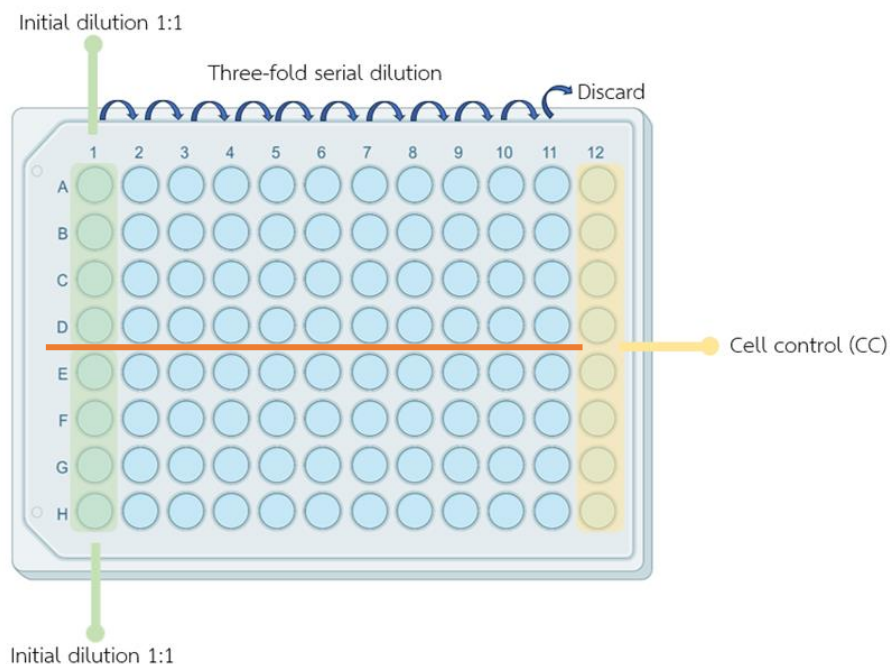


Figure 4: Plate design for pseudotype viral titration

### SARS-CoV-2-lentiviral pseudotype neutralization and statistical analysis

All serum samples were heat-inactivated at 56°C for 30 minutes and 2-fold serially diluted starting from 1:10 to 40,960 (**figure 5**). All samples were tested in duplicate. The sera were incubated with 50  $\mu$ L of 100 TCID<sub>50</sub> of the WT SARS-CoV-2 pseudotype at 37°C for 1 hr. Afterward, 50  $\mu$ L of 3x10<sup>4</sup> HEK Blue™ hACE2 cells were added into the mixture and incubated at 37 °C for 60 hrs. A dilution that yielded the 50% reduction of infection as compared to virus control wells was reported as PVNT<sub>50</sub>. For GFP reporter, the GFP spots were analyzed and counted by CTL - Immunospot® S6 ultimate (CTL, Cleveland, OH, USA). Serum samples that produced negative results at a dilution ratio of 1:10 will be designated with a PVNT<sub>50</sub> titer value of 5.

### VNT

Live virus neutralization titers were performed at a certified biosafety level 3 facility, Department of Microbiology, Faculty of Science, Mahidol University, Thailand. The procedure of MN assay was described previously [80]. In detail, 1:10 heat-inactivated immunized sera were 2-fold serially diluted in DMEM + 2% FBS. After serum dilution, 100 times of the TCID<sub>50</sub> of the SARS-CoV-2 virus isolated from a confirmed COVID-19 patient at Bamrasnaradura Infectious Diseases Institute, Nonthaburi (SARS-CoV-2/01/human/Jan2020/Thailand) is added and incubated at 37 °C for 1 hr. Serum-virus combinations are placed in 1x10<sup>4</sup> pre-seeded Vero-E6 cells. After 2 days of infection, ice-cold 1:1 methanol/acetone was added to fix and permeabilize cells for 20 min at 4 °C. Fixed cells were washed three times with PBS-T, then soak in blocking buffer (1XPBS with 2% BSA and 0.1% Tween 20) for 1 hr. SARS-CoV/SARS-CoV-2 nucleocapsid mAb (40143-R001; Sino Biological, United States) was diluted 1:5,000 in 1XPBS with 0.5% BSA and 0.1% Tween 20 and incubated for 2 h at 37°C to detect viral antigen after three PBS-T washes. Addition of 1:2,000 HRP-conjugated goat anti-rabbit polyclonal antibody (P0448; Dako, Denmark) to the plates was performed after three PBS-T washes. After 1 h incubation at 37°C, plates were washed 3 times, then 50  $\mu$ L SureBlue TMB 1 peroxidase substrate was added

(SeraCare Life Sciences, US) to each well, and incubate at room temperature for 10 min in the dark. The reaction was stop with 50  $\mu$ l 1N HCl. The absorbance was read at 450 and 620 nm using microplate reader. A 50% specific signal calculation determined a neutralizing endpoint for quadruplicate 100TCID<sub>50</sub> wells and negative control wells (CC). The average A450/620 was calculated. The endpoint titer was expressed as the reciprocal of the highest dilution of serum with average A450/620 value (duplicate wells) less than X, where  $X = [(average\ A450/620\ of\ 100TCID_{50}\ wells) - (average\ A450/620\ of\ CC\ wells)]/2 + (average\ A450/620\ of\ CC\ wells)$ . Serum samples which tested negative at a dilution of 1:10 was assigned an MN<sub>50</sub> titer of 10.

#### **Pseudotype neutralization test (performed at the National Science and Technology Development Agency (PVNT NSTDA))**

The firefly luciferase reporter was used to produce and titrate pseudotype viruses of SARS-CoV-2. Sera were heat-inactivated at 56 °C for 30 min before testing. Serum samples were incubated with  $1 \times 10^4$  RLU/mL pseudotype at 37 °C for 1 hr, diluted in DMEM with 10% FBS, and transferred to a tissue culture-treated, white opaque 96-well microplate. HEK 293T/TMPRSS2 cells ( $1 \times 10^4$  cells) were suspended in 50  $\mu$ L DMEM with 10% FBS and included in each well. A 48-hr 37 °C, 5% CO<sub>2</sub> incubation was performed. After removing supernatants, 25  $\mu$ L of Bright-Glo™ luciferase substrate (Promega, Madison, WI, USA) was added to each. The Synergy, HTX multi-mode reader (BioTek, Winooski, USA) was used to assess PVNT titer-related luciferase signals (RLU/mL) and normalize with the no-serum control response. Each serum sample's neutralizing activity was estimated using the half-maximal inhibitory dilution (ID<sub>50</sub>) [83, 84].

## sVNT

sVNT was conducted in accordance with the manufacturer's instructions (GenScript, Piscataway, New Jersey, United States of America). Briefly, diluted sera (1:10) were pre-incubated at 37 °C for 30 minutes with RBD conjugated with HRP. The mixtures were then placed on hACE2-coated plates and incubated for 15 minutes at 37 °C. After washing, 100  $\mu$ L of TMB was added to each well and incubated for 15 minutes at room temperature in the dark. Immediately after adding 50  $\mu$ L of stop solution (0.2 N sulfuric acid), the absorbance at 450 nm was measured. The percentage of inhibition was determined by comparing the OD values of the sample and the negative control [85].

## ELISA (Abbott SARS-CoV-2 IgG II Quant assay)

The SARS-CoV-2 IgG II Quant assay is a chemiluminescent microparticle immunoassay (CMIA) that operates in an automated, two-step approach (performed by HIV-NAT laboratory, AIDS Research Center, Thai Red Cross Society). It was used for quantitation of IgG antibodies targeting RBD of the S1 subunit of the spike protein of SARS-CoV-2 in human serum and plasma.

All 4 testing platforms used to compare to PVNT<sub>50</sub> described above was summarized target and signal detection method in **table 8**.

Table 8: Summary of cell or antigen target and signal detection of the different testing platforms.

Testing platform	Target	Signal detection method
VNT	Cell based VERO E6	Enzymatic chemical reaction - HRP
PVNT <sub>50</sub> NSTDA	Cell based HEK293 hACE2 TMPRSS2	Enzymatic chemical reaction - luciferase
sVNT	Protein based hACE2	Enzymatic chemical reaction - HRP
ELISA	Protein based RBD	Enzymatic chemical reaction - HRP
PVNT <sub>50</sub>	Cell based HEK Blue™ hACE2	Photoluminescence photon emission-based - GFP

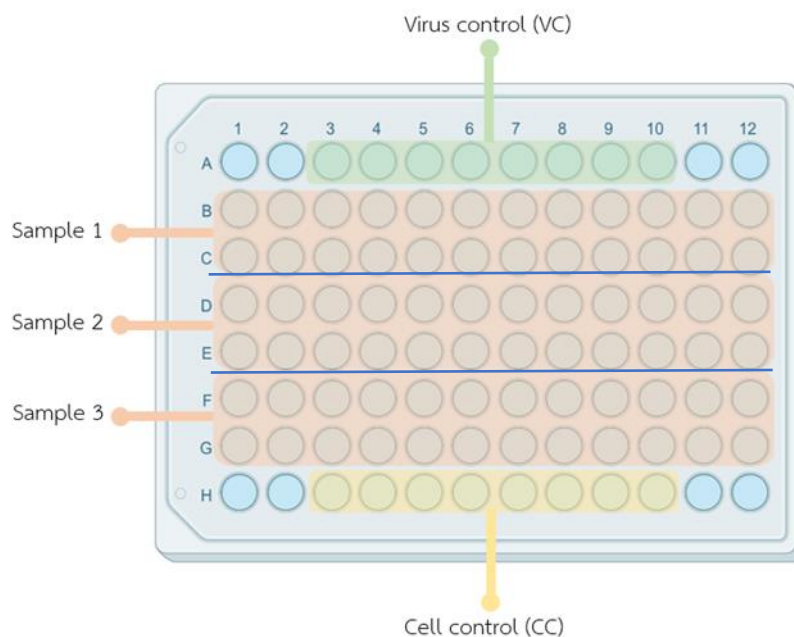


Figure 5: Plate design for pseudotype neutralization assay.

### Statistical analysis

The results obtained from the analyzers were subjected to determine the  $PVNT_{50}$  analysis using the probit analysis software SPSS (version 28, IBM, Chicago, USA).

Correlation between methods were analyzed by Passing–Bablok regression analysis. Bias and 95% limits of agreement assessments were performed using Bland–Altman plot (MedCalc, Version 22.013).

### Ethics statement

This study was approved by Institutional Biosafety Committee of the Faculty of Veterinary Science, Chulalongkorn University (IBC2131027).

## CHAPTER V

## RESULTS

## Construction of recombinant plasmid expressing SARS-CoV-2-WT Spike protein

As shown in **figure 6**, the gene encoded for the SARS-CoV-2-WT spike (S) protein was successfully subcloned into pHDM expression plasmid. It was confirmed by double digestion using restriction enzymes *SalI* and *EcoRI*. The bands at approximately 4.8 kb and 3.8 kb corresponded to pHDM expression plasmid and S gene, respectively.

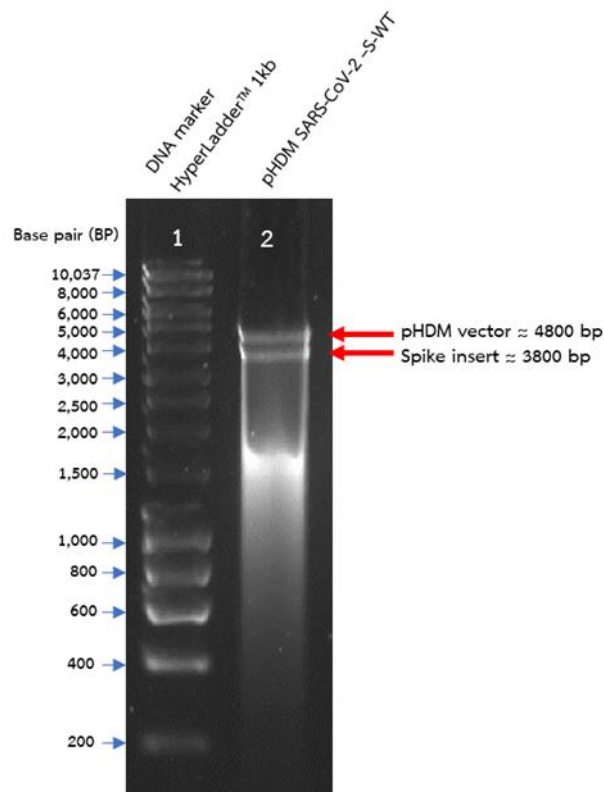
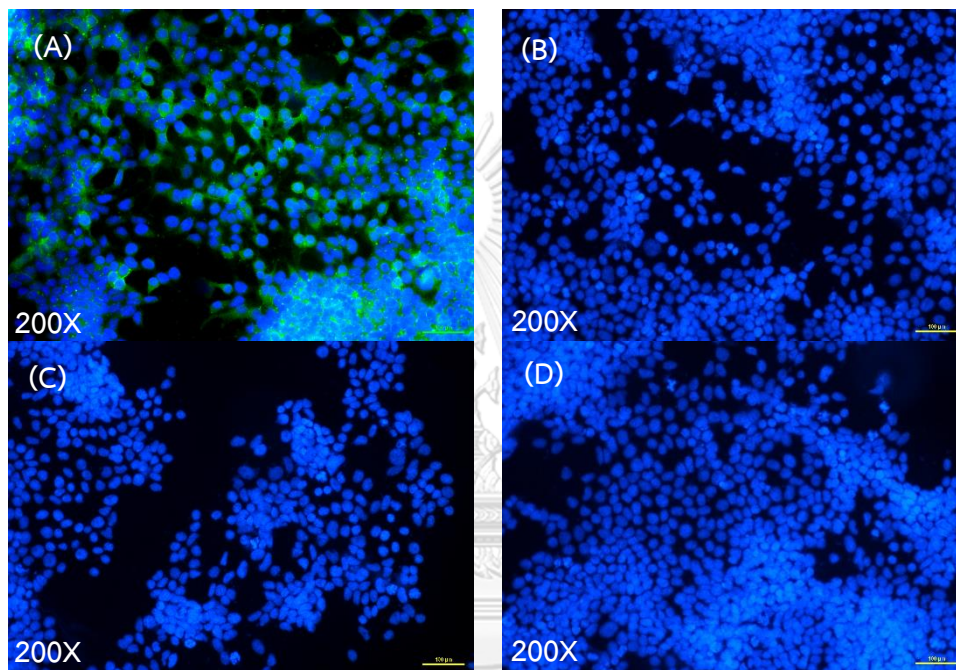


Figure 6: Restriction digestion products in 1% agarose gel electrophoresis with product size of 4.8 kb (upper red arrow) and 3.8 kb (lower red arrow), respectively. Lane 1: 1 kb hyper ladder and lane 2: pHDM contains SARS-CoV-2-S-WT gene.

### Target protein expression analysed by indirect immunofluorescent assay (IFA)

Spike protein expression was detected by indirect immunofluorescent assay (IFA). As shown in **figure 7**, S protein expression could be detected by anti-S1 polyclonal antibody (green). No signal of spike protein expression was observed in transfected control conditions.



*Figure 7: Immunofluorescence staining of SARS-CoV-2-S protein expression in HEK293T cells. Cells were transfected with pHDM-SARS-CoV-S-WT (A), empty pHDM (B) transfection reagents: PEI and serum-free media (C), and untransfected cells (D) for 24 hrs. FITC: green, DAPI: Blue. Cells were visualized under fluorescence microscope (200X magnification). The scale is 100  $\mu$ m.*

### Pseudotype collection time optimization

As shown in **table 9**, 2<sup>nd</sup>, and 3<sup>rd</sup> generation SARS-CoV-2 pseudotypes were collected at two separate time points at 48 and 72-hr post transfection. The difference in pseudotype yield collected at 2 time-points was less than 1-log in both generations. Thus, we pooled the pseudotype samples obtained from both time periods in order to maximize the amount of pseudotype for the further experimentation.

*Table 9: The titer of SARS-CoV-2 pseudotype produced at different collection time.*

Generation	Collection time (hr)	Titer (TCID <sub>50</sub> /mL)
2 <sup>nd</sup> with GFP	48	8.50x10 <sup>3</sup>
	72	8.45x10 <sup>3</sup>
3 <sup>rd</sup> with luciferase	48	1.94x10 <sup>4</sup>
	72	2.55x10 <sup>4</sup>

### SARS-CoV-2-lentiviral pseudotype production (luciferase reporter system)

At 48 and 60 hrs post-transfection with 1<sup>st</sup> generation plasmids (pNL4-3.Luc.R-E- and pHDM-SARS-CoV-2 S-WT), cell culture supernatant was harvested, pooled and subjected for pseudotype titration in HEK-Blue™ hACE2 cells. At 60 hrs post-infection, luciferase activity was measured. The result showed that the RLU signal of SARS-CoV-2-WT was low (with approximately 2,000 RLU in undiluted samples and was undetectable after 9-fold dilution) when compared to positive control (VSVG and bald controls) which showed the average RLU of approximately 5-log and 3-log, respectively. The background of this system was approximately 1-log as shown in **figure 8**.

The application of the luciferase reporter system was investigated for the production of 2<sup>nd</sup> and 3<sup>rd</sup> generation pseudotypes. The cell culture supernatant of the 2<sup>nd</sup> generation (pHAGE-CMV-Luc2-IRES-ZsGreen-W, psPAX2 pHDM-SARS-CoV-2 S-

WT) and 3<sup>rd</sup> generation pseudotype production (pHAGE-CMV-Luc2-IRES-ZsGreen-W, pHDM-Hgpm2, HDM-tat1b, pRC-CMV-Rev1b, and pHDM-SARS-CoV-2 S-WT) were collected and underwent pseudotype titration using the same procedure as performed in the 1<sup>st</sup> generation.

The result showed that the RLU signal of 2<sup>nd</sup> generation SARS-CoV-2-WT was approximately  $10^6$  log RLU in undiluted samples and undetectable after 243-fold dilution (**figure 9**). RLU signal of 3<sup>rd</sup> generation SARS-CoV-2-WT was approximately  $10^6$  log RLU in undiluted samples and undetectable after 19,683-fold dilution (**figure 10**). In summary, both generations yielded the RLU higher than 4-log when compared to cut-off. The TCID<sub>50</sub> titers of SARS-CoV-2-S-WT pseudotype in different generations were calculated and summarized in **table 10**.

Titration curve of SARS-CoV-2-WT pseudotype produced by 1<sup>st</sup> generation plasmids

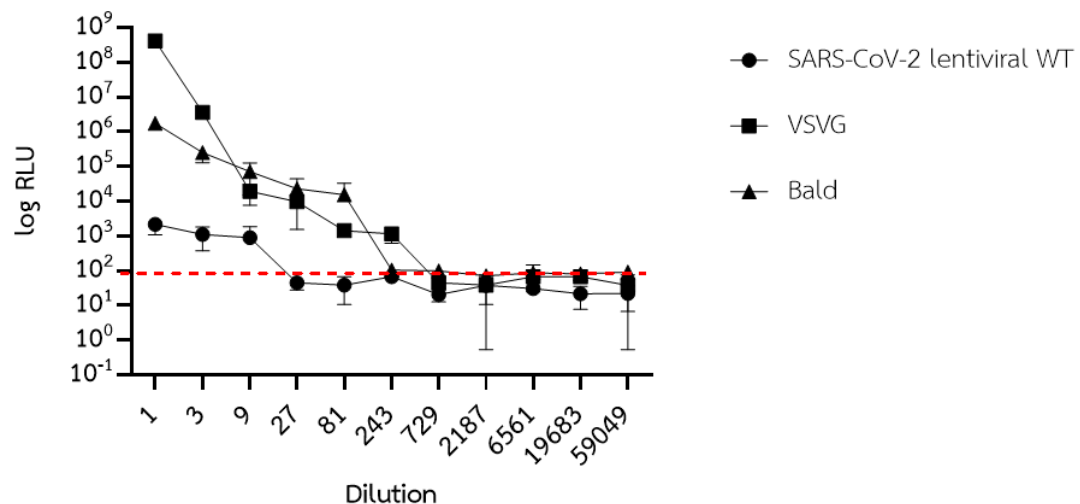


Figure 8: Relationship between RLU on X-axis and dilution on Y-axis at 60-hr post-titration of 1<sup>st</sup> generation of pseudotype SARS-CoV-2-WT, VSVG and bald controls. The experiment was performed in triplicates. Circle, square and triangle represent

SARS-CoV-2-S-WT, VSVG and bald respectively. Which red dashed line represents cut-off at  $10^2$ . Line represents mean with SD.

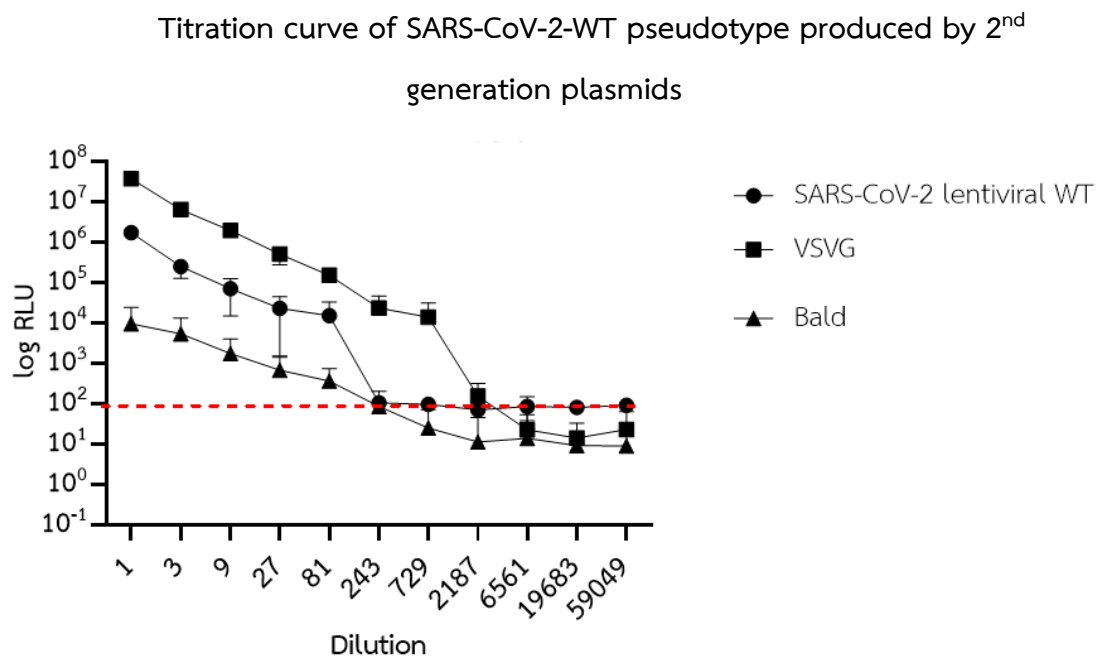


Figure 9: Relationship between RLU on X-axis and dilution on Y-axis at 60-hr post-titration of 2<sup>nd</sup> generation of pseudotype SARS-CoV-2-WT, VSVG and bald controls.

The experiment was performed in triplicates. Circle, square and triangle represent SARS-CoV-2-S-WT, VSVG and bald respectively. Which red dashed line represents cut-off at  $10^2$ . Line represents mean with SD.

Titration curve of SARS-CoV-2-WT pseudotype produced by 3<sup>rd</sup> generation  
plasmids

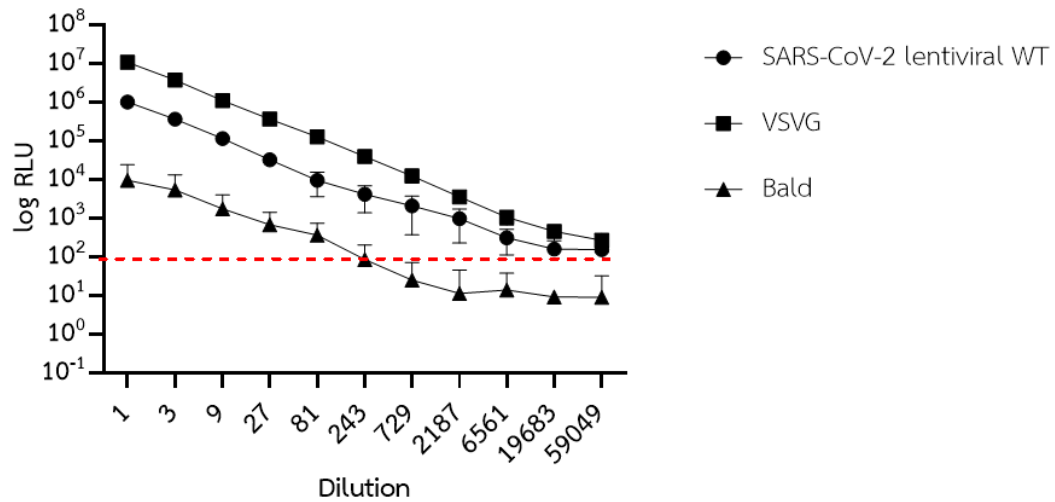


Figure 10: Relationship between RLU on X-axis and dilution on Y-axis at 60-hr post-titration of 3<sup>rd</sup> generation of pseudotype SARS-CoV-2-WT, VSVG and bald controls. The experiment was performed in triplicates. Circle, square and triangle represent SARS-CoV-2-S-WT, VSVG and bald respectively. Which red dashed line represents cut-off at 10<sup>2</sup>. Line represents mean with SD.

### SARS-CoV-2-lentiviral pseudotype production (GFP reporter system)

Production of pseudotype using GFP expression system was compared only between 2<sup>nd</sup> and 3<sup>rd</sup> generation production systems. The results revealed that after 24 hrs of transfection with combination of plasmids required for pseudotype production, GFP signal was observed in pMD2.G (served as positive control) and SARS-CoV-2-S-WT transfected cells. GFP signal could not be detected in untransfected cells. This could confirm the reliability of our transfection protocol. When comparing the GFP signal at this timepoint, the 2<sup>nd</sup> generation production system significantly expresses higher GFP signal than that of the 3<sup>rd</sup> generation (**figure 11**). However, **figure 11** represents only single comparison between 2 generations, further confirmation by pseudotype titration is required to determine the exact titer. At 48 and 72 hrs post-transfection with plasmid required for 2<sup>nd</sup> (pCCGW, psPAX2 and pHDM-SARS-CoV-2 S-WT) or 3<sup>rd</sup> generation pseudotype production (pHAGE-CMV-Luc2-IRES-ZsGreen- W, pHDM-Hgpm2, HDM-tat1b, pRC-CMV-Rev1b and pHDM-SARS-CoV-2 S-WT), cell culture supernatants were harvested, pooled and subjected for pseudotype titration in HEK-Blue™ hACE2 cells. At 60 hrs post-infection, GFP spots of 2<sup>nd</sup> and 3<sup>rd</sup> generation of SARS-CoV-2 pseudotypes were detected and counted by CTL-Immunospot® S6 ultimate as shown in **figure 12 and 13**. The TCID<sub>50</sub> titers of 2<sup>nd</sup> and 3<sup>rd</sup> generations SARS-CoV-2-S-WT pseudotype were calculated and summarized in **table 10**.

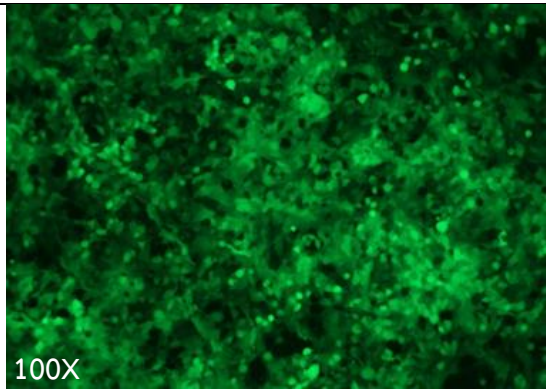
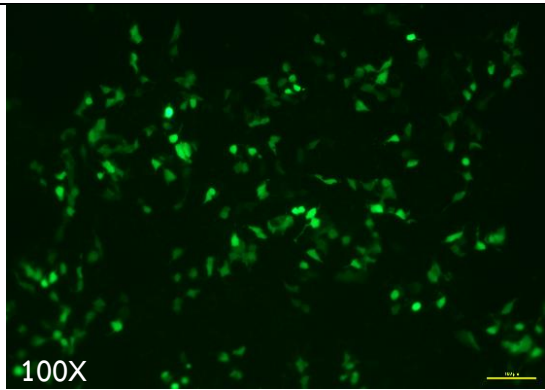
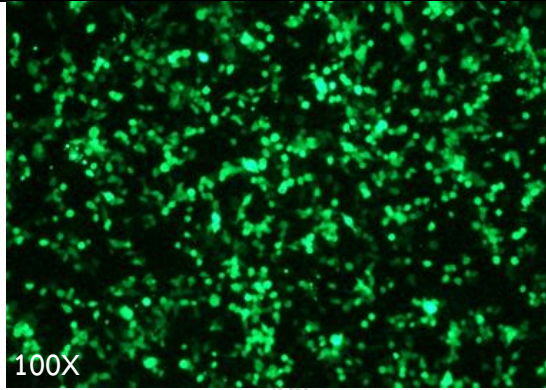
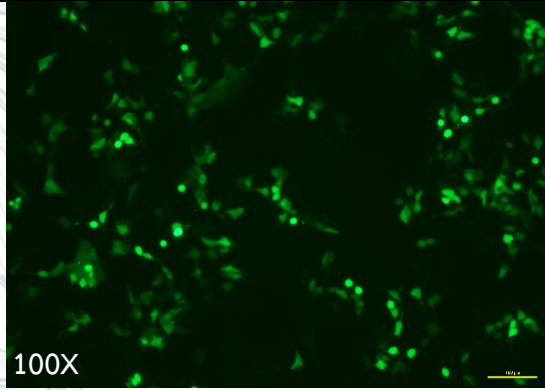
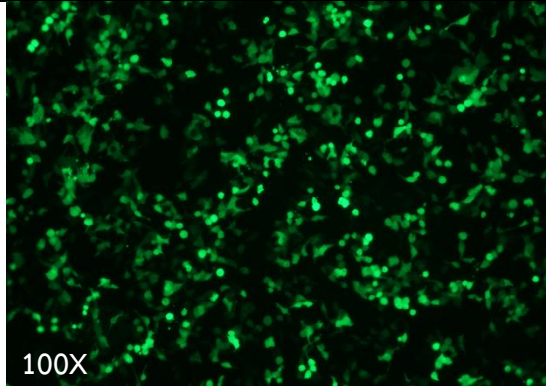
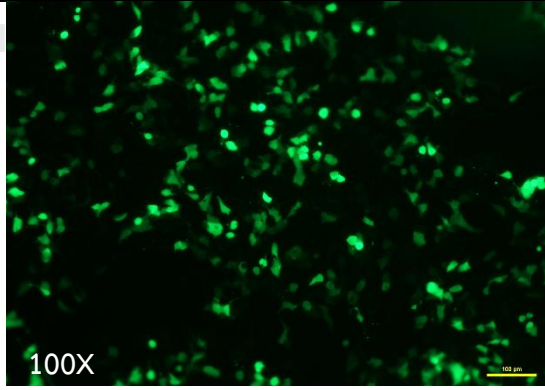
2 <sup>nd</sup> generation	3 <sup>rd</sup> generation
 <p data-bbox="336 689 411 723">100X</p> <p data-bbox="331 768 863 801">Transfected with pCCGW, psPAX2 and pMD2.G</p>	 <p data-bbox="922 689 997 723">100X</p> <p data-bbox="911 734 1474 869">Transfected with pHAGE-CMV-Luc2-IRES-ZsGreen-W, pHDM-Hgpm2, HDM-tat1b, pRC-CMV-Rev1b and pMD2.G</p>
 <p data-bbox="336 1223 411 1256">100X</p> <p data-bbox="331 1301 863 1379">Transfected with pCCGW, psPAX2, pHDM SARS-CoV-2-S-WT</p>	 <p data-bbox="922 1223 997 1256">100X</p> <p data-bbox="911 1267 1474 1402">Transfected with pHAGE-CMV-Luc2-IRES-ZsGreen-W, pHDM-Hgpm2, HDM-tat1b pRC-CMV-Rev1b and pHDM SARS-CoV-2-S-WT</p>
 <p data-bbox="336 1751 411 1785">100X</p> <p data-bbox="331 1830 831 1863">Transfected with pCCGW and psPAX2 (Bald)</p>	 <p data-bbox="922 1751 997 1785">100X</p> <p data-bbox="911 1796 1474 1930">Transfected with pHAGE-CMV-Luc2-IRES-ZsGreen-W, pHDM-Hgpm2, HDM-tat1b pRC-CMV-Rev1b (Bald)</p>

Figure 11: HEK293T cell 24-hr post transfection with 2<sup>nd</sup> generation (left) and 3<sup>rd</sup> generation (right) plasmids. GFP signal (green) were visualized under fluorescence microscope (100X magnification). The scale is 100  $\mu$ m.

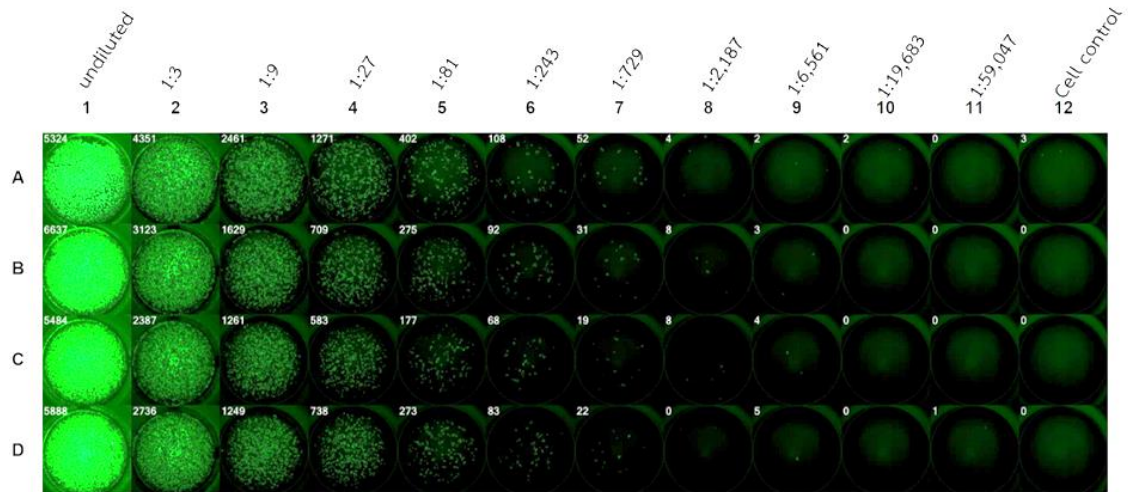
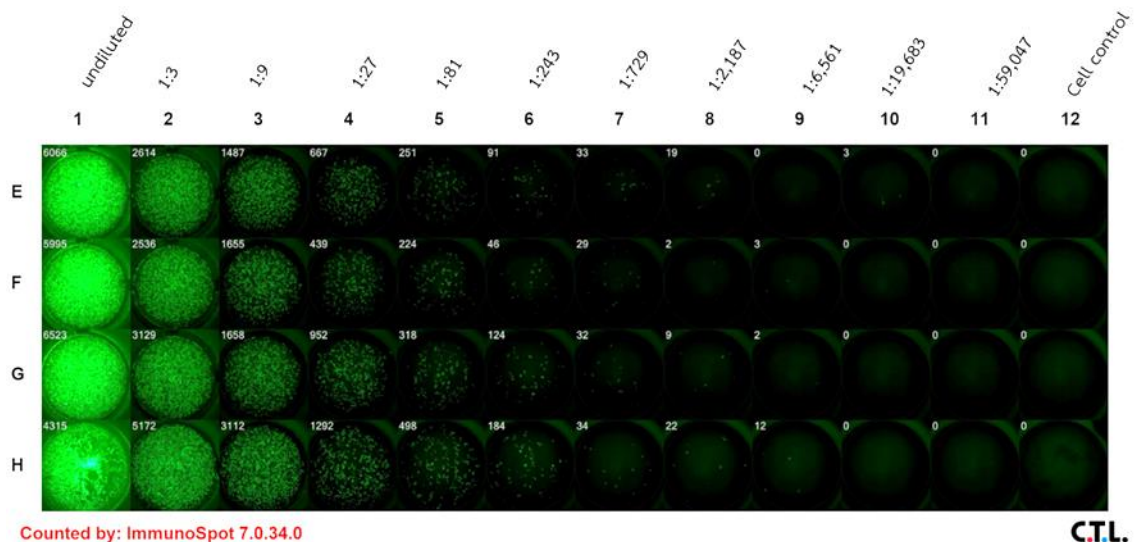


Figure 12: HEK-Blue™ hACE2 cell 60-hr post titration using 2<sup>nd</sup> generation of SARS-CoV-2 detected GFP signal (green) and counted by CTL-Immunospot® S6 Ultimate. Pseudotype sample was 3-fold serially diluted in quadruplicate from column 1-11



(from undilute to 1:59,047), column 12 represent cell control.

*Figure 13: HEK-Blue™ hACE2 cell 60-hr post titration using 3<sup>rd</sup> generation of SARS-CoV-2 detected GFP signal (green) and counted by CTL-Immunospot® S6 Ultimate. Pseudotype sample was 3-fold serially diluted quadruplicate covering column 1-11 (from undilute to 1:59,047), column 12 represent cell control. SARS-CoV-2*

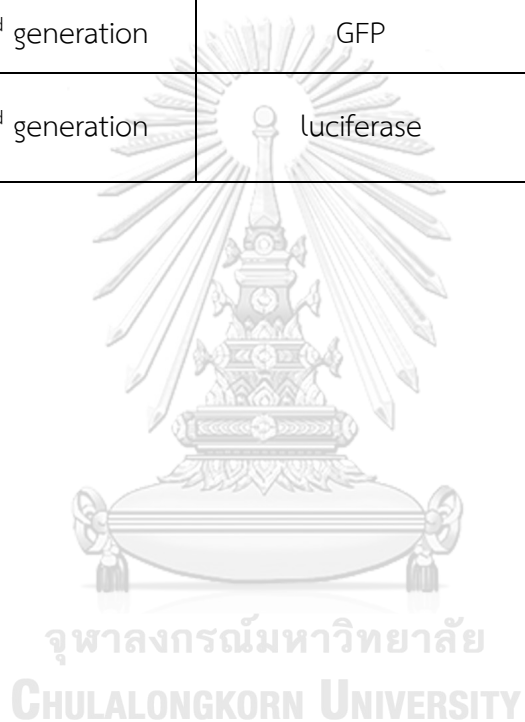
#### **pseudotype titer determination**

All the pseudotype SARS-CoV-2 titer determination results were summarized in **table 10**. The results demonstrated that 1<sup>st</sup>, 2<sup>nd</sup> and 3<sup>rd</sup> generations using luciferase reporter system yielded the lowest titer in 1<sup>st</sup> generation, higher titer in 2<sup>nd</sup> generation and the highest titer in 3<sup>rd</sup> generation, respectively. GFP reporter system tested in 2<sup>nd</sup> and 3<sup>rd</sup> generations showed the moderate titers. Of note, the minimum titer required for PVNT test was approximately  $2 \times 10^3$  TCID<sub>50</sub>/mL for pseudotype system which separate from base line and provide enough titer for neutralization test. We therefore selected 2<sup>nd</sup> generation of GFP reporter system for further PVNT analysis.

Although the 2<sup>nd</sup> and 3<sup>rd</sup> generation pseudotype of luciferase system also yields a high titer, the variation between run or between replication were obviously observed (results not shown). Moreover, additional procedures in luciferase activity detection including transferring of supernatant to another plate, addition of D-luciferin (luciferase substrate) step, could yield a high imprecision of this method. Thus, the 3<sup>rd</sup> generation pseudotype of luciferase system was not selected for PVNT analysis.

Table 10: Titer comparison between different pseudotype generations and reporter systems.

Plasmid concentration	Generation	Reporting system	Titer (TCID <sub>50</sub> /mL)
12 µg	1 <sup>st</sup> generation	Luciferase	3.09×10 <sup>2</sup>
	2 <sup>nd</sup> generation	GFP	8.45×10 <sup>3</sup>
	2 <sup>nd</sup> generation	luciferase	2.82 ×10 <sup>3</sup>
	3 <sup>rd</sup> generation	GFP	2.13×10 <sup>3</sup>
	3 <sup>rd</sup> generation	luciferase	2.51×10 <sup>4</sup>



### SARS-CoV-2-lentiviral pseudotype neutralization

At 60-hr post-neutralization, the non-neutralized SARS-CoV-2 pseudotype were detected and counted by CTL-Immunospot® S6 ultimate as shown in **figure 14**.

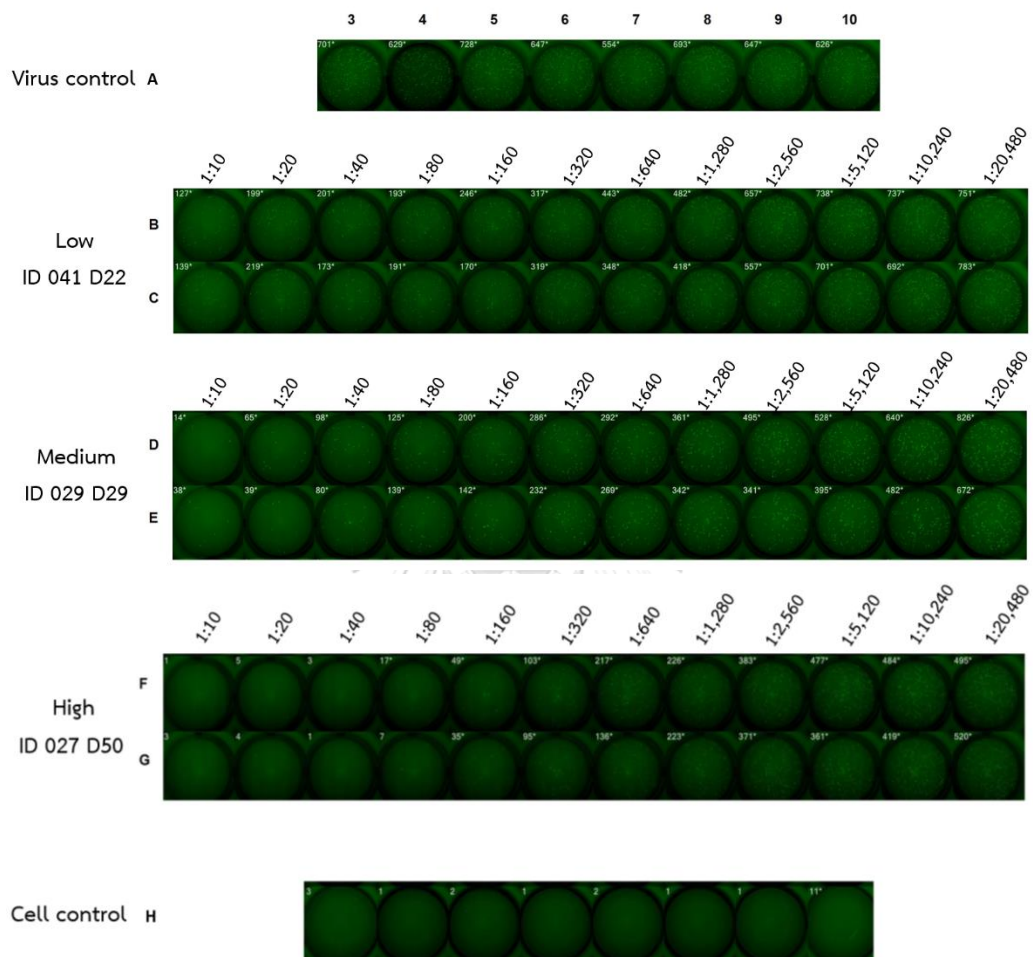


Figure 14: The 96-well plate configuration of SARS-CoV-2 WT 2<sup>nd</sup> generation neutralization test. GFP signal (green) in HEK-Blue™ hACE2 was detected and counted by CTL-Immunospot® S6 Ultimate. Row A: Virus control, row B to C: low titer ID 041 D22, row D to E: medium titer ID 029 D29, row F to G: high titer ID 027 D50, all sera sample was 2-fold serially diluted duplicate covering column 1-12 (from undilute to 1:20,480) and row H: CC.

### Sensitivity and specificity

A total of 128 samples were used for evaluation of sensitivity and specificity by comparing with MN<sub>50</sub> that was used as reference method in this study. PVNT<sub>50</sub> showed 98.91% sensitivity and 100% specificity when compared with MN<sub>50</sub> results (**table 11**). One sample out of 92 samples (1.1%) with false result by PVNT<sub>50</sub> was the low titer sample analyzed by VNT (MN<sub>50</sub> titer = 1:20). These results demonstrate a high sensitivity and specificity of our in-house PVNT method when compared to the reference method (VNT).

Table 11: Sensitivity and specificity results of PVNT

	VNT <sub>50</sub> positive	VNT <sub>50</sub> Negative	Total
PVNT <sub>50</sub> Positive	91 (true positive)	0 (false positive)	91
PVNT <sub>50</sub> Negative	1 (false negative)	36 (true negative)	37
Total	92	36	128
	Sensitivity = 98.91%	Specificity = 100%	

#### Sensitivity

$$\begin{aligned} \text{Sensitivity} &= \text{true positive}/(\text{true positive} + \text{false negative}) \\ &= 91/(91+1) \\ &= 0.9891 \end{aligned}$$

$$\% \text{ Sensitivity} = 0.9891 \times 100 = 98.91$$

#### Specificity

$$\begin{aligned} \text{Specificity} &= \text{true negative}/(\text{true negative} + \text{false positive}) \\ &= 36/(36+0) \\ &= 1 \end{aligned}$$

$$\% \text{ Specificity} = 1 \times 100 = 100$$

Comparison of PVNT<sub>50</sub> and SARS-CoV-2 IgG using convalescent patient sera.

From 11 samples of convalescence sera (Accuset™, Seracare), 10 samples were tested positive and 1 sample was tested negative by CMIA (Abbott ARCHITECT), defined by signal to cut-off (s/co) ratio. By using this serum panel, 100% agreement of the results between PVNT<sub>50</sub> and SARS-CoV-2 IgG (Abbott ARCHITECT) were observed (figure 15).

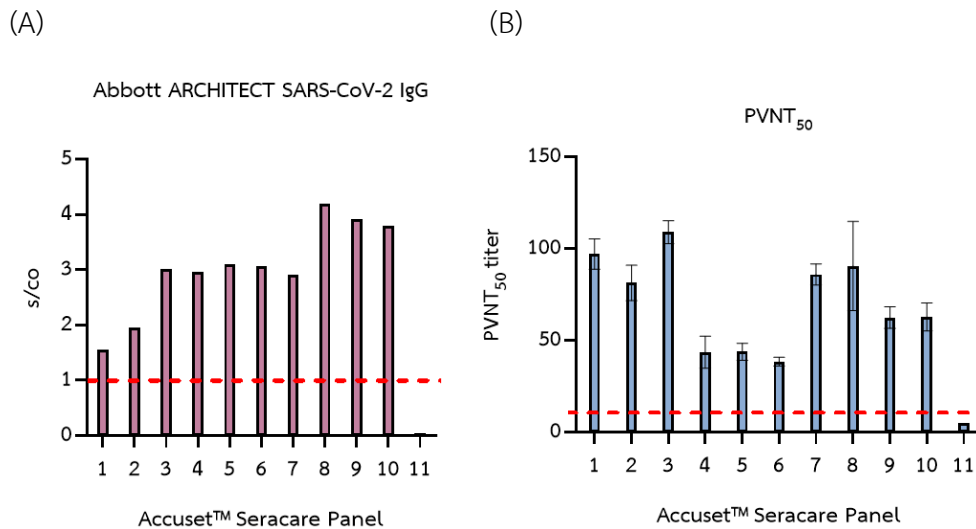


Figure 15: Demonstrates the comparison of results between Accuset™ Seracare panel for CMIA (Abbott ARCHITECT SARS-CoV-2 IgG) (A) and PVNT<sub>50</sub> (B). The red dashed line represents the positive cut-off of the tests. Each bar represents mean with SD. PVNT was performed in triplicates.

### Validation of neutralizing titer analyzed by PVNT<sub>50</sub> with the standardized neutralizing titer (IU/mL) using WHO serum panel.

To compare our PVNT<sub>50</sub> with other methods, we validate the neutralizing titer analyzed by our PVNT<sub>50</sub> using WHO serum panel (WHO Standard NIBSC code:20/268) which reported the neutralizing titer in international unit (IU/mL). Four samples of NIBSC code:20/268 (including NIBSC code 20/140, 20/144, 20/148 and 20/150) with neutralizing titer ranged from 44-1,473 IU/mL were validated against our PVNT<sub>50</sub>. The correlation was shown in **table 12**, with the correlation coefficient of 1.0 and yielded an equation of  $y = 0.7968x + 9.4048$ . The results were also shown in **figure 16**.

Table 12: Validation of PVNT<sub>50</sub> titers using standard sera.

Code	Run 1	Run 2	Run 3	Average PVNT <sub>50</sub>
NIBSC 20/140 (Low 44 IU/mL)	34.55	49.986	47.61	44.05
NIBSC 20/144 (Low 95 IU/mL)	87.30	121.38	99.21	102.63
NIBSC 20/148 (Medium 210 IU/mL)	117.85	390.0	261.0	256.28
NIBSC 20/150 (High 1,473 IU/mL)	2,002.69	1,571.52	1,935.0	1,836.40

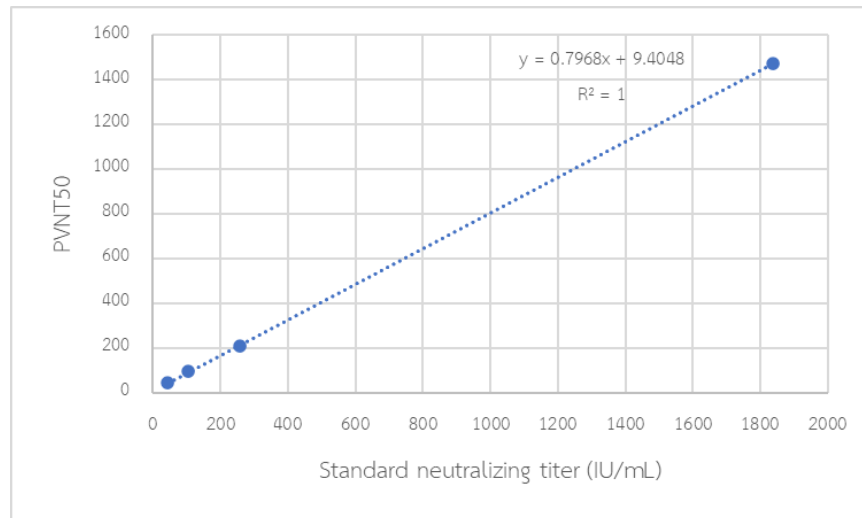


Figure 16: Correlation of PVNT<sub>50</sub> and neutralizing antibody concentration after validated against the standardized serum panel.

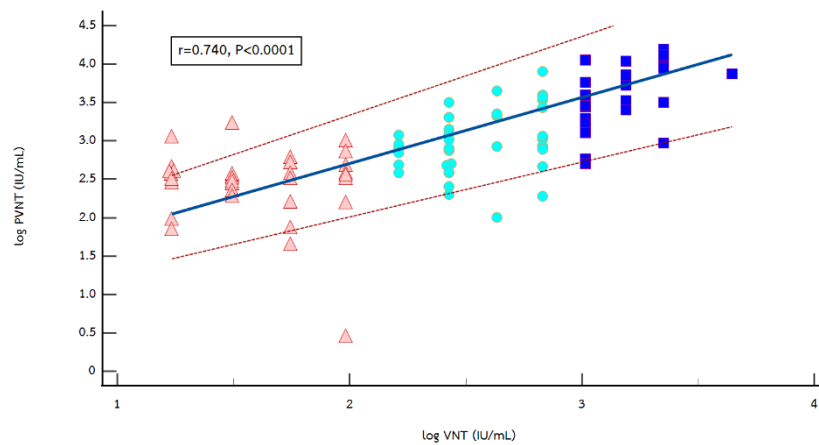


Comparison of PVNT results with other SARS-CoV-2 antibody detection methods using ChulaCoV-19 immunized sera (summarized in table 13).

#### PVNT vs VNT

Comparison between  $\log PVNT_{50}$  and  $VNT_{50}$  after converted into IU/mL using Passing-balok regression revealed a moderate correlation ( $r=0.740$ ,  $P<0.0001$ ) as shown in figure 17(A). Bland-Altman analysis showed a mean bias of  $-0.4735$  (95% CI:  $-0.5791$  to  $-0.3678$ ) figure 17(B).

(A)



(B)

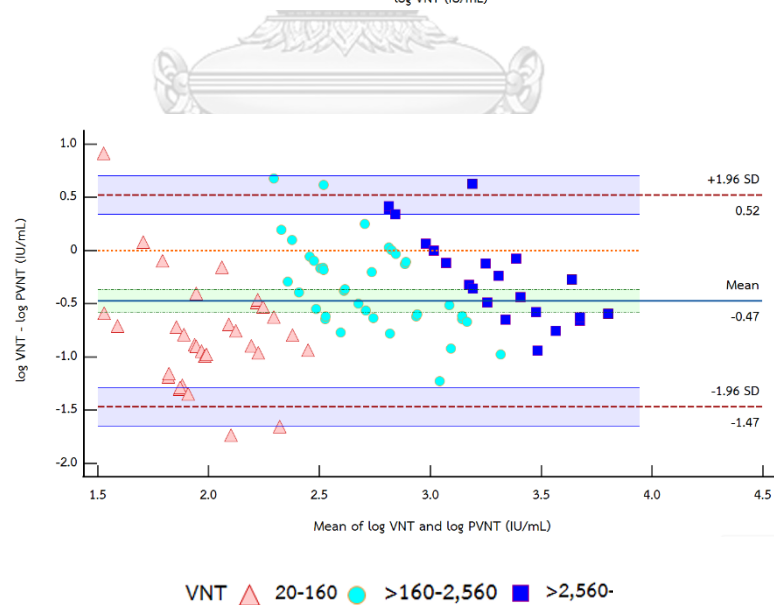


Figure 17: Passing-bablok regression analysis of log VNT and log PVNT (A), Bland-Altman analysis for mean difference of log VNT and log PVNT (B).

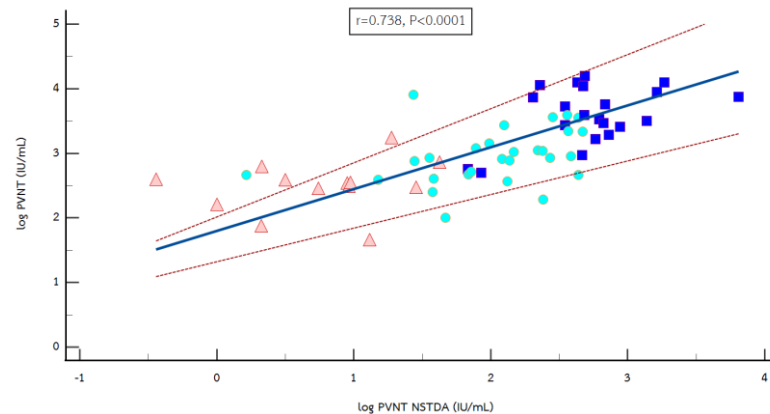
Figure 17: (continued)

Red triangle, green circle and blue square represent titers of 20-160, >160-2,560 and >2,560, respectively analyzed by VNT<sub>50</sub>.

### PVNT vs PVNT-NSTDA

Comparison between our PVNT titers with the PVNT titers analyzed at NSTDA (Dr. Anan Jongkeawwattana's Lab), designated as PVNT-NSTDA. The results were converted into IU/mL. Passing-bablok regression analysis showed a moderate correlation ( $r=0.738$ ,  $P<0.0001$ ) in the PVNT values between 2 laboratories, **figure 18(A)**. In Bland-Altman analysis demonstrated that our PVNT tended to yield a higher result at low titer samples but yield a higher result at high titer samples. A mean bias of PVNT results between laboratories was 1.08 (95% CI: -1.60 to -1.12) **figure 18(B)**.

(A)



(B)

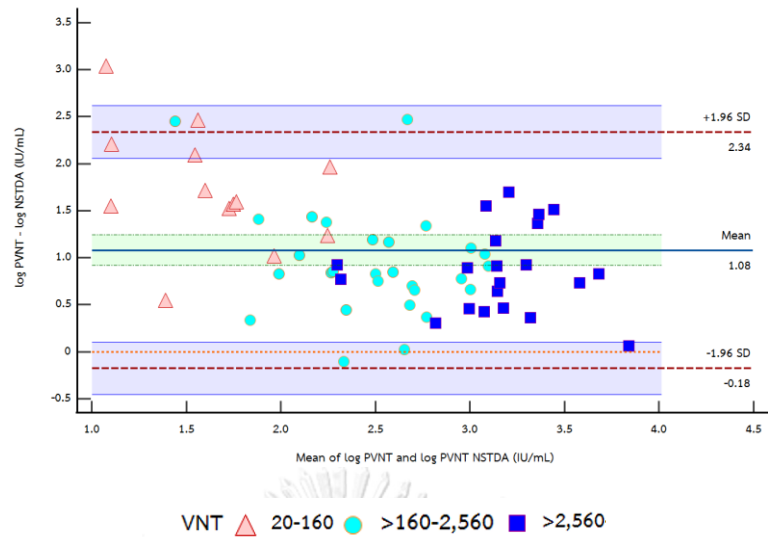
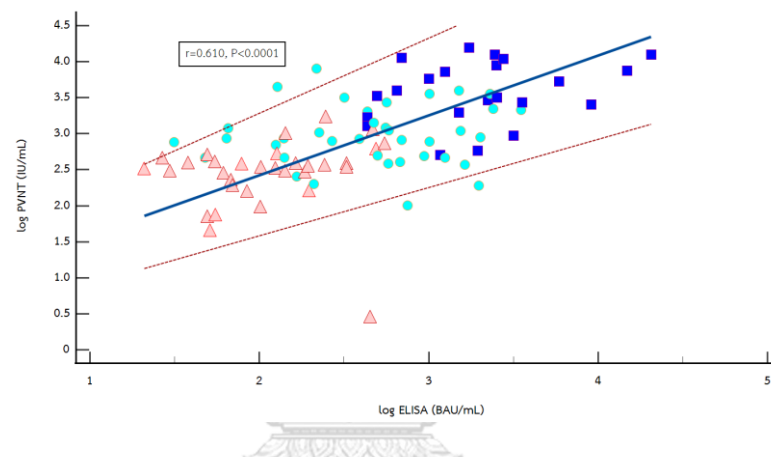


Figure 18: Passing-bablok regression of log PVNT and log PVNT-NSTDA (IU/mL) (A) and Bland-Altman analysis of log PVNT and log PVNT-NSTDA (IU/mL) (B). Red triangle, green circle and blue square represent titers of 20-160, >160-2,560 and >2,560, respectively analyzed by VNT<sub>50</sub>.

### PVNT vs ELISA anti-SAR-CoV-2 IgG

Comparison between log PVNT<sub>50</sub> (IU/mL) and anti-SAR-CoV-2 IgG (BAU/mL) using Passing-bablok regression observed a moderate correlation ( $r=0.610$ ,  $P<0.0001$ ) as shown in **figure 19(A)**. Mean bias between 2 methods was of  $-0.33$  (95% CI:  $-0.45$  to  $-0.20$ ) obtained by Bland-Altman analysis, **figure 19(B)**.

(A)



(B)

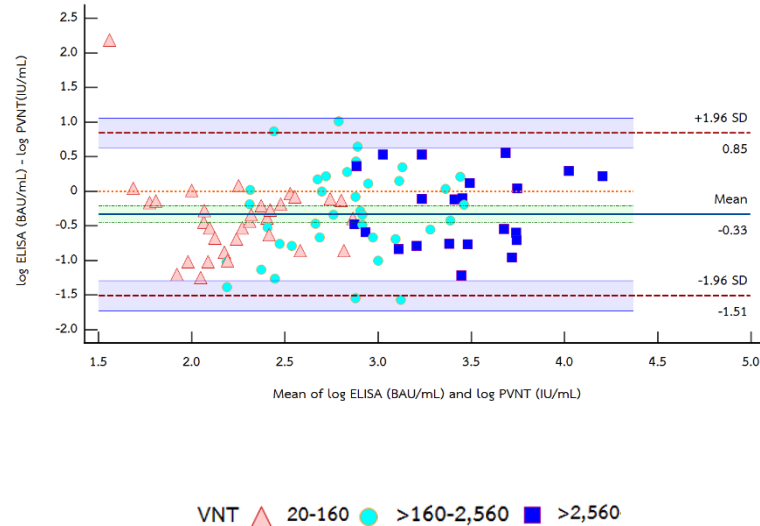


Figure 19: Passing-bablok regression analysis of log PVNT (IU/mL) and log ELISA (BAU/mL) (A) and, Bland-Altman analysis for mean difference of log PVNT (IU/mL) and log ELISA (BAU/mL) (B). Red triangle, green circle and blue square represent

titers of 20-160, >160-2,560 and >2,560, respectively analyzed by VNT<sub>50</sub>. **PVNT vs sVNT**

Comparison between log PVNT<sub>50</sub> (IU/mL) and sVNT (% inhibition) using Passing-balok regression observed a moderate correlation ( $r=0.637$ ,  $P<0.0001$ ) as shown in **figure 20**. Most of the sample with >80% inhibition results showed PVNT higher than 100 IU/mL.

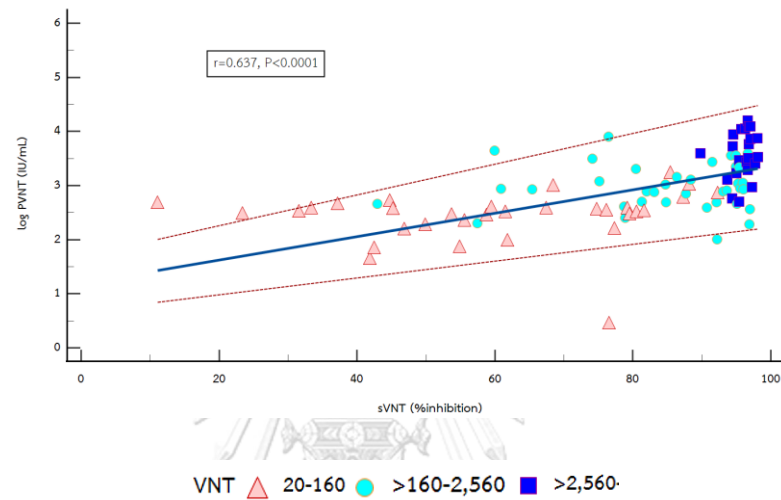
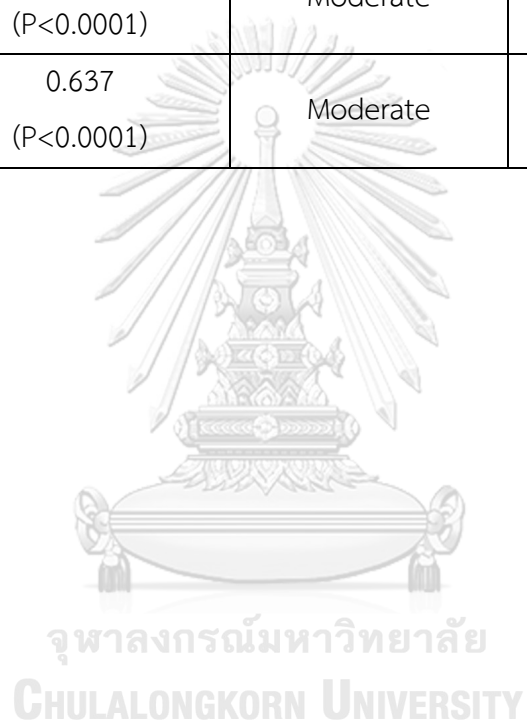


Figure 20: Passing-bablok regression analysis of log PVNT (IU/mL) and sVNT. Red triangle, green circle and blue square represent titers of 20-160, >160-2,560 and >2,560, respectively analyzed by VNT<sub>50</sub>.

Table 13: Summary of results comparison between PVNT and other techniques.

Test	Correlation coefficient	Spearman correlation[86]	Mean bias
VNT	0.740 (P<0.0001)	Moderate	-0.5646 (95% CI: -0.67 to -0.46)
PVNT NSTDA	0.738 (P<0.0001)	Moderate	1.08 (95% CI: -1.60 to -1.12)
ELISA	0.610 (P<0.0001)	Moderate	-0.33 (95% CI: -0.46 to -0.20)
sVNT	0.637 (P<0.0001)	Moderate	-



### Construction of recombinant plasmid expressing Spike protein of SARS-CoV-2 variants: Delta (B1.617.2) and Omicron BA.4/5

As shown in **figure 21**, the gene encoded for the SARS-CoV-2- spike (S) protein of Delta (B1.617.2) and Omicron BA.4/5 were successfully subcloned into pHDM expression plasmid. They were confirmed by double digestion using restriction enzymes *Sall* and *EcoRI*. The digested bands showed the size at approximately 4.8 kb and 3.8 kb corresponding to pHDM expression plasmid and S gene, respectively.

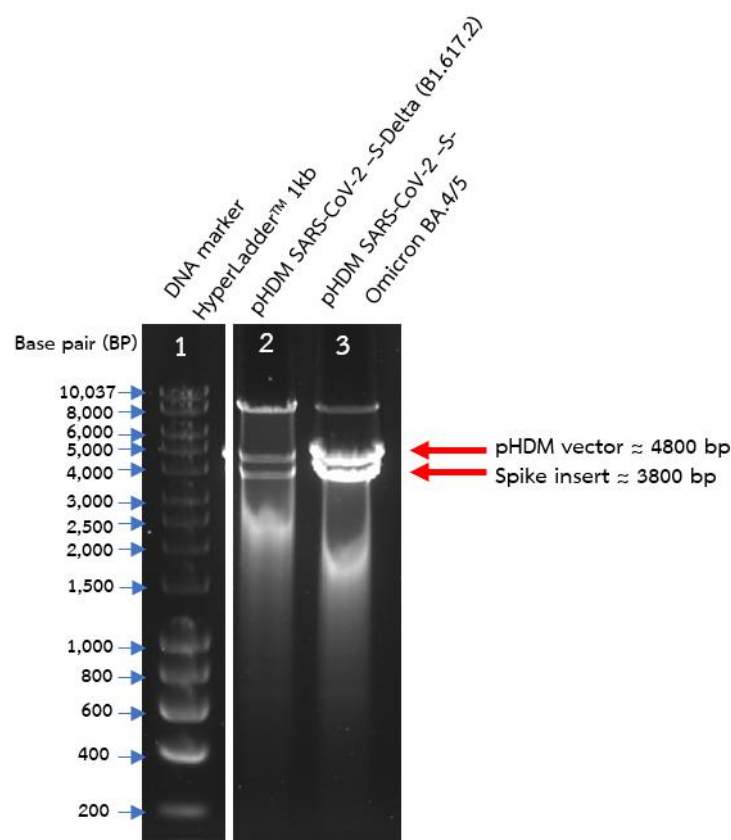


*Figure 21: Restriction digestion products in 1% agarose gel electrophoresis with product size of 4.8 kb (upper red arrow) and 3.8 kb (lower red arrow), respectively. Lane 1: 1 kb hyper ladder, lane 2: pHDM contains SARS-CoV-2-S-Delta (B.1.617.2) gene and lane 3: pHDM contains SARS-CoV-2-S-Omicron BA.4/5.*

### Target protein expression analysis by indirect immunofluorescent assay (IFA)

Spike protein expression was detected by indirect immunofluorescent assay (IFA). As shown in **figure 22**, S protein expression could be detected by anti-S1 polyclonal antibody (green). No FITC signal was observed in empty pHDM transfected cells. Cellular nuclei were counter stained with DAPI (Blue).

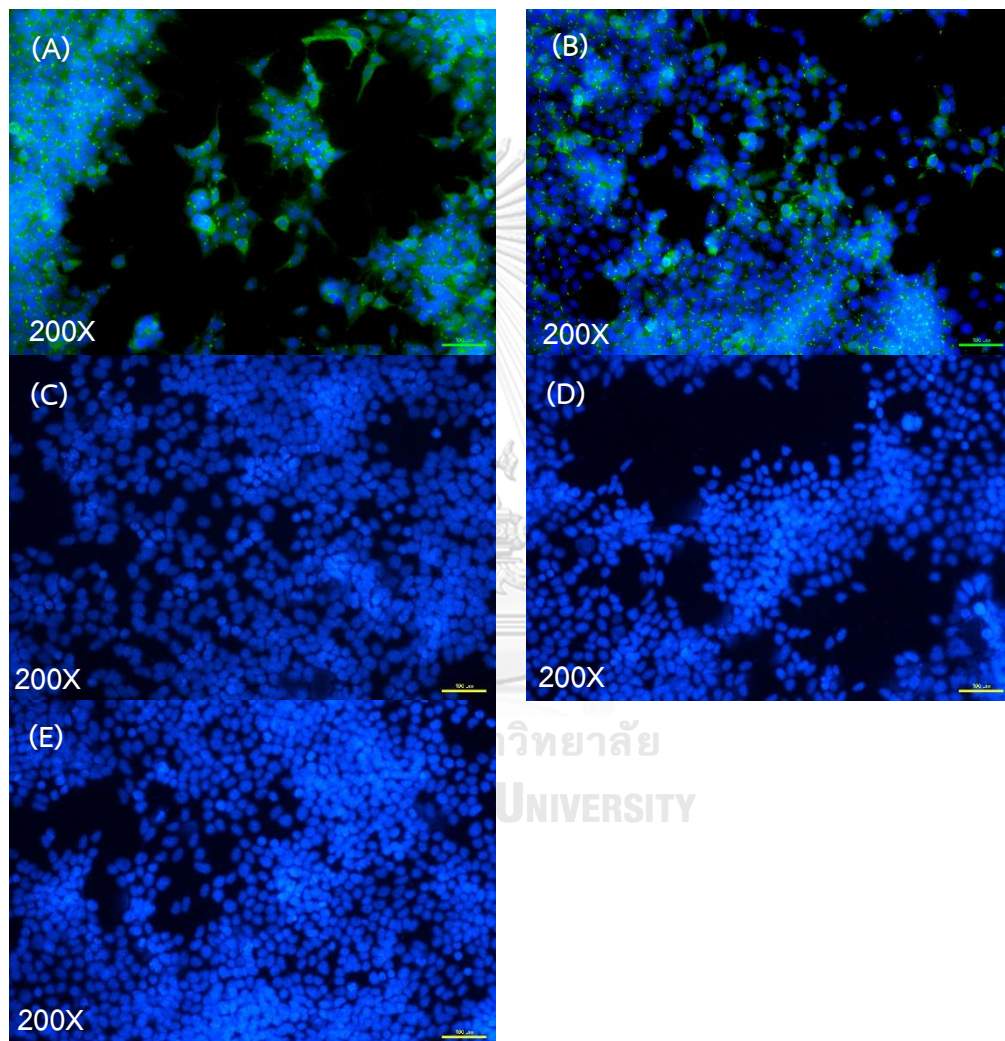


Figure 22: Immunofluorescence staining SARS-CoV-2 S protein expression in HEK293T cells. Cells were transfected with pHDM-SARS-CoV-2-S-Delta (B.1.617.2) plasmid (A), pHDM-SARS-CoV-S-Omicron BA.4/5 plasmid (B), empty pHDM transfected (C), transfected with transfection reagent: PEI and serum-free media (D) and Figure 22: (continued)

*untransfected cells (E) for 24 hrs. FITC: green, DAPI: Blue. Cells were visualized under fluorescence microscope (200X magnification). The scale is 100  $\mu$ m.*

### **SARS-CoV-2-S-Delta(B.1.617.2) and Omicron BA.4/5 lentiviral pseudotype production (GFP reporter system)**

Based on the prior successful production of SARS-CoV-2-S-WT. An identical technique is employed to generate two variants of SARS-CoV-2 pseudotype including Delta (B.1.617.2) and Omicron BA.4/5 using 2<sup>nd</sup> generation plasmid with GFP reporter system. The GFP signal within the producing cells after VSVG and both variants of SARS-CoV-2 spike plasmids at 24 hrs post-transfection were shown in **figure 23**. At 48 and 72 hrs post-transfection (pCCGW, psPAX2 and pHDM-SARS-CoV-2-S-Delta (B.1.617.2) or Omicron BA.4/5), cell culture supernatants were harvested, pooled, and subjected for pseudotype titration in HEK-Blue™ hACE2 cells. At 60 hrs post-infection, number of GFP spots of 2<sup>nd</sup> generation of SARS-CoV-2 pseudotype were detected and counted by CTL-Immunospot® S6 ultimate. The TCID<sub>50</sub> titers of SARS-CoV-2-S- Delta (B.1.617.2) and Omicron BA.4/5 was calculated and summarized in **table 14**. Low pseudotype titer were obtained in both SARS-CoV-2 Delta (B.1.617.2) and Omicron BA.4/5 variants which insufficient for neutralization testing. Additional optimization is required for the pseudotype production of SARS-CoV-2 variants in order to achieve a sufficient TCID<sub>50</sub> titer.

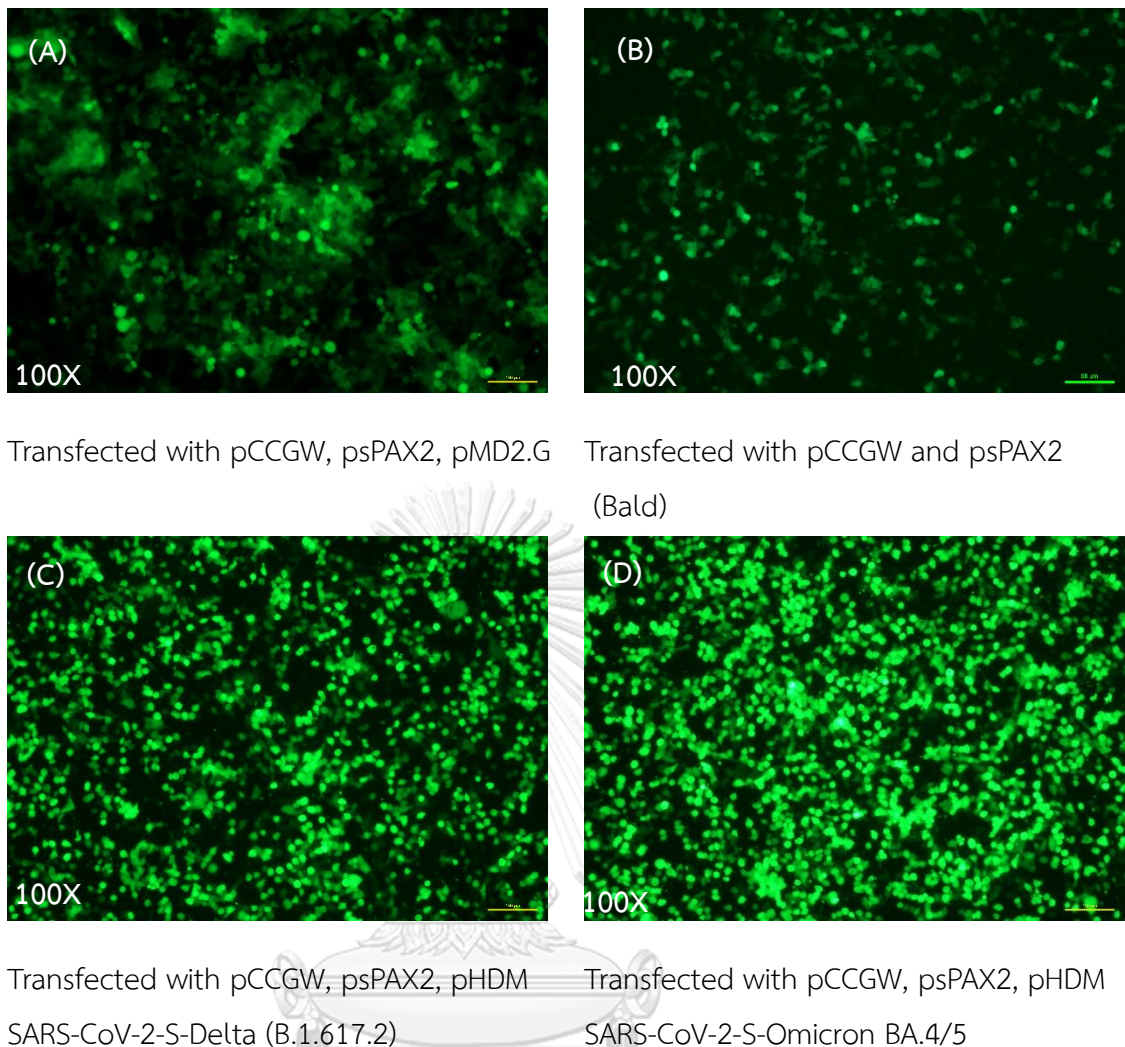


Figure 23: HEK293T cell 24-hr post transfection with 2<sup>nd</sup> generation plasmids transfected with pCCGW, psPAX2 and pMD2.G (A), pCCGW and psPAX2 (Bald) (B), pCCGW, psPAX2, pHDM SARS-CoV-2-S-Delta (B.1.617.2) (C) and pCCGW, psPAX2, pHDM SARS-CoV-2-S-Omicron BA.4/5 (D). GFP signal (green) were visualized under fluorescence microscope (100X magnification). The scale is 100  $\mu$ m.

Table 14: Titer summary of SARS-CoV-2-S-Delta (B.1.617.2) and Omicron BA.4/5.

Variant	Plasmid concentration	Generation	Reporting system	Titer (TCID <sub>50</sub> /mL)
SARS-CoV-2-S-Delta (B.1.617.2)	12 µg	2 <sup>nd</sup> generation	GFP	34.6
SARS-CoV-2-S-Omicron BA.4/5		2 <sup>nd</sup> generation	GFP	26.3



## CHAPTER VI

### DISCUSSION AND CONCLUSION

Determining neutralization activity against SARS-CoV-2 poses challenges since the gold standard assay generally relies on live virus neutralization. This assay requires a BSL-3 laboratory, well-trained personnel, and well-characterized virus with established protocols.

To address this limitation, various methods have been developed, including ELISA tests, sVNT (which use the same principle as ELISA), and pseudotype virus neutralization [3, 19-24]. ELISA-based tests offer advantages such as speed and safety, but they can only detect binding antibodies (or blocking of RBD/ACE2 interaction in the case of sVNT). Hence, the detection of antibody binding domains or the neutralizing epitopes residing outside the protein used in the assay, such as the N-terminal of the S protein, may be missed [85, 87].

The utilization of the pseudotype virus neutralization assay is regarded as a viable alternative for the assessment of neutralizing antibody levels in vaccinees or have recovered from an infection. The test can be conducted within BSL-2 laboratories, which possess reduced containment restrictions. Therefore, this technique has the potential to be utilized as a high-throughput screening approach for individuals who are infected or have had vaccinations, particularly in laboratory environments [88].

This study provides a comprehensive analysis and methodology for the generation of lentiviral-pseudotype viral particles that carry the spike protein of SARS-CoV-2. Through the process of protocol comparison, the production of pseudotype virus was achieved by utilizing the 2<sup>nd</sup> and 3<sup>rd</sup> generations of plasmids that contained GFP and luciferase reporting systems.

The utilization of the transfer plasmid pHAGE-CMV-luc2-IRES-ZsGreen-W in the development of the 3<sup>rd</sup> generation pseudotype has revealed that the luciferase reporting system exhibits a greater titer compared to the GFP reporting system. This disparity can be attributed to the presence of the IRES element on the plasmid,

denoted as Luc2-IRES-ZsGreen, which features the luciferase gene preceding the GFP gene. Consequently, the reduced efficacy of ribosome binding results in diminished expression of second gene, GFP in this case [89, 90]. According to the data presented in **table 9**, the titer achieved using the luciferase reporting system in the 3<sup>rd</sup> generation lentiviral system was found to be greater when compared to the titer obtained using the GFP reporting system. This finding aligns with the earlier study conducted by Muzukuchi, H et al (ref).

It is noteworthy that, based on our observations after working with these two reporter systems, detection of luciferase activity showed higher variation between wells/replicates. The detection step must be performed by cell lysis and measured within 1 hr after the addition of the substrate (beetle-luciferin). Moreover, specific white polystyrene optical-bottom cell culture plates are required. These additional required procedures, reagents, and materials yield an approximately 50-fold higher cost per plate. Therefore, we selected the 2<sup>nd</sup> generation pseudotype with GFP reporter for further study, as it is more practical; the GFP signal remains stable for a week, there is lower signal variation between replicates, and the analysis cost is lower. However, there have been studies demonstrating sensitivity issues in some cases.

Failure in SARS-CoV-2-S-WT pseudotype production using the 1<sup>st</sup> generation plasmids with the luciferase reporter showed a low titer, possibly due to an optimal plasmid ratio used for transfection. In our study, the pNL4-3.Luc.R-E-:pHDM-SARS-CoV2-S-WT ratio was 2:1. Higher plasmid ratios, ranging from 3:1 and DNA mass up to 25 µg, have been used to yield a high pseudotype virus titer [3]. In addition, it has been studied that the plasmid quantity used for transfection varies with the size of the transgene of interest when using plasmids of different sizes [91]. The study examines the shortcomings observed in SARS-CoV-2 variant pseudotype, specifically focusing on the Delta (B.1.617.2) and Omicron BA.4/5 by utilizing the 2<sup>nd</sup> generation plasmids containing the GFP reporter exhibited low titer. In addition, it has been studied that sodium butyrate increase 5-fold titer [92, 93]. Thus, further investigation on plasmid ratio optimization or even viral concentration protocols is needed [94, 95].

Considering VNT as the gold standard, our pseudotype virus demonstrates excellent sensitivity and specificity profiles. One sample with a false negative result in our PVNT is the sample with a low  $MN_{50}$  titer (1:20), very close to the positive cut-off of the MN protocol.

As mentioned earlier, several assays are used to measure SARS-CoV-2 neutralizing antibody levels. However, the reported values were not directly compared due to the lack of standardized reporting for virus neutralization titers and standardized assays. Therefore, we used standardized sera to harmonize our method with other reports. This procedure translated our  $PVNT_{50}$  titer into IU/mL before comparing it with the results reported by VNT, PVNT-NSTDA, and ELISA.

The correlation of our PVNT with the VNT standard method showed a moderate correlation ( $r = 0.740$ ,  $P < 0.0001$ ), as illustrated in **Figure 14A**. A similar finding was reported by Yu et al., yielding  $r = 0.747$  [96]. The difference in neutralizing antibody levels between these two methods is probably due to the different target cells used (Vero E6 for VNT vs. HEK Blue™ hACE2 for PVNT). Additionally, a different detection method was used; VNT employed specific antibodies to detect SARS-CoV-2 nucleocapsid in permeabilized infected cells, while our method relied on the detection of the GFP signal in pseudotype-infected HEK293 cells.  $MN_{50}$  titer (1:20), very close to the positive cut-off of the MN protocol.

Surprisingly, only a moderate correlation ( $r = 0.738$ ,  $P < 0.0001$ ) between the two PVNT laboratories (our PVNT vs. PVNT-NSTDA) was noted. Although the platform is the same, there are some details that might contribute to the different results. Firstly, the PVNT-NSTDA protocol used HEK293-ACE2-TMPRSS2 expressing target cells, while our PVNT used HEK Blue™™ hACE2 as the target cell, which might differ in pseudotype permissiveness. Secondly, PVNT-NSTDA employed luciferase as a detection system, which has been reported to be very sensitive with a lower signal-to-noise ratio when compared to GFP [97]. These might affect the readouts and yield a difference in neutralizing antibody values.

As expected, a low correlation between PVNT and ELISA-based methods, including anti-RBD IgG and ELISA (sVNT), was observed ( $r = 0.610$ ,  $P < 0.0001$ ), as these techniques do not determine neutralizing activity but only the binding antibody

against the RBD protein. Similar results of low or moderate correlation were reported [98]. Additional analysis to establish the relationship between PVNT and sVNT was performed. We found that at approximately 200 IU/mL and 1,900 IU/mL of neutralizing antibody analyzed by PVNT, there were around 55% and 90% inhibition analyzed by sVNT, respectively.

The limitation of this study, according to the data shown in **table 8**, is that four out of the five testing methods employed enzymatic chemical reactions for detection. However, PVNT<sub>50</sub> utilized photoluminescence photon emission-based - GFP for detection, as it employed a cell-based technique in testing. The autofluorescence features of cells might lead to overestimation in titer determination or false negative in assays. The employment of enzymatic chemical reaction technology might overcome this issue. Moreover, the enzymatic chemical process possesses a signal amplification, and probably increase the assay sensitivity.

The other limitations of this study include the fact that most of the samples used for the correlation study were ChulaCoV-19 immunized sera. Further validation using convalescent patient sera could potentially provide more information about the assay's performance. Additional production of more recent circulating variants is also crucial to gain more applications for next-generation vaccine immunogenicity, as well as for serological studies.

In conclusion, our pseudotype neutralization assay demonstrated comparable performance in terms of its sensitivity, specificity, and correlation with the gold standard method. It could be applied as a high-throughput tool for measuring neutralizing antibodies in both vaccinated and naturally infected individuals.

## APPENDIX A

## REAGENTS

0.25% Trypsin EDTA	Gibco, USA
10 mg/mL Puromycin	Invivogen ,USA
10 mg/mL Puromycin	Invivogen ,USA
100 mg/mL Zeocin®	Invivogen ,USA
100X Antibiotics-Antimycotics	Gibco, USA
100X L-glutamine	Gibco, USA
50 mg/mL Normocin®	Invivogen ,USA
50X PBS buffer	Vivantis, Malaysia
50X TAE buffer	Vivantis, Malaysia
Absolute ethanol	Emsure, Germany
Agarose	Vivantis, Malaysia
Ampicillin	General Drug house, Thailand
DMEM	Gibco, USA
Fetal bovine serum (FBS)	Gibco, USA
Isopropranol (2-propranol)	Emsure, Germany
Kanamycin	Thai Meiji Pharmaceutical, Thailand
Luria-Bertani (LB) agar	Culgene, USA
Luria-Bertani (LB) broth	Culgenex, USA
Luria-Bertani(LB) agar	Culgenex, USA
ONE glo luciferase	Promega, USA
PEI, Branch	Sigma-Aldrich, Germany
Polybrene	Sigma-Aldrich, Germany
Sodium hydrogen bicarbonate	Panreac Appllichem, Spain

**APPENDIX B**  
**INSTRUMENTS AND MATERIALS**

0.45 µM syringe filter	Corning, USA
1 mL pipette tip	QSP, USA
1.5 microcentrifuge tube	Axygen, USA
10 mL serological pipette	SPL, Korea
12-well plate	SPL, Korea
15 mL conical tube	Thermo Scientific, USA
25 mL serological pipette	SPL, Korea
5 ml serological pipette	SPL, Korea
5 ml syringe	Nipro, Japan
50 mL conical tube	Thermo Scientific, USA
6-well plate	SPL, Korea
96-well plate flat bottom	SPL, Korea
96-well plate U bottom	SPL Korea
Autoclave, HICLAVE	Hirayama, Japan
Balance (2 digits)	Adam, UK
Biohazard safety cabinet class II	Faster, Italy
Cell culture flask (T25, T75 and T175)	Thermo Scientific, USA
CO <sub>2</sub> humidified incubator	Binder, Germany
Electronic pipette	Sartorius, Germany
High speed centrifuge MX-301	Tomy, Japan
Hot air oven	Memmert, Germany
Immunospot® S6 Ultimate	CTL, USA
Incubator shaker Innova 42	Scientific Laboratory Supplies, UK
Inverted fluorescent microscopy	Nikon, Japan
Microcentrifuge	Eppendorf, Germany
Microplate reader Varioskan Flash	Thermo Scientific, USA
Nanodrop	Thermo Scientific, USA
Presto™ Mini Plasmid Kit (PDH300)	Geneaid, Taiwan

QIAGEN® Plasmid Midi Kits	Qiagen, USA
QIAquick PCR Purification Kit	Qiagen, USA
Reservoir	SPL, Korea



## APPENDIX C

## ENZYMES

Restriction enzyme <i>EcoRI</i>	NEB, England
Restriction enzyme <i>Sall</i>	NEB, England
T4 DNA Ligase	NEB, England



**APPENDIX D****ANTIBODY**

SARS-CoV-2 (2019-nCoV) Spike Antibody, Sino biological, USA

Rabbit PAb, Antigen Affinity Purified (Cat no.  
40591-T62).

FITC Donkey anti-rabbit IgG (min. x-reactivity) Biolegend, USA  
(Cat no. 406403)



APPENDIX E  
REAGENTS PREPARATION

10% DMEM		
1X DMEM		87 mL
FBS		10 mL
100X L-glutamine		1 mL
100X Antibiotic antimycotic		1 mL
Stored at 4 °		
		
10% DMEM		
1X DMEM		96.89 mL
FBS		1 mL
100X L-glutamine		1 mL
10 mg/mL Puromycin		10 µL
100 mg/mL Zeocin		100 µL
50 mg/mL Normocin		200 µL
Stored at 4 °		
จุฬาลงกรณ์มหาวิทยาลัย <b>CHULALONGKORN UNIVERSITY</b>		
1X PBS		
50X PBS		2 mL
DW qs to		100 mL
1X TAE buffer		
50X TEA buffer		2 mL
DW qs to		100 mL

**APPENDIX F**  
**AMINO ACID SEQUENCE**

Amino acid sequence MN908947.1 Wuhan seafood market pneumonia virus isolate  
Wuhan-Hu-1, complete

MFVFLVLLPLVSSQCVNLTRTQLPPAYTNSFTRGVYYPDKVFRSSVLHSTQDLFLPFFSNVTWFHAI  
HVSQTNGTKRFDNPVLPFNDGVYFASTEKSNIIRGWIFGTLLDSKTQSLLIVNNATNVVIVKCEFQFC  
NDPFLGVYYHKNNKSWMESEFRVYSSANNCTFEYVSQPFLMDLEGKQGNFKNLREFVFKNIDGYFK  
IYSKHTPINLVRDLPQGFSALEPLVDLPIGINITRFQTLALHRSYLTPGDSSSGWTAGAAAYVGYLQP  
RTFLLKYNENGTITDAVDCALDPLSETKCTLKSFTVEKGIYQTSNFRVQPTESIVRFPNITNLCPFGEVF  
NATRFASVYAWNRKRISNCVADYSVLYNSASFSTFKCYGVSPTKLNDLCFTNVYADSFVIRGDEVROIA  
PGQTGKIADYNYKLPDDFTGCVIAWNSNLDKSKVGGNYNYLYRLFRKSNLKPFERDISTEIQAGSTP  
CNGVEGFNCYFPLOSYPQPTNGVGYQPYRWVLSFELLHAPATVCGPKKSTNLVKNKCVNFNFNNG  
LTGTGVLTESNKKFLPFQQFGRDIADTTDAVRDPQTLLEILDITPCSFGGVSVITPGTNTSNQVAVLYQD  
VNCTEVPVAIHADQLTPTWRVYSTGSNVFQTRAGCLIGAEHVNNSYECDIPIGAGICASYQTQTNSPR  
RARSVASQSIIAYTMSLGAENSVAYSNNIAIPTNFTISVTTEILPVSMTKTSVDCTMYICGDSTECSNLL  
LOYGSFCTQLNRALTGIAVEQDKNTOEVFAQVKQIYKTPPIKDFGGFNFSQILPDPSKPSKRSFIEDLL  
FNKVTLADAGFIKQYGDCLGDIAARDLICAQKFNGLTVLPLLTDemiaQYTSALLAGTITSGWTFGA  
GAALQIPFAMQMAYRFNGIGVTQNVLYENQKLIANQFNNSAIGKIQDSLSSTASALGKLQDVVNQNAQ  
ALNTLVKQLSSNFGAISSVLNDILSRDKVEAEVQIDRLITGRLOSLQTYVTQQLIRAAEIRASANLAAT  
KMSECVLGQSKRVDFCGKGYHLMSPQSAPHGVFLHVTYVPAQEKNFHTTAPAICHGKAHFPREG  
VFVSNGTHWFVTQRNFYEPQIITDNTFVSGNCDVWIGVNNNTVYDPLQPELDSFKEELDKYFKNHTS  
PDVDLGDISGINASVVNIQKEIDRLNEVAKNLNESLIDLQELGKYEQYIKWPWYIWLGFIAGLIAIVMVTI  
MLCCMTSCCSCLKGCCSCGS

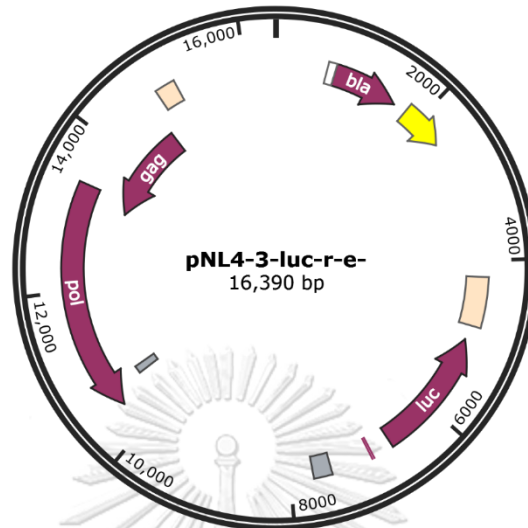
Amino acid sequence Delta (B.1.617.2)

MFVFLVLLPLVSSQCVNLRTRTQLPPAYTNSFTRGVVYYPDKVFRSSVLHSTQDLFLPFFSNVTWFHAI  
HVSGTNGTKRFDNPVLPFNDGVYFASTEKSNIIRGWIFGTTLDSKTQSLLIVNNATNVVIKVFCEQFC  
NDPFLDVYYHKNNKSWMESVYSSANNCTFEYVSQPFLMDLEGKQGNFKNLREFVFKNIDGYFKIYS  
KHTPINLVRDLPQGFSALEPLVDLPIGINITRFQTLALHRSYLTGDSSSGWTAGAAAYVGYLQPRT  
FLLKYNENGTITDAVDCALDPLSETKCTLKSFTEKGIYQTSNFRVQPTESIVRFPNITNLCPFGEVFN  
ATRFASVYAWNRRKRISNCVADYSVLYNSASFSTFKCYGVSPTKLNLDLCTNVYADSFVIRGDEVRQIAP  
GQTGKIADYNYKLPDDFTGCVIAWNSNNLDSKVGGNYNRYRFRKSNLKPFERDISTEIYQAGSKPC  
NGVQGFNCYFPLQSYGFQPTNGVGYQPYRVVWLSFELLHAPATVCGPKKSTNLVKNKCVNFNFNGL  
TGTGVLTESNKKFLPFQQFGRDIADTTDAVRDPQTLTLEILDITPCSFGGVSVITPGTNTSNQVAVLYQG  
VNCTEVPVAIHADQLTPTWRVYSTGSNVFQTRAGCLIGAEHVNNSYECDIPIGAGICASYQTQTNRRR  
RARSVASQSIIAYTMSLGAENSVAYSNNNSIAIPTNFTISVTTEILPVSMTKTSVDCTMYICGDSTECSNLL  
LQYGSFCTQLNRALTGIAVEQDKNTQEVFAQVKQYKTPPIKDFGGFNFSQILPDPSPKRSFIEDLL  
FNKVTLADAGFIKQYGDCLGDIAARDLICAQKFNGLTVLPPLLTDEMIAQYTSALLAGTITSGWTFGA  
GAALQIPFAMQMAYRFNGIGVTQNVLYENQKLIANQFNNSAIGKIQDSLSTASALGKLQNVVNQNAQ  
ALNTLVKQLSSNFGAISSVLNDILSRLDPPEAEVQIDRLITGRLOSLQTYVTQQLIRAAEIRASANLAAT  
KMSECVLGQSKRVDFCGKGYHLMSPQSAHPGVVFLHVTVYVPAQEKNFTTAPAICHGDKAHFPREG  
VFVSNGTHWFVTQRNFYEPQIITDNTFVSGNCDVVIGIVNNTVYDPLQPELDSFKEELDKYFKNHST  
PDVDLGDISGINASVVNIQKEIDRLNEVAKNLNESLIDLQELGKYEQYIKWPWYIWLGFIAGLIAVMVTI  
MLCCMTSCCCLKGCCSCGS

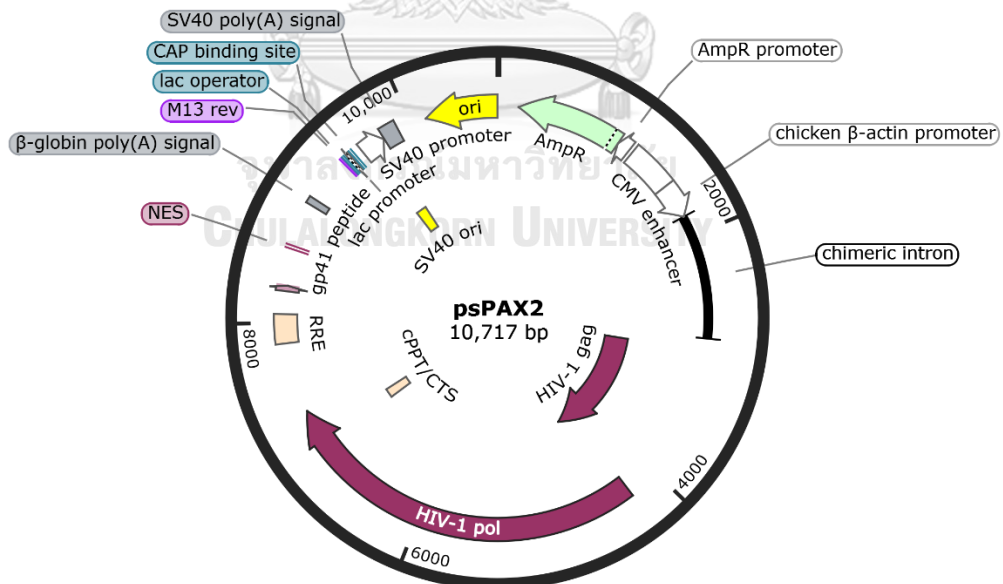
Amino acid sequence Omicron BA.4/5

MFVFLVLLPLVSSQCVNLITRTQSYTNSFTRGVVYPDKVFRSSVLHSTQDLFLPFFSNVTWFHAIISGT  
 NGTKRFDNPVLPFNDGVYFASTEKSNIRGWIFGTTLDLSTQSLIVNNATNVVIVKVEFQFCNDPFLD  
 VYYHKNNKSWMESEFRVYSSANNCTFEYVSQPFLMDLEGKQGNFKNLREFVFNIDGYFKIYSKHTP  
 INLGRDLPQGFSALEPLVDLPIGINITRFQTLALHRSYLTGDSGSSGWTAGAAAYVGYLQPRTFLLK  
 YNENGTITDAVDCALDPLSETKCTLSFTVEKGIYQTSNFRVQPTESIVRFPNITNLCPFDEVFNATRF  
 ASVYAWNRKRISNCVADYSVLYNFAPFFAFKCYGVSPTKLNLDLCTNVYADSFVIRGNEVRQIAPGQT  
 GNIADYNYKLPDDFTGCVIAWNSNKLDSKVGGNVYRYRFRKSNLKPFRDISTEIQAGNKPCNGV  
 AGVNCYFPLQSYGFRPTYGVGHQPYRVVLSFELLHAPATVCGPKKSTNLVKNKCVNFNFNGLTGT  
 GVLTESNKKFLPFQQFGRDIADTTDAVRDPQTLLEILDITPCSFGGVSVITPGTNTSNQVAVLYQGVNC  
 TEVPAIHADQLTPTWRVYSTGNSVNFQTRAGCLIGAIEVNNNSYECDIPIGAGICASYQTQTKSHRRAR  
 SVASQSIIAYTMSLGAENSVAYSNNSIAIPTNFTISVTTEILPVSMTKTSVDCTMYICGDSTECSNLLLQY  
 GSFCTQLKRALTGIAVEQDKNTQEVFAQVKQIYKTPPIKYFGGFNFSQILPDPSPKSKRSFIEDLLFNKV  
 TLADAGFIKQYGDCLGDIAARDLICAQKFNGLTVLPPLLTDEMIAQYTSALLAGTITSGWTFGAGAAL  
 QIPFAMQMAYRFNGIGVTQNVLYENQKLIANQFNSAIGKIQDSLSTASALGKLQDVNHNAAQALNT  
 LVKQLSSKFGAISSVLNDILSRLDPPEAEVQIDRLITGRLQSLQTYVTQQLIRAAEIRASANLAATKMSE  
 CVLGQSKRVDFCGKGYHLSFPQSAPHGVVFLHVTYVPAQEKNFHTTAPAICHGKAHFPREGVFVS  
 NGTHWFVTQRNFYEQIITTDNTEFVSGNCDVVIGIVNNTVYDPLQPELDSFKEELDKYFKNHTSPDV  
 DLGDISGINASVVNIQKEIDRLNEVAKNLNESLIDLQELGKYEQYIKWPWYIWLGFIAGLIAIVMVTIML  
 CCMTSCCSCLKGCCSCGSC

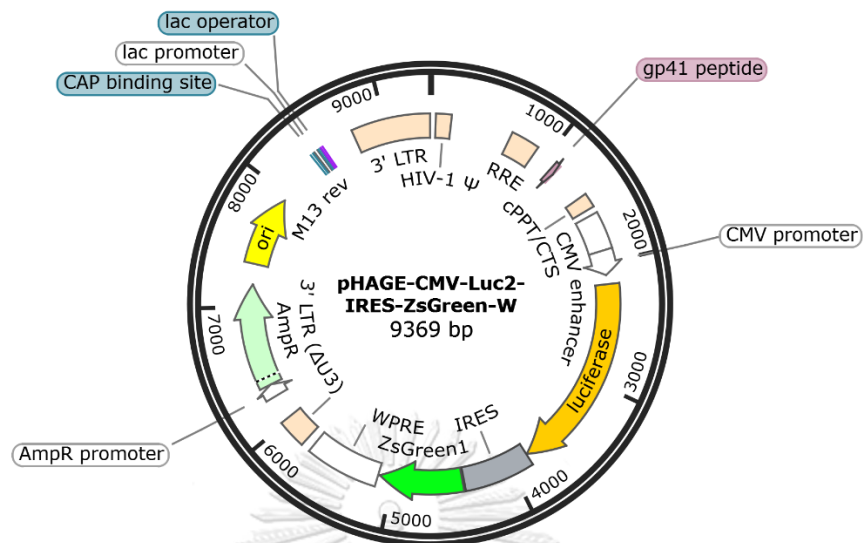
APPENDIX G  
PLASMID MAP



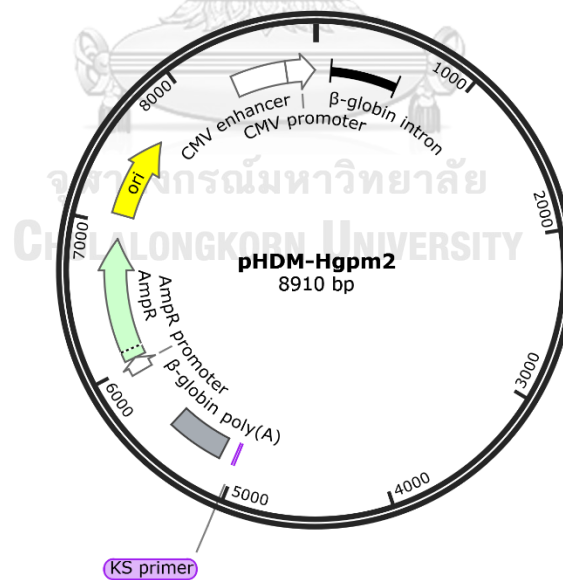
Plasmid pNL4-3.Luc.R-E, by “SnapGene software (from Insightful Science; available at [snapgene.com](http://snapgene.com))”



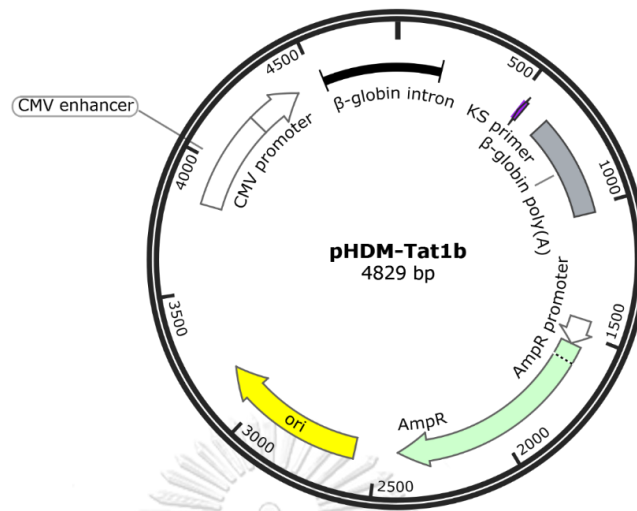
Plasmid psPAX2, by “SnapGene software (from Insightful Science; available at [snapgene.com](http://snapgene.com))”



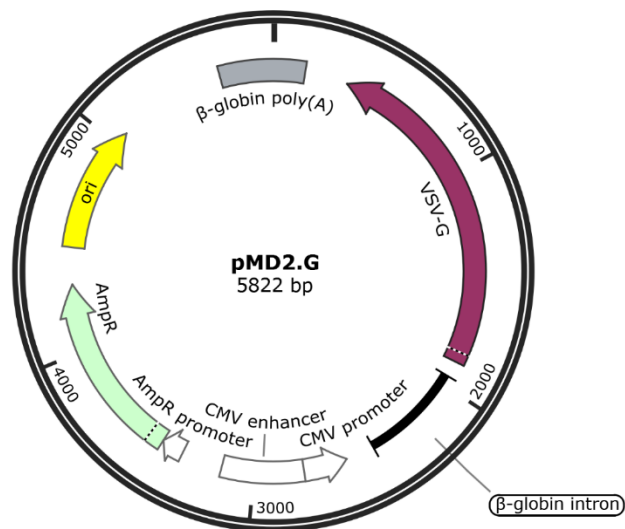
Plasmid pHAGE-CMV-Luc2-IRES-ZsGreen-W, by “SnapGene software (from Insightful Science; available at [snapgene.com](http://snapgene.com))”



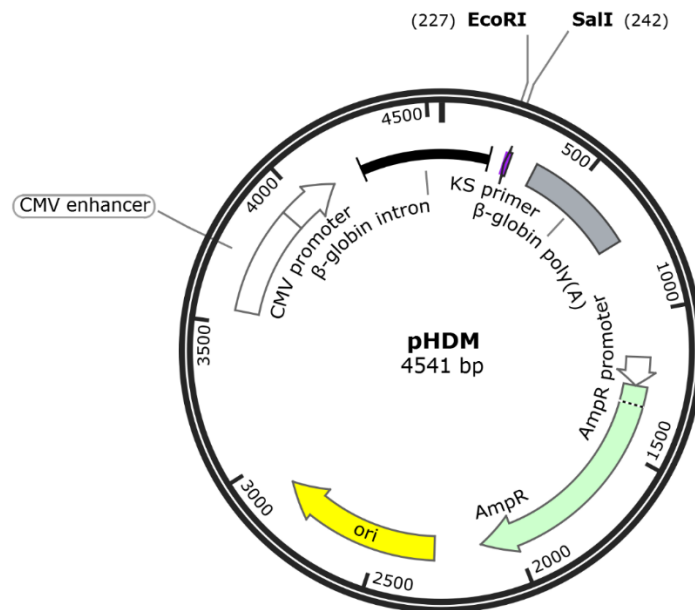
Plasmid pHDM-Hgpm2, by “SnapGene software (from Insightful Science; available at [snapgene.com](http://snapgene.com))”



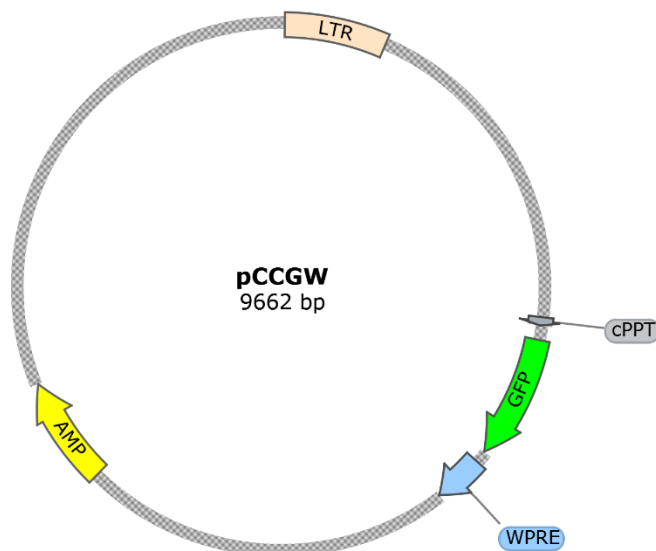
Plasmid pHDM-Tat1b, by “SnapGene software (from Insightful Science; available at [snapgene.com](http://snapgene.com))”



Plasmid pMD2.G, “SnapGene software (from Insightful Science; available at [snapgene.com](http://snapgene.com))”



Plasmid pHDM, by “SnapGene software (from Insightful Science; available at [snapgene.com](http://snapgene.com))”



plasmid pCCGW, by “SnapGene software (from Insightful Science; available at [snapgene.com](http://snapgene.com))”

## APPENDIX H

## SUMMARY NEUTRALIZING DATA

Summary neutralizing data in low titer (20-160) group

Low titer (20-160)						
Sample no.	ID	MN (IU/mL)	ELISA Abbott Total IgG (BAU/mL)	PVNT NSTDA (IU/mL)	svNT	PVNT (IU/mL)
1	006 D22	31.24	67.89	-	55.60	229.85
2	008 D22	96.07	84.52	-	46.88	161.06
3	011 D22	17.16	465.87	-	88.13	1,149.49
4	016 D22	96.07	101.66	-	31.55	344.46
5	020 D22	55.47	126.98	-	44.72	536.49
6	025 D22	96.07	328.12	-	79.19	392.39
7	029 D22	55.47	20.93	-	61.46	331.83
8	032 D22	55.47	78.48	-	45.22	385.32
9	035 D22	17.16	54.5	-	59.49	413.72
10	036 D22	96.07	450.27	-	76.56	2.92
11	041 D22	17.16	101.36	-	61.78	98.29
12	042 D22*	17.16	19.3	-	33.14	0
13	048 D22	31.24	69.47	-	49.91	193.99
14	049 D22	31.24	124.42	-	80.48	335.34
15	055 D22	17.16	26.74	-	37.19	467.10
16	056 D22	31.24	243.09	-	74.71	370.07
17	059 D22	96.07	49.37	-	11.09	491.59
18	061 D22	17.16	141.66	-	79.53	306.80
19	066 D22	96.07	142.11	-	68.43	1,023.86
20	071 D22	17.16	49.36	-	42.51	71.69
21	004 D29	31.24	61.24	5.52	58.78	288.16
22	005 D29	55.47	51.19	13.10	41.84	46.09
23	011 D29	55.47	487.68	2.13	87.32	624.76
24	017 D29	17.16	37.94	0.36	33.38	395.28
25	018 D29	17.16	29.49	9.20	23.38	308.28
26	021 D29	55.47	54.84	2.12	54.84	75.41
27	041 D29	55.47	196.27	0.00	77.29	162.90
28	044 D29	31.24	185.72	28.63	53.69	298.94
29	045 D29	17.16	163.41	3.16	67.42	393.18
30	047 D29	96.07	326.36	8.99	81.60	349.47
31	049 D29	31.24	245.46	18.95	85.39	1,755.98
32	050 D29	31.24	193.13	9.48	76.12	357.81
33	051 D29	96.07	546.71	42.43	92.29	736.90

\*False negative

## Summary neutralizing data in medium titer (&gt;160-2,560) group

Medium (>160-2,560)						
Sample no.	ID	MN (IU/mL)	ELISA Abbott Total IgG (BAU/mL)	PVNT NSTDA (IU/mL)	sVNT	PVNT (IU/mL)
34	002 D22	162.34	63.89	-	60.89	867.38
35	014 D22	162.34	65.46	-	75.17	1,190.96
36	015 D22	162.34	47.78	-	84.84	492.10
37	027 D22	267.62	433.26	-	80.46	2,017.44
38	028 D22	267.62	269.46	-	82.00	785.25
39	030 D22	267.62	209.86	-	57.45	201.41
40	031 D22	162.34	124.82	-	87.71	706.76
41	033 D22	267.62	316.53	-	74.14	3,159.80
42	034 D22	430.38	127.86	-	59.94	4,470.07
43	007 D29	267.62	31.45	27.86	83.07	764.19
44	010 D29	267.62	165.73	37.64	78.90	253.71
45	012 D29	162.34	139.4	35.68	65.43	855.04
46	013 D29	267.62	140.37	1.65	42.92	464.04
47	014 D29	675.22	1,249.67	437.70	95.12	464.04
48	015 D29	267.62	937.38	72.02	92.10	492.30
49	016 D29	267.62	499.27	68.72	81.33	498.19
50	020 D29	675.22	1,014.26	436.01	94.97	3,586.78
51	022 D29	162.34	578.78	15.10	90.76	387.37
52	024 D29	675.22	217.53	27.28	76.43	8,028.57
53	028 D29	675.22	2,308.91	283.08	94.25	3,602.38
54	029 D29	267.62	225.16	147.60	84.72	1,043.27
55	030 D29	675.22	1,541.24	239.21	95.24	1,086.64
56	031 D29	675.22	692.82	121.48	93.63	823.11
57	035 D29	267.62	678.70	38.31	78.70	406.95
58	036 D29	430.38	3,519.27	470.01	95.38	2,154.12
59	066 D29	430.38	2,401.39	367.52	94.90	2,215.36
60	067 D29	267.62	555.63	77.58	88.36	1,211.75
61	003 D50	675.22	2,018.18	385.44	95.53	898.25
62	006 D50	430.38	749.86	46.74	92.24	101.14
63	014 D50	675.22	1,505.7	360.82	96.66	3,951.58
64	015 D50	675.22	1,981.67	241.33	96.92	191.33
65	016 D50	267.62	472.96	97.11	86.33	1,425.77
66	017 D50	675.22	579.32	220.11	95.94	1,110.07
67	018 D50	430.38	390.83	271.12	95.99	848.68
68	022 D50	267.62	1,639.69	132.59	96.97	369.13

Medium (>160-2,560)						
Sample no.	ID	MN (IU/mL)	ELISA Abbott Total IgG (BAU/mL)	PVNT NSTDA (IU/mL)	sVNT	PVNT (IU/mL)
69	028 D50	675.22	1,008.34	137.52	93.06	777.69
70	029 D50	675.22	563.14	125.52	91.52	2,732.52



## Summary neutralizing data in high titer (&gt;2,560) group

High (>2,560)						
Sample no.	ID	MN (IU/mL)	ELISA Abbott Total IgG (BAU/mL)	PVNT NSTDA (IU/mL)	sVNT	PVNT (IU/mL)
71	069 D22	1,033.44	434.65	-	93.70	1,287.09
72	002 D29	1,033.44	2,238.35	665.71	95.44	2,930.38
73	008 D29	1,033.44	1004.15	682.04	96.78	5,776.01
74	023 D29	1,033.44	650.22	482.95	89.81	3,951.58
75	025 D29	1,543.05	5,887.09	350.17	94.48	5,296.53
76	027 D29	2,247.64	20,532.62	1,856.76	96.82	12,448.02
77	032 D29	1,033.44	692.82	228.07	96.29	11,308.13
78	033 D29	1,543.05	2,756.7	474.46	95.73	10,949.74
79	063 D29	1,543.05	494.86	617.91	98.10	3,340.81
80	069 D19	1,033.44	434.65	583.27	95.05	1,676.06
81	002 D50	2,247.64	2,461.53	428.02	97.07	12,441.81
82	011 D50	2,247.64	2,515.06	1,632.56	94.55	8,857.86
83	012 D50	2,247.64	2,532.91	1,372.36	96.71	3,178.19
84	014 D50	1,033.44	1,505.7	729.50	96.66	1,948.53
85	021 D50	1,033.44	1,169.21	85.06	95.43	503.19
86	024 D50	2,247.64	1,735.13	485.37	96.61	15,774.35
87	025 D50	1,033.44	3,559.64	347.75	96.50	2,706.06
88	026 D50	4,427.70	14,819.99	6,441.85	98.05	7,439.39
89	027 D50	1,543.05	9,144.12	881.14	97.74	2,552.20
90	033 D50	2,247.64	3,178.67	464.31	97.28	931.12
91	034 D50	1,543.05	1,250.75	203.72	97.07	7,281.38
92	054 D50	1,033.44	1,945.66	68.14	94.35	575.96

## Summary neutralizing data in negative group

Sample no.	ID	MN <sub>50</sub> titer	MN <sub>50</sub> titer (IU/mL)	PVNT <sub>50</sub> titer	PVNT <sub>50</sub> titer (IU/mL)
1	004 D2	10	0	5	0
2	006 D2	10	0	5	0
3	007 D2	10	0	5	0
4	011 D2	10	0	5	0
5	012 D2	10	0	5	0
6	014 D2	10	0	5	0
7	016 D2	10	0	5	0
8	017 D2	10	0	5	0
9	018 D2	10	0	5	0
10	022 D2	10	0	5	0
11	023 D2	10	0	5	0
12	037 D2	10	0	5	0
13	038 D2	10	0	5	0
14	039 D2	10	0	5	0
15	040 D2	10	0	5	0
16	041 D2	10	0	5	0
17	042 D2	10	0	5	0
18	043 D2	10	0	5	0
19	044 D2	10	0	5	0
20	045 D2	10	0	5	0
21	046 D2	10	0	5	0
22	047 D2	10	0	5	0
23	048 D2	10	0	5	0
24	049 D2	10	0	5	0
25	050 D2	10	0	5	0
26	051 D2	10	0	5	0
27	052 D2	10	0	5	0
28	053 D2	10	0	5	0
29	054 D2	10	0	5	0
30	055 D2	10	0	5	0
31	056 D2	10	0	5	0
32	057 D2	10	0	5	0
33	058 D2	10	0	5	0
34	059 D2	10	0	5	0
35	060 D2	10	0	5	0
36	061 D2	10	0	5	0

Summary of PVNT<sub>50</sub> and SARS-CoV-2 IgG using convalescent patient sera.

Accuset™ SeraCare	Abbott ARCHITECT SARS-CoV-2 IgG (s/co)	PVNT <sub>50</sub> titer		
		Run 1	Run 2	Run 3
Panel 1	1.56	88.4	104.8	98.1
Panel 2	1.96	75.7	75.7	92.5
Panel 3	3.01	101.8	113.3	111.9
Panel 4	2.96	33.6	50.3	46.8
Panel 5	3.10	49.2	40.9	41.5
Panel 6	3.07	37.5	36.7	41.3
Panel 7	2.91	89.5	79.3	89.1
Panel 8	4.19	111.9	64.1	95.6
Panel 9	3.92	58.9	69.3	59.3
Panel 10	3.79	53.9	66.5	67.9
Panel 11	0.03	5	5	5

## REFERENCES

1. Cui, J., F. Li, and Z.L. Shi, *Origin and evolution of pathogenic coronaviruses*. Nat Rev Microbiol, 2019. **17**(3): p. 181-192.
2. Drain, P.K., *Rapid Diagnostic Testing for SARS-CoV-2*. New England Journal of Medicine, 2022. **386**(3): p. 264-272.
3. Wu, F., et al., *A new coronavirus associated with human respiratory disease in China*. Nature, 2020. **579**(7798): p. 265-269.
4. Hu, B., et al., *Characteristics of SARS-CoV-2 and COVID-19*. Nature Reviews Microbiology, 2021. **19**(3): p. 141-154.
5. Bhattacharya, M., et al., *D614G mutation and SARS-CoV-2: impact on S-protein structure, function, infectivity, and immunity*. Appl Microbiol Biotechnol, 2021. **105**(24): p. 9035-9045.
6. Volz, E., et al., *Evaluating the Effects of SARS-CoV-2 Spike Mutation D614G on Transmissibility and Pathogenicity*. Cell, 2021. **184**(1): p. 64-75.e11.
7. Zhang, Y., H. Xi, and M. Juhas, *Biosensing Detection of the SARS-CoV-2 D614G Mutation*. Trends in Genetics, 2021. **37**(4): p. 299-302.
8. Kalker, R., et al., *SARS-CoV-2 Spike Pseudoviruses: A Useful Tool to Study Virus Entry and Address Emerging Neutralization Escape Phenotypes*. Microorganisms, 2021. **9**(8).
9. Alkhatib, M., et al., *SARS-CoV-2 Variants and Their Relevant Mutational Profiles: Update Summer 2021*. Microbiol Spectr, 2021. **9**(3): p. e0109621.
10. Li, C.K., et al., *T cell responses to whole SARS coronavirus in humans*. J Immunol, 2008. **181**(8): p. 5490-500.
11. Shah, V.K., et al., *Overview of Immune Response During SARS-CoV-2 Infection: Lessons From the Past*. Frontiers in Immunology, 2020. **11**.
12. Okba, N.M.A., et al., *Severe Acute Respiratory Syndrome Coronavirus 2-Specific Antibody Responses in Coronavirus Disease Patients*. Emerg Infect Dis, 2020. **26**(7): p. 1478-1488.
13. Hajissa, K., et al., *The SARS-CoV-2 Antibodies, Their Diagnostic Utility, and Their*

- Potential for Vaccine Development*. Vaccines (Basel), 2022. **10**(8).
14. West, R., et al., *COVID-19 Antibody Tests: A Valuable Public Health Tool with Limited Relevance to Individuals*. Trends Microbiol, 2021. **29**(3): p. 214-223.
  15. Thiriard, A., et al., *Antibody response in children with multisystem inflammatory syndrome related to COVID-19 (MIS-C) compared to children with uncomplicated COVID-19*. Frontiers in Immunology, 2023. **14**.
  16. Abduljalil, J.M., *Laboratory diagnosis of SARS-CoV-2: available approaches and limitations*. New Microbes New Infect, 2020. **36**: p. 100713.
  17. Mallano, A., A. Ascione, and M. Flego, *Antibody Response against SARS-CoV-2 Infection: Implications for Diagnosis, Treatment and Vaccine Development*. Int Rev Immunol, 2022. **41**(4): p. 393-413.
  18. Gumanova, N.G., et al., *Detection of Anti-SARS-CoV-2-S1 RBD-Specific Antibodies Prior to and during the Pandemic in 2011-2021 and COVID-19 Observational Study in 2019-2021*. Vaccines (Basel), 2022. **10**(4).
  19. Lo Sasso, B., et al., *Evaluation of Anti-SARS-Cov-2 S-RBD IgG Antibodies after COVID-19 mRNA BNT162b2 Vaccine*. Diagnostics (Basel), 2021. **11**(7).
  20. Fogolari, M., et al., *Neutralizing Antibodies against SARS-CoV-2 Beta and Omicron Variants Inhibition Comparison after BNT162b2 mRNA Booster Doses with a New PETIA sVNT Assay*. Diagnostics, 2023. **13**(5): p. 889.
  21. Tan, C.W., et al., *A SARS-CoV-2 surrogate virus neutralization test based on antibody-mediated blockage of ACE2–spike protein–protein interaction*. Nature Biotechnology, 2020. **38**(9): p. 1073-1078.
  22. Liu, K.T., et al., *Overview of Neutralization Assays and International Standard for Detecting SARS-CoV-2 Neutralizing Antibody*. Viruses, 2022. **14**(7).
  23. Perera, R.A.P.M., et al., *Evaluation of a SARS-CoV-2 Surrogate Virus Neutralization Test for Detection of Antibody in Human, Canine, Cat, and Hamster Sera*. Journal of clinical microbiology, 2021. **59**(2): p. e02504-20.
  24. Zhu, Z., et al., *Potent cross-reactive neutralization of SARS coronavirus isolates by human monoclonal antibodies*. Proc Natl Acad Sci U S A, 2007. **104**(29): p. 12123-8.
  25. Diamond, M.S. and T.-D. Kanneganti, *Innate immunity: the first line of defense*

- against SARS-CoV-2. *Nature Immunology*, 2022. **23**(2): p. 165-176.
26. Zhu, Q., et al., *Innate and adaptive immune response in SARS-CoV-2 infection- Current perspectives*. *Frontiers in Immunology*, 2022. **13**.
  27. Liu, G. and Y. Zhao, *Toll-like receptors and immune regulation: their direct and indirect modulation on regulatory CD4+ CD25+ T cells*. *Immunology*, 2007. **122**(2): p. 149-56.
  28. Schultze, J.L. and A.C. Aschenbrenner, *COVID-19 and the human innate immune system*. *Cell*, 2021. **184**(7): p. 1671-1692.
  29. Thorne, L.G., et al., *SARS-CoV-2 sensing by RIG-I and MDA5 links epithelial infection to macrophage inflammation*. *bioRxiv*, 2020: p. 2020.12.23.424169.
  30. Zhou, X. and Q. Ye, *Cellular Immune Response to COVID-19 and Potential Immune Modulators*. *Front Immunol*, 2021. **12**: p. 646333.
  31. Maison, D.P., Y. Deng, and M. Gerschenson, *SARS-CoV-2 and the host-immune response*. *Frontiers in Immunology*, 2023. **14**.
  32. Bertoletti, A., A.T. Tan, and N. Le Bert, *The T-cell response to SARS-CoV-2: kinetic and quantitative aspects and the case for their protective role*. *Oxford Open Immunology*, 2021. **2**(1).
  33. Swain, S.L., K.K. McKinstry, and T.M. Strutt, *Expanding roles for CD4+ T cells in immunity to viruses*. *Nature Reviews Immunology*, 2012. **12**(2): p. 136-148.
  34. Moss, P., *The T cell immune response against SARS-CoV-2*. *Nature Immunology*, 2022. **23**(2): p. 186-193.
  35. Le Bert, N., et al., *SARS-CoV-2-specific T cell immunity in cases of COVID-19 and SARS, and uninfected controls*. *Nature*, 2020. **584**(7821): p. 457-462.
  36. Hermens, J.M. and C. Kesmir, *Role of T cells in severe COVID-19 disease, protection, and long term immunity*. *Immunogenetics*, 2023. **75**(3): p. 295-307.
  37. Qi, H., et al., *The humoral response and antibodies against SARS-CoV-2 infection*. *Nature Immunology*, 2022. **23**(7): p. 1008-1020.
  38. Winter, A.K. and S.T. Hegde, *The important role of serology for COVID-19 control*. *Lancet Infect Dis*, 2020. **20**(7): p. 758-759.
  39. Muruato, A.E., et al., *A high-throughput neutralizing antibody assay for COVID-19*

- diagnosis and vaccine evaluation*. Nat Commun, 2020. **11**(1): p. 4059.
40. Zainol Rashid, Z., et al., *Diagnostic performance of COVID-19 serology assays*. Malays J Pathol, 2020. **42**(1): p. 13-21.
  41. Kundu, D., et al., *The role and diagnostic accuracy of serology for COVID-19*. BMC Infectious Diseases, 2022. **22**(1): p. 390.
  42. Watzinger, F., et al., *Real-time quantitative PCR assays for detection and monitoring of pathogenic human viruses in immunosuppressed pediatric patients*. J Clin Microbiol, 2004. **42**(11): p. 5189-98.
  43. Gong, F., et al., *Evaluation and Comparison of Serological Methods for COVID-19 Diagnosis*. Frontiers in Molecular Biosciences, 2021. **8**.
  44. Mahallawi, W.H., *A serological assay to detect human SARS-CoV-2 antibodies*. Journal of Taibah University Medical Sciences, 2021. **16**(1): p. 57-62.
  45. James, J., et al., *Comparison of Serological Assays for the Detection of SARS-CoV-2 Antibodies*. Viruses, 2021. **13**(4).
  46. Wang, Y., et al., *Unique epidemiological and clinical features of the emerging 2019 novel coronavirus pneumonia (COVID-19) implicate special control measures*. J Med Virol, 2020. **92**(6): p. 568-576.
  47. Machado, B.A.S., et al., *The Main Molecular and Serological Methods for Diagnosing COVID-19: An Overview Based on the Literature*. Viruses, 2020. **13**(1).
  48. Embregts, C.W.E., et al., *Evaluation of a multi-species SARS-CoV-2 surrogate virus neutralization test*. One Health, 2021. **13**: p. 100313.
  49. Mouna, L., et al., *Validation of a SARS-CoV-2 Surrogate Virus Neutralization Test in Recovered and Vaccinated Healthcare Workers*. Viruses, 2023. **15**(2).
  50. Lichtenegger, S., et al., *Development of a Rapid Live SARS-CoV-2 Neutralization Assay Based on a qPCR Readout*. Journal of Clinical Microbiology, 2022. **60**(7): p. e00376-22.
  51. Mather, S., et al., *Current progress with serological assays for exotic emerging/re-emerging viruses*. Future Virology, 2013. **8**(8): p. 745-755.
  52. Payne, S., *Chapter 4 - Methods to Study Viruses*, in *Viruses*, S. Payne, Editor. 2017, Academic Press. p. 37-52.
  53. Luo, Y.R., et al., *A SARS-CoV-2 Label-Free Surrogate Virus Neutralization Test*

- and a Longitudinal Study of Antibody Characteristics in COVID-19 Patients. *J Clin Microbiol*, 2021. **59**(7): p. e0019321.
54. Whitt, M.A., *Generation of VSV pseudotypes using recombinant  $\Delta$ G-VSV for studies on virus entry, identification of entry inhibitors, and immune responses to vaccines.* *J Virol Methods*, 2010. **169**(2): p. 365-74.
  55. Xiang, Q., et al., *Application of pseudovirus system in the development of vaccine, antiviral-drugs, and neutralizing antibodies.* *Microbiological Research*, 2022. **258**: p. 126993.
  56. Li, Q., et al., *Current status on the development of pseudoviruses for enveloped viruses.* *Reviews in medical virology*, 2018. **28**(1): p. e1963.
  57. Salazar-García, M., et al., *Pseudotyped Vesicular Stomatitis Virus-Severe Acute Respiratory Syndrome-Coronavirus-2 Spike for the Study of Variants, Vaccines, and Therapeutics Against Coronavirus Disease 2019.* *Frontiers in Microbiology*, 2022. **12**.
  58. Wright, E., et al., *Investigating antibody neutralization of lyssaviruses using lentiviral pseudotypes: a cross-species comparison.* *J Gen Virol*, 2008. **89**(Pt 9): p. 2204-2213.
  59. Zhou, S., et al., *A safe and sensitive enterovirus A71 infection model based on human SCARB2 knock-in mice.* *Vaccine*, 2016. **34**(24): p. 2729-36.
  60. Sierra, S., B. Kupfer, and R. Kaiser, *Basics of the virology of HIV-1 and its replication.* *Journal of Clinical Virology*, 2005. **34**(4): p. 233-244.
  61. *Human Immunodeficiency Virus (HIV).* *Transfus Med Hemother*, 2016. **43**(3): p. 203-22.
  62. Chen, M. and X.E. Zhang, *Construction and applications of SARS-CoV-2 pseudoviruses: a mini review.* *Int J Biol Sci*, 2021. **17**(6): p. 1574-1580.
  63. Dull, T., et al., *A third-generation lentivirus vector with a conditional packaging system.* *J Virol*, 1998. **72**(11): p. 8463-71.
  64. Carnell, G.W., et al., *Pseudotype-Based Neutralization Assays for Influenza: A Systematic Analysis.* *Frontiers in Immunology*, 2015. **6**.
  65. Milone, M.C. and U. O'Doherty, *Clinical use of lentiviral vectors.* *Leukemia*,

2018. **32**(7): p. 1529-1541.
66. Tani, H., S. Morikawa, and Y. Matsuura, *Development and Applications of VSV Vectors Based on Cell Tropism*. Frontiers in Microbiology, 2012. **2**.
67. Almahboub, S.A., et al., *Evaluation of Neutralizing Antibodies Against Highly Pathogenic Coronaviruses: A Detailed Protocol for a Rapid Evaluation of Neutralizing Antibodies Using Vesicular Stomatitis Virus Pseudovirus-Based Assay*. Front Microbiol, 2020. **11**: p. 2020.
68. Yan, Y., et al., *Chemiluminescence and Bioluminescence Imaging for Biosensing and Therapy: In Vitro and In Vivo Perspectives*. Theranostics, 2019. **9**: p. 4047-4065.
69. Close, D.M., et al., *Comparison of human optimized bacterial luciferase, firefly luciferase, and green fluorescent protein for continuous imaging of cell culture and animal models*. J Biomed Opt, 2011. **16**(4): p. 047003.
70. Lo, M.K., S.T. Nichol, and C.F. Spiropoulou, *Evaluation of luciferase and GFP-expressing Nipah viruses for rapid quantitative antiviral screening*. Antiviral research, 2014. **106**: p. 53-60.
71. Zuverink, M. and J.T. Barbieri, *From GFP to  $\beta$ -lactamase: advancing intact cell imaging for toxins and effectors*. Pathog Dis, 2015. **73**(9): p. ftv097.
72. Keelapang, P., et al., *Heterologous prime-boost immunization induces protection against dengue virus infection in cynomolgus macaques*. J Virol, 2023: p. e0096323.
73. Meyer, B., et al., *Validation and clinical evaluation of a SARS-CoV-2 surrogate virus neutralisation test (sVNT)*. Emerg Microbes Infect, 2020. **9**(1): p. 2394-2403.
74. Neerukonda, S.N., et al., *Establishment of a well-characterized SARS-CoV-2 lentiviral pseudovirus neutralization assay using 293T cells with stable expression of ACE2 and TMPRSS2*. PLOS ONE, 2021. **16**(3): p. e0248348.
75. von Rhein, C., et al., *Comparison of potency assays to assess SARS-CoV-2 neutralizing antibody capacity in COVID-19 convalescent plasma*. Journal of virological methods, 2021. **288**: p. 114031-114031.
76. Gager, P.C. and A.L. Vincent, *Serum Virus Neutralization Assay for Detection*

- and Quantitation of Serum-Neutralizing Antibodies to Influenza A Virus in Swine*, in *Animal Influenza Virus*, E. Spackman, Editor. 2014, Springer New York: New York, NY. p. 313-324.
77. Amanat, F., et al., *A serological assay to detect SARS-CoV-2 seroconversion in humans*. *Nature Medicine*, 2020. **26**(7): p. 1033-1036.
  78. Khoury, D.S., et al., *Measuring immunity to SARS-CoV-2 infection: comparing assays and animal models*. *Nat Rev Immunol*, 2020. **20**(12): p. 727-738.
  79. Case, J.B., et al., *Neutralizing Antibody and Soluble ACE2 Inhibition of a Replication-Competent VSV-SARS-CoV-2 and a Clinical Isolate of SARS-CoV-2*. *Cell Host & Microbe*, 2020. **28**(3): p. 475-485.e5.
  80. Peletta, A., et al., *DNA Vaccine Administered by Cationic Lipoplexes or by In Vivo Electroporation Induces Comparable Antibody Responses against SARS-CoV-2 in Mice*. *Vaccines (Basel)*, 2021. **9**(8).
  81. Ramakrishnan, M.A., *Determination of 50% endpoint titer using a simple formula*. *World J Virol*, 2016. **5**(2): p. 85-6.
  82. Lei, C., et al., *On the Calculation of TCID<sub>50</sub> for Quantitation of Virus Infectivity*. *Virol Sin*, 2021. **36**(1): p. 141-144.
  83. Koonpaew, S., et al., *A Single-Cycle Influenza A Virus-Based SARS-CoV-2 Vaccine Elicits Potent Immune Responses in a Mouse Model*. *Vaccines*, 2021. **9**(8): p. 850.
  84. Ferrara, F. and N. Temperton, *Pseudotype Neutralization Assays: From Laboratory Bench to Data Analysis*. *Methods Protoc*, 2018. **1**(1).
  85. Prompetchara, E., et al., *DNA vaccine candidate encoding SARS-CoV-2 spike proteins elicited potent humoral and Th1 cell-mediated immune responses in mice*. *PLOS ONE*, 2021. **16**(3): p. e0248007.
  86. Chan, Y.H., *Biostatistics 104: correlational analysis*. *Singapore Med J*, 2003. **44**(12): p. 614-9.
  87. Chi, X., et al., *A neutralizing human antibody binds to the N-terminal domain of the Spike protein of SARS-CoV-2*. *Science*, 2020. **369**(6504): p. 650-655.
  88. Huang, Y., et al., *Structural and functional properties of SARS-CoV-2 spike protein: potential antiviral drug development for COVID-19*. *Acta*

- Pharmacologica Sinica, 2020. **41**(9): p. 1141-1149.
89. Mizuguchi, H., et al., *IRES-Dependent Second Gene Expression Is Significantly Lower Than Cap-Dependent First Gene Expression in a Bicistronic Vector*. Molecular Therapy, 2000. **1**(4): p. 376-382.
90. Pelletier, J. and N. Sonenberg, *Internal initiation of translation of eukaryotic mRNA directed by a sequence derived from poliovirus RNA*. Nature, 1988. **334**(6180): p. 320-325.
91. Gándara, C., V. Affleck, and E.A. Stoll, *Manufacture of Third-Generation Lentivirus for Preclinical Use, with Process Development Considerations for Translation to Good Manufacturing Practice*. Hum Gene Ther Methods, 2018. **29**(1): p. 1-15.
92. Sena-Esteves, M., et al., *Optimized large-scale production of high titer lentivirus vector pseudotypes*. J Virol Methods, 2004. **122**(2): p. 131-9.
93. Sena-Esteves, M., et al., *Optimized large-scale production of high titer lentivirus vector pseudotypes*. Journal of Virological Methods, 2004. **122**(2): p. 131-139.
94. Nie, J., et al., *Quantification of SARS-CoV-2 neutralizing antibody by a pseudotyped virus-based assay*. Nature Protocols, 2020. **15**(11): p. 3699-3715.
95. King, B., et al., *Technical considerations for the generation of novel pseudotyped viruses*. Future Virology, 2015. **11**.
96. Yu, J., et al., *Deletion of the SARS-CoV-2 Spike Cytoplasmic Tail Increases Infectivity in Pseudovirus Neutralization Assays*. J Virol, 2021. **95**(11).
97. Tsai, W.Y., et al., *A real-time and high-throughput neutralization test based on SARS-CoV-2 pseudovirus containing monomeric infrared fluorescent protein as reporter*. Emerg Microbes Infect, 2021. **10**(1): p. 894-904.
98. Bošnjak, B., et al., *Low serum neutralizing anti-SARS-CoV-2 S antibody levels in mildly affected COVID-19 convalescent patients revealed by two different detection methods*. Cellular & Molecular Immunology, 2021. **18**(4): p. 936-944.



จุฬาลงกรณ์มหาวิทยาลัย  
**CHULALONGKORN UNIVERSITY**

## VITA

**NAME** Kunlanan Charsangbong

**DATE OF BIRTH** 23 January 1991

**PLACE OF BIRTH** Bangkok, Thailand

**INSTITUTIONS ATTENDED** Silpakorn University, 2010-2015  
Doctor of Pharmacy (Pharm.D.)

**HOME ADDRESS** 63/1 Mittraphap 19, Naimaund subdistrict, Maung District,  
Nakhonratchasima Province Thailand, 30000

**PUBLICATION** Charsangbong K, Rojjananavin N, Nedumpun T, Ketloy C, Prompetchara E, Techakriengkrai N 2023. Development of a pseudotype-based neutralization test for SARS-CoV-2 antibody measurement. The proceedings of the 22nd Chulalongkorn University Veterinary Conference CUVC 2023: Accelerating impactful innovative research for global health, food security & pet wellness, Bangkok, Thailand 19-21 April, 2023: 391-392.

Charsangbong K, Rojjananavin N, Nedumpun T, Prompetchara E, Techakriengkrai N. Estimating anti-SARS-CoV-2 antibody titre by a pseudotype-based neutralization test. The Proceedings of the 21st Chulalongkorn University Veterinary Conference CUVC2022: Research in Practice, Bangkok, Thailand 27-29 April, 2022: 233-234.

May Phyu Tein Maw, Charsangbong K, Kasilerk J, Chavalit P, Piyapolrunroj N. Effect of candelabra bush (*Senna alata*) herbal infusion tea on the functions of multidrug resistance proteins. Thai Journal of Pharmaceutical Sciences. 2018, 55-58.